US011071617B2

(12) **United States Patent**
MacEwan et al.

(10) **Patent No.: US 11,071,617 B2**
(45) **Date of Patent: *Jul. 27, 2021**

(54) **BIOMEDICAL PATCHES WITH ALIGNED FIBERS**

(71) Applicant: **Washington University**, St. Louis, MO (US)

(72) Inventors: **Matthew R. MacEwan**, St. Louis, MO (US); **Jingwei Xie**, St. Louis, MO (US); **Zack Ray**, St. Louis, MO (US); **Younan Xia**, St. Louis, MO (US)

(73) Assignee: **Washington University**, St. Louis, MO (US)

(*) Notice: Subject to any disclaimer, the term of this patent is extended or adjusted under 35 U.S.C. 154(b) by 0 days.

This patent is subject to a terminal disclaimer.

(21) Appl. No.: **17/063,924**

(22) Filed: **Oct. 6, 2020**

(65) **Prior Publication Data**

US 2021/0030525 A1 Feb. 4, 2021

Related U.S. Application Data

(63) Continuation of application No. 16/795,057, filed on Feb. 19, 2020, now Pat. No. 10,888,409, which is a (Continued)

(51) **Int. Cl.**
A61F 2/00 (2006.01)
A61F 2/02 (2006.01)
(Continued)

(52) **U.S. Cl.**
CPC ***A61F 2/02*** (2013.01); ***A61F 2/0063*** (2013.01); ***A61F 2/105*** (2013.01); ***A61L 15/22*** (2013.01);
(Continued)

(58) **Field of Classification Search**
CPC .. A61F 2/02; A61F 2/0063; A61F 2002/0068; A61L 15/22; A61L 15/42;
(Continued)

(56) **References Cited**

U.S. PATENT DOCUMENTS

2,068,703 A 1/1937 Powdermaker
3,280,229 A 10/1966 Simons
(Continued)

FOREIGN PATENT DOCUMENTS

AU 2011268321 B2 10/2015
AU 2012390291 B2 9/2017
(Continued)

OTHER PUBLICATIONS

3rd International Conference on Electrospinning Conference Program dated Aug. 4-7, 2004, www.ceramics.org/electrospin2014.
(Continued)

Primary Examiner — Alvin J Stewart
(74) *Attorney, Agent, or Firm* — Armstrong Teasdale LLP

(57) **ABSTRACT**

A multi-laminar electrospun nanofiber scaffold for use in repairing a defect in a tissue substrate is provided. The scaffold includes a first layer formed by a first plurality of electrospun polymeric fibers, and a second layer formed by a second plurality of electrospun polymeric fibers. The second layer is combined with the first layer. A first portion of the scaffold includes a higher density of fibers than a second portion of the scaffold, and the first portion has a higher tensile strength than the second portion. The scaffold is configured to degrade via hydrolysis after at least one of a predetermined time or an environmental condition. The scaffold is configured to be applied to the tissue substrate containing the defect, and is sufficiently flexible to facilitate
(Continued)

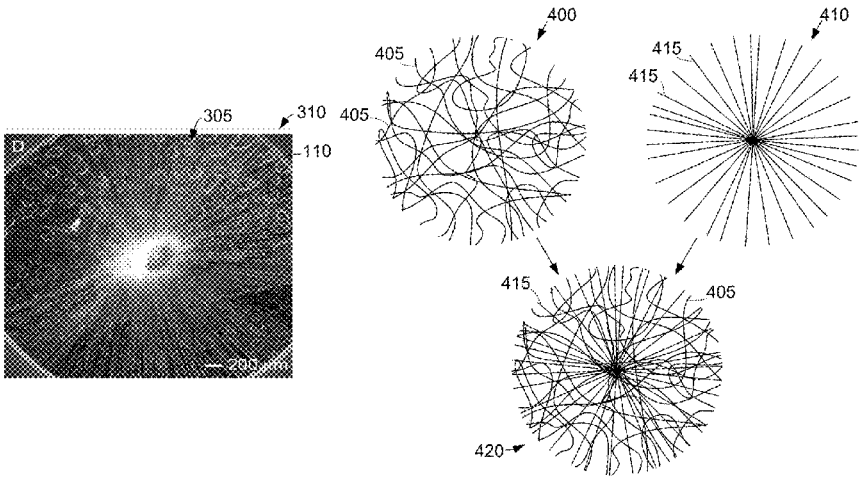

application of the scaffold to uneven surfaces of the tissue substrate, and to enable movement of the scaffold by the tissue substrate.

30 Claims, 23 Drawing Sheets

Related U.S. Application Data

continuation of application No. 16/540,548, filed on Aug. 14, 2019, now Pat. No. 10,617,512, which is a continuation of application No. 15/497,691, filed on Apr. 26, 2017, which is a continuation of application No. 13/703,210, filed as application No. PCT/US2011/040691 on Jun. 16, 2011, now Pat. No. 10,149,749.

(60) Provisional application No. 61/355,712, filed on Jun. 17, 2010.

(51) **Int. Cl.**

B29C 48/05	(2019.01)
B29C 48/14	(2019.01)
A61L 15/22	(2006.01)
A61L 15/42	(2006.01)
A61L 27/14	(2006.01)
A61L 27/50	(2006.01)
D01D 5/00	(2006.01)
D04H 1/728	(2012.01)
D04H 3/016	(2012.01)
D04H 3/073	(2012.01)
A61F 2/10	(2006.01)
C12M 1/12	(2006.01)

(52) **U.S. Cl.**

CPC ***A61L 15/42*** (2013.01); ***A61L 27/14*** (2013.01); ***A61L 27/50*** (2013.01); ***B29C 48/05*** (2019.02); ***B29C 48/142*** (2019.02); ***D01D 5/0076*** (2013.01); ***D01D 5/0092*** (2013.01); ***D04H 1/728*** (2013.01); ***D04H 3/016*** (2013.01); ***D04H 3/073*** (2013.01); *C12M 25/14* (2013.01)

(58) **Field of Classification Search**

CPC A61L 27/14; A61L 27/50; D01D 5/0076; D01D 5/0092

See application file for complete search history.

(56) **References Cited**

U.S. PATENT DOCUMENTS

3,338,992	A	8/1967	Kinney	
3,341,394	A	9/1967	Kinney	
3,502,763	A	3/1970	Hartmann	
3,542,615	A	11/1970	Dobo et al.	
3,692,618	A	9/1972	Dorschner et al.	
3,740,302	A	6/1973	Soehngen	
3,802,817	A	4/1974	Matsuki et al.	
3,849,241	A	11/1974	Butin et al.	
3,909,009	A	9/1975	Cvetko et al.	
4,044,404	A	8/1977	Martin et al.	
4,340,563	A	7/1982	Appel et al.	
4,468,428	A	8/1984	Early et al.	
4,738,740	A	4/1988	Pinchuk et al.	
4,965,110	A	10/1990	Berry	
5,024,789	A	6/1991	Berry	
5,079,080	A	1/1992	Schwarz	
5,306,550	A	4/1994	Nishiyama et al.	
5,464,450	A	11/1995	Buscemi et al.	
5,591,335	A	1/1997	Barboza et al.	
5,626,611	A	5/1997	Liu et al.	
5,795,584	A	8/1998	Totakura et al.	
5,851,937	A	12/1998	Wu et al.	
5,997,568	A	12/1999	Liu	
6,147,135	A	11/2000	Yuan et al.	
6,162,535	A	12/2000	Turkevich et al.	
6,171,338	B1	1/2001	Talja et al.	
6,180,848	B1	1/2001	Flament et al.	
6,183,670	B1	2/2001	Torobin et al.	
6,265,333	B1	7/2001	Dzenis et al.	
6,306,424	B1	10/2001	Vyakarnam et al.	
6,391,060	B1	5/2002	Ory et al.	
6,596,296	B1	7/2003	Nelson et al.	
6,630,231	B2	10/2003	Perez et al.	
6,649,807	B2	11/2003	Mizutani	
6,685,956	B2	2/2004	Chu et al.	
6,689,374	B2	2/2004	Chu et al.	
6,713,011	B2	3/2004	Chu et al.	
6,753,454	B1	6/2004	Smith et al.	
6,797,655	B2	9/2004	Rudisill	
6,946,506	B2	9/2005	Bond et al.	
7,134,857	B2	11/2006	Andrady et al.	
7,172,765	B2	2/2007	Chu et al.	
7,192,604	B2	3/2007	Brown et al.	
7,655,070	B1	2/2010	Dallas et al.	
7,759,082	B2	7/2010	Bowlin et al.	
7,799,262	B1	9/2010	Kim	
7,879,093	B2 *	2/2011	Wei	A61L 27/48 623/11.11
7,981,353	B2	7/2011	Mitchell et al.	
8,066,932	B2	11/2011	Xu	
8,273,369	B2	9/2012	Moloye-Olabisi	
8,809,212	B1	8/2014	Dirk et al.	
8,852,621	B2 *	10/2014	Patel	D01D 5/0076 424/423
9,074,172	B2	7/2015	Johnson	
9,085,830	B2	7/2015	Mitchell et al.	
9,393,097	B2	7/2016	McCullen et al.	
9,487,893	B2	11/2016	Moore et al.	
9,539,365	B2	1/2017	Kasuga et al.	
9,737,632	B2	8/2017	Johnson et al.	
9,884,027	B2	2/2018	Johnson	
9,938,373	B2	4/2018	Wang et al.	
10,016,464	B2	7/2018	Murphy et al.	
10,080,687	B2 *	9/2018	MacEwan	A61F 13/00017
10,124,089	B2 *	11/2018	MacEwan	A61L 27/60
10,149,749	B2 *	12/2018	MacEwan	A61L 15/22
10,166,315	B2	1/2019	Johnson et al.	
10,227,568	B2	3/2019	Johnson	
10,233,427	B2	3/2019	Johnson	
10,239,262	B2	3/2019	Johnson	
10,294,449	B2	5/2019	Johnson	
10,335,154	B2	7/2019	Johnson et al.	
10,381,672	B2	8/2019	Lee et al.	
10,406,346	B2	9/2019	Scott-Carnell et al.	
10,413,574	B2	9/2019	Fong et al.	
10,420,856	B2	9/2019	Arinzeh et al.	
10,441,403	B1	10/2019	MacEwan et al.	
10,441,685	B2 *	10/2019	MacEwan	D01D 5/0076
10,588,734	B2 *	3/2020	MacEwan	D04H 3/073
10,617,512	B2 *	4/2020	MacEwan	D04H 3/073
10,632,228	B2 *	4/2020	MacEwan	A61L 27/18
10,682,444	B2 *	6/2020	MacEwan	B32B 5/26
10,738,152	B2	8/2020	Wang et al.	
10,888,409	B2	1/2021	MacEwan	
11,000,358	B2	5/2021	MacEwan	
2002/0081732	A1	6/2002	Bowlin et al.	
2002/0090725	A1	7/2002	Simpson et al.	
2002/0173213	A1	11/2002	Chu et al.	
2002/0192251	A1	12/2002	Collin	
2003/0004579	A1	1/2003	Rousseau et al.	
2003/0054035	A1	3/2003	Chu et al.	
2004/0013819	A1	1/2004	Hou et al.	
2004/0018226	A1	1/2004	Wnek et al.	
2004/0037813	A1 *	2/2004	Simpson	A61L 27/34 424/93.7
2004/0096532	A1	5/2004	Dubson et al.	
2004/0102614	A1	5/2004	Islam et al.	
2005/0104258	A1	5/2005	Lennhoff	

(56) **References Cited**

U.S. PATENT DOCUMENTS

2005/0167311 A1 8/2005 Tonsfeldt et al.
2005/0222591 A1 10/2005 Gingras et al.
2006/0094320 A1 5/2006 Chen et al.
2006/0153904 A1 7/2006 Smith et al.
2006/0193578 A1 8/2006 Ouderkirk et al.
2006/0014460 A1 9/2006 Isele et al.
2006/0204539 A1 9/2006 Atala et al.
2006/0240110 A1 10/2006 Kick et al.
2006/0246798 A1 11/2006 Reneker et al.
2006/0263417 A1 11/2006 Lelkes et al.
2006/0264140 A1 11/2006 Andrady et al.
2007/0073344 A1 3/2007 Jahns et al.
2007/0152378 A1 7/2007 Kim
2007/0155273 A1 7/2007 Chu et al.
2007/0225631 A1 9/2007 Bowlin et al.
2007/0269481 A1* 11/2007 Li A61L 27/18 424/423
2008/0065123 A1 3/2008 Yli-Urpo et al.
2008/0112998 A1 5/2008 Wang et al.
2008/0207798 A1 8/2008 Hellring et al.
2008/0208358 A1* 8/2008 Bellamkonda A61L 27/48 623/23.72
2008/0220042 A1* 9/2008 Hashi A61K 38/58 514/1.1
2008/0237934 A1 10/2008 Reneker et al.
2009/0028921 A1 1/2009 Arinzeh
2009/0074832 A1* 3/2009 Zussman A61L 27/3847 424/423
2009/0075354 A1 3/2009 Reneker et al.
2009/0155326 A1 6/2009 Mack et al.
2009/0162468 A1 6/2009 Barinov et al.
2009/0171467 A1 7/2009 Mann et al.
2009/0202616 A1 8/2009 Chong et al.
2009/0214614 A1 8/2009 Everland et al.
2009/0228021 A1 9/2009 Leung
2009/0317446 A1 12/2009 Tan et al.
2010/0003305 A1 1/2010 Pattanaik
2010/0047309 A1 2/2010 Lu et al.
2010/0061962 A1* 3/2010 Li A61L 27/3817 424/93.7
2010/0076377 A1 3/2010 Ehrenreich et al.
2010/0092687 A1 4/2010 Sumida et al.
2010/0093093 A1 4/2010 Leong et al.
2010/0119564 A1 5/2010 Kasuga et al.
2010/0120115 A1 5/2010 Ogle et al.
2010/0166854 A1 7/2010 Michniak Kohn et al.
2010/0174368 A1 7/2010 Lynch et al.
2010/0179659 A1 7/2010 Li et al.
2010/0185219 A1 7/2010 Gertzman et al.
2010/0190254 A1 7/2010 Chian et al.
2010/0233115 A1* 9/2010 Patel A61L 15/26 424/78.08
2010/0273258 A1* 10/2010 Lannutti C12M 35/08 435/366
2010/0291182 A1 11/2010 Palasis et al.
2010/0292791 A1* 11/2010 Lu A61F 2/0811 623/13.12
2010/0297208 A1* 11/2010 Fry A61P 17/02 424/422
2010/0330419 A1 12/2010 Cui et al.
2010/0331980 A1* 12/2010 Lee A61L 27/26 623/14.13
2011/0087277 A1 4/2011 Vola et al.
2011/0098826 A1* 4/2011 Mauck A61F 2/442 623/23.72
2011/0101571 A1 5/2011 Reneker
2011/0111012 A1 5/2011 Pepper et al.
2011/0150973 A1 6/2011 Bowlin et al.
2011/0152897 A1 6/2011 Bates
2011/0174158 A1 7/2011 Walls et al.
2011/0180951 A1* 7/2011 Teo D01D 5/0046 264/109
2011/0242310 A1 10/2011 Beebe, Jr. et al.
2011/0280919 A1 11/2011 Moloye-Olabisi et al.
2011/0287082 A1* 11/2011 Smith A61L 27/56 424/444
2012/0015331 A1* 1/2012 Wood A61L 27/3804 433/215
2012/0029654 A1 2/2012 Xu et al.
2012/0040581 A1 2/2012 Kim
2012/0123342 A1 5/2012 Andrews et al.
2012/0165957 A1 6/2012 Everland et al.
2012/0225039 A1 9/2012 Li et al.
2012/0265300 A1 10/2012 Mauck et al.
2012/0310260 A1 12/2012 Hamlin et al.
2013/0035704 A1 2/2013 Dudai
2013/0110138 A1* 5/2013 Hurtado A61L 27/54 606/152
2013/0115457 A1 5/2013 Haynie et al.
2013/0197663 A1* 8/2013 MacEwan A61L 15/42 623/23.72
2013/0251762 A1* 9/2013 Wei A61K 9/70 424/400
2013/0338791 A1 12/2013 McCullen et al.
2014/0030315 A1 1/2014 Johnson
2014/0128345 A1 5/2014 Woodrow et al.
2014/0272225 A1 9/2014 Johnson
2014/0303727 A1 10/2014 Atlas et al.
2014/0322512 A1 10/2014 Pham et al.
2015/0045818 A1 2/2015 Kim et al.
2015/0132423 A1 5/2015 Johnson
2015/0190285 A1* 7/2015 MacEwan A61F 13/00987 602/43
2015/0250927 A1* 9/2015 MacEwan A61L 15/64 606/151
2015/0297791 A1* 10/2015 Patel A61L 27/18 424/422
2015/0342719 A1 10/2015 Patel et al.
2016/0022873 A1 1/2016 Besner et al.
2016/0083868 A1 3/2016 Park
2016/0136330 A1 5/2016 Benkirane-Jessel et al.
2016/0302869 A1 10/2016 Chopra
2016/0317706 A1 11/2016 Johnson
2017/0119886 A1 5/2017 Johnson et al.
2017/0182206 A1 6/2017 Johnson et al.
2017/0182211 A1 6/2017 Raxworthy et al.
2017/0319323 A1 11/2017 MacEwan
2017/0319742 A1 11/2017 Johnson et al.
2017/0326270 A1* 11/2017 MacEwan A61L 27/18
2018/0116973 A1 5/2018 Jonnson
2018/0161185 A1 6/2018 Kresslein et al.
2018/0174367 A1* 6/2018 Marom A61B 34/10
2018/0221537 A1 8/2018 Johnson et al.
2018/0237952 A1 8/2018 Johnson et al.
2018/0245243 A1 8/2018 Krieger et al.
2018/0368917 A1 12/2018 Dekel et al.
2019/0015563 A1* 1/2019 MacEwan A61L 27/58
2019/0021837 A1* 1/2019 MacEwan A61L 15/42
2019/0054036 A1 2/2019 Johnson et al.
2019/0102880 A1* 4/2019 Parpara G06T 17/10
2019/0105128 A1* 4/2019 Velazquez G06T 17/20
2019/0134267 A1 5/2019 Francis et al.
2019/0134570 A1 5/2019 Pintauro et al.
2019/0153398 A1 5/2019 Johnson
2019/0175786 A1 6/2019 Cohen et al.
2019/0249127 A1 8/2019 Johnson
2019/0269829 A1 9/2019 Johnson
2019/0271098 A1 9/2019 Johnson et al.
2019/0330419 A1 10/2019 Song et al.
2019/0365520 A1* 12/2019 MacEwan D04H 1/728
2019/0365958 A1* 12/2019 MacEwan A61L 15/26
2019/0374227 A1 12/2019 Johnson et al.
2020/0000570 A1* 1/2020 MacEwan D01D 5/0092
2020/0060800 A1 2/2020 MacEwan et al.
2020/0197153 A1* 6/2020 MacEwan A61L 15/22
2020/0229679 A1 7/2020 Zhao et al.
2020/0242767 A1 7/2020 Zhao et al.
2020/0390932 A1 12/2020 MacEwan
2021/0001014 A1 1/2021 MacEwan

(56) **References Cited**

U.S. PATENT DOCUMENTS

2021/0030525	A1	2/2021	MacEwan et al.
2021/0052362	A1	2/2021	MacEwan et al.

FOREIGN PATENT DOCUMENTS

CA	2094908	C	2/2000
CA	2802482	A1	12/2011
CA	2386810	C	9/2013
DE	102014107826	A1	12/2014
EP	0515522	B1	10/1993
EP	0571415		7/1995
EP	0757127		2/1997
EP	2045375		3/2011
EP	2582868	B1	3/2018
EP	2897561		4/2020
EP	3508641		8/2020
EP	3741896		11/2020
GB	1286858		8/1972
GB	2181207		4/1987
GB	2195251		4/1988
JP	H03161563	A	7/1991
JP	3487722	B2	1/2004
JP	2005534828	A	11/2005
JP	2006283241	A	10/2006
JP	2006328562	A	12/2006
JP	4979264	B2	11/2007
JP	2007303021	A	11/2007
JP	2008223186	A	9/2008
JP	2009061109	A	3/2009
JP	2011509786	A	3/2011
JP	4769871		9/2011
JP	2012528464	A	11/2012
JP	2013518996	A	5/2013
JP	2013534979	A	9/2013
JP	6295258	A	3/2018
JP	6328672		5/2018
KR	100439871	B1	7/2004
KR	20060118937	A	11/2006
KR	1020070047873	A	5/2007
KR	101703095	A	10/2013
SG	186379	A1	1/2013
SG	11201502207	W	4/2015
WO	WO 1991/001695		2/1991
WO	2001027365	A1	4/2001
WO	WO 02/00149		1/2002
WO	2004016839	A1	2/2004
WO	2006096791	A2	9/2006
WO	2006123858	A1	11/2006
WO	2007086910	A2	8/2007
WO	2008069760	A1	6/2008
WO	WO 2009/093023		7/2009
WO	2010041944	A1	4/2010
WO	WO 2010/042651		4/2010
WO	2010112564	A2	10/2010
WO	2010138619	A2	12/2010
WO	2011095141	A1	8/2011
WO	2011159889	A2	12/2011
WO	WO 2012/080706		6/2012
WO	WO 2013/025819		2/2013
WO	2013050428	A1	4/2013
WO	2013078051	A1	5/2013
WO	2013106822	A1	7/2013
WO	2014031721	A1	2/2014
WO	2014046669	A1	3/2014
WO	2014145864	A1	9/2014
WO	2014152906	A2	9/2014
WO	2015048224	A1	4/2015
WO	2015116917	A1	8/2015
WO	2015153011	A1	10/2015
WO	2016176559	A1	11/2016
WO	2017024263	A1	2/2017
WO	2017035500	A1	3/2017
WO	2017044982	A1	3/2017
WO	2017079328	A1	5/2017
WO	WO 2017/196325		11/2017
WO	2018112203	A1	6/2018
WO	2018144858	A1	8/2018

OTHER PUBLICATIONS

Davis, et al., "A biodegradable composite artificial tendon," Journal of Materials Science: Materials in Medicine, 3:359-364 (1992).

Doshi, et al., "Electrospinning Process and Applications of Electrospun Fibers," J. Electrostatics 35(2-3): 151-160 (1995).

Dzenis et al., "Hierarchical nano-/micromaterials based on electrospun polymer fibers: Predictive models for thermomechanical behavior," Journal of Computer-Aided Materials Design, 3(1-3): 403-408 (1996).

Dzenis et al., "Polymer Hybrid Nano/Micro Composites," Proceedings of the American Society for Composites Ninth Technical Conference, pp. 657-665, 1994.

Li et al., "Direct Fabrication of Composite and Ceramic Hollow Nanofibers by Electrospinning," Nano Lett. 2004, 4(5): 933-938.

Li, et al., "Electrospinning Nanofibers as Uniaxially Aligned Arrays and Layer-by-Layer Stacked Films," Adv. Mater. 2004, 16(4): 361-366.

Li et al., "Electrospinning of Nanofibers: Reinventing the Wheel?" Adv. Mater. Nov. 2004, 16(14): 1151-1170.

Li, et al., "Electrospinning of Polymeric and Ceramic Nanofibers as 20 Uniaxially Aligned Arrays" Nano Lett. 2003, 3, 1167-1171.

Tormala, et al., "Ultra-High-Strength absorbable self-reinforced polyglycolide (SR-PGA) composite rods for internal fixation of bone fractures: In vitro and in vivo study" Journal of Biomedical Materials Research, 25(1): 1-22 (1991).

Xie, et al., Conductive core-sheath nanofibers and their potential applications in neural tissue engineering. Adv Funct Mater 2009; 19(14): 2312-2318.

Xie, et al., Neurites outgrowth on nanofiber scaffolds with different orders, structures, and surface properties. ACS Nano 2009; 3(5): 1151-1159.

Xie et al., Putting electrospun nanofibers to work for biomedical research. Macromol Rapid Commun 2008; 29(22): 1775-1792.

ASTM Standard F2450-10, "Guide for Assessing Microstructure of Polymeric Scaffolds for Use in Tissue-Engineered Medical Products" ASTM International, West Conshohocken, PA, 10 pages (Mar. 27, 2013).

Barbol et al., "Biocompatibility evaluation of dura mater substitutes in an animal model," Neurological Research, 23(8): 813-820 (2001).

Beachley et al., "Polymer nanofibrous structures: Fabrication, biofunctionalization, and cell interactions," Progress in Polymer Science, 35(7): 868-892 (2010).

Beheshtkhoo et al., "Fabrication and Properties of Collagen and Polyurethane Polymeric Nanofibers Using Electrospinning Techniques," Journal of Environmental Treatment Techniques, 7(4): 802-807 (2019).

Zong et al., "Structure and process relationship of electrospun bioabsothable nanofiber membranes," Polymer, 43(16): 4403-4412 (2002).

Bhattarai et al. "Electrospun chitosa-based nanofibers and their cellular compatibility", Biomaterials, 26(31): 6176-6184 (2005).

Chen et al., "Preparation and characterization of coaxial electrospun thermoplastic polyurethane/collagen compound nanofibers for tissue engineering applications," Colloids and Surfaces B: Biointerfaces, 79(2): 315-325 (2010).

Chen et al., "Preparation and Study of TPU/Collagen Complex Nanofiber via Electrospinning," AATCC Review, 10(2): 59-63 (2010).

Choi et al., "Formation of interfiber bonding in electrospun poly(etherimide) nanofiber web," Journal of Materials Science, 39(4): 1511-1513 (2004).

Cole et al., "A comparative long-term assessment of four soft tissue substitutes," Aesthetic Surgery Journal, 31(6): 674-681 (2011).

Cui et al., "Controlled assembly of poly(vinyl pyrrolidone) fibers through an electric-field-assisted electrospinning method," Applied Physics A, 103(1): 167-172 (2011).

(56) **References Cited**

OTHER PUBLICATIONS

Figallo et al., "Micropatterned biopolymer 3D scaffold for static and dynamic culture of human fibroblasts," Biotechnology Progress, 23(1): 210-216 (2007).
Foy et al., "Allergic reaction to a bovine dural substitute following spinal cord untethering," Case Report, Journal of Neurosurgery: Pediatrics, 1(2): 167-169 (2008).
Gibson et al., "Electrospun Fiber Mats: Transport Properties," AIChE Journal, 45(1): 190-195 (1999).
Liu et al., "Tensile Mechanics of Electrospun Multiwalled Nanotube/Poly(methyl methacrylate) Nanofibers," Advanced Materials, 19(9): 1228-1233 (2007).
Martinez-Lage et al. "Accidental transmission of Creutzfeldt-Jakob disease by dural cadaveric grafts" Journal of Neurology, Neurosurgery & Psychiatry, 57(9): 1091-1094 (1994).
McMillan et al. "Small diameter poro poly (ϵ-caprolactone) films enhance adhesion and growth of human cultured epidermal keratinocyte and dermal fibroblast cells," Tissue Engineering, 13(4): 789-798 (2007).
Mi, Fwu-Log et al. "Asymmetric chitosan membranes prepared by dry/wet phase separation: a new type of wound dressing for controlled antibacterial release," Journal of Membrane Science, 212(1-2): 237-254 (2003).
Park et al., "Apparat for Preparing Electrospun Nanofibers: Designing and Electrospinning process for Nanofiber Fabrication," Polymer International, 56(11): 1361-1366 (2007).
Pham et al. "Electrospun poly (ϵ-caprolactone) microfiber and multilayer nanofiber/microfiber scaffold: characterization of scaffolds and measurement of cellular infiltration," Biomacromolecules, 7(10): 2796-2805 (2006).
Shin et al., "Electrospun PLGA nanofiber scaffolds for articular cartilage reconstruction: mechanical stability, degradation and cellular responses under mechanical stimulation in vitro," Journal of Biomaterials Science, Polymer Edition, 17(1-2): 103-119 (2006).
Tan et al., "Tensile test of a single nanofiber ing an atomic force microscope tip," Applied Physics Letters, 86(7): 073115-1:3 (2004).
Teo et al., "Electrospun scaffold tailored for tissue-specific extracellular matrix," Biotechnology Journal, 1(9): 918-929 (2006).
Thomas et al. "Electrospun bioactive nanocomposite scaffolds of polycaprolactone and nanohydroxyapatite for bone tissue engineering," Journal of Nanoscience Nanotechnology, 6(2): 487-93 (2006).
Vaz et al. "Design of scaffold for blood vessel tissue engineering ing a multiple-layering electrospinning technique," Acta Biomaterialia, 1(5): 572-582 (2005).
"Wikipedia, "Polyhydroxyethylmethacrylate,"" downloaded on Dec. 18, 2019 downloaded from https://en.wikipedia.org/wiki/Polyhydroxyethylmethacrylate (3 pages).
Wise, Histologic proof that acellular dermal matrices (ADM)-Enduragen DermaMalrix and DuraMatrix-are not repopulaled or nonviable and that AlloDerm may be repopulated but degraded synchronoly, Aesthetic Surgery Journal, 32(3): 355-358 (2012).
Xie et al. "Radially Aligned Electrospun Nanofibers as Dural Substitutes for Wound Closure and Tissue Regeneration Applicalions," ACS Nano, 4(9): 5027-5036 (2010).
Zerris et al. "Repair of the dura mater with processed collagen devices," Journal of Biomedical Materials Research Part B: Applied Biomaterials, 83B(2): 580-588 (2007).
Australian Examination Report No. 1 issued for Application No. 2012390291 dated May 31, 2017 (4 pages).
Australian Examination Report issued for Application No. 2011268321, dated Apr. 17, 2015 (4 pages).
Australian Examination Report No. 1 issued for Application No. 2017232208 dated Jan. 8, 2018 (4 pages).
Brazilian Technical Report for related Application No. 112012032169-2, dated Feb. 20, 2019 (4 pages).
Canadian Examiner's Report issued for Application No. 2,885,682, dated Jun. 4, 2018 (5 pages).
European Extended Search Report issued for Application No. 11796426.2, dated Mar. 27, 2014 (6 pages).
European Examination Report issued for Application No. 12884789.4 dated Feb. 13, 2018 (5 pages).
European Partial Search Report issued for Application No. 12884789.4, dated Feb. 29, 2016 (8 pages).
European Extended Search Report issued for Application No. 12884789.4, dated Jun. 16, 2016 (12 pages).
European Search Report issued for Application No. 16901840.5, dated Dec. 2, 2019 (15 pages).
European Search Report and Written Opinion for Application No. 18164340, dated May 17, 2019, (5 pages).
GCC Examination Report in Application No. 2017-33397, dated Apr. 15, 2019 (4 pages).
Indian Examination Report issued for Application No. 11141/DELNP/2012, dated Jun. 21, 2018 (7 pages).
Indian First Examination Report for Application No. 2299/DELNP/2015, dated Oct. 24, 2019, (6 pages) English translation.
Japanese Office action issued for Application No. 2013-515511, dated Oct. 28, 2014 (1 page).
Japanese Office translation issued for Application No. 2015-533026, dated Jun. 27, 2017 (4 pages).
Japanese Office Action Summary issued for Application No. 2015-533026, dated Oct. 18, 2016 (5 pages).
PCT International Search Report and Written Opinion issued for Application No. PCT/2012/056548, dated Apr. 26, 2013 (12 pages).
PCT International Search Report in International Application No. PCT/16/32001, dated Aug. 11, 2016 (1 page).
PCT International Search Report and Written Opinion issued for Application No. PCT/2011/040691, dated Feb. 24, 2012 (14 pages).
PCT International Preliminary Report on Patentability for PCT/2011/040691, dated Dec. 19, 2012 (9 pages).
Singapore Search Report issued for Application No. 201209288.8, dated May 15, 2014 (17 pages).
Singapore Search and Examination Report for 2012092888, dated Jan. 30, 2015 (8 pages).
Singapore Examination Report issued for Application No. 11201502207W, dated Jun. 13, 2017 (8 pages).
U.S. Appl. No. 62/154,286, filed Apr. 29, 2015, Johnson.
Australian Examination Report No. 1 issued for Application No. 2016406314 dated Oct. 29, 2020 (4 pages).
Australian Examination Report No. 2 issued for Application No. 2016406314 dated Mar. 12, 2021.
Bognitzki et al., "Preparation of Fibers with Nanoscaled Morphologies: Electrospinning of Polmer Blends" Polymer Enginering and Science, Jun. 2001, vol. 41, No. 6, pp. 982-989.
Bognitzki et al., "Nanostructured Fibers via Electrospinning**", Advanced Mater. 2001, 13. No. 1, Jan. 5, pp. 70-72.
Brazil Technical Report for related Application No. BR112015006301-2, dated Oct. 15, 2020, 5 pages.
Camposeo et al., "Lobal Mechanical Properties of Electrospun Fibers Correlate to Their Internal Nanostructure" Nano Lett. 2013, pp. 13, 5056-5062.
Cheng et al, "Engineering the Microstructure of Electrospun Fibrous Scaffolds by Microtopography," Biomacromolecules 14:1349-1360 (2013), doi: 10.1021/bm302000n).
China Examiners Report issued for Application No. 201680087078.9, dated Jan. 20, 2021 with translation in 28 pages.
Declaration of Gary E. Wnek, PH.D. in support of Petition for Inter Partes Review of U.S. Pat. No. 10,632,228, date: Jan. 2021.
Deitzel et al. "The effect of processing variables on the morphology of electrospun nanofibers and textiles" Polymer 42 (2001) pp. 261-272.
Dubsky et al., "Nanofibers prepared by needleless electrospinning technology as scaffolds for wound healing," J Mater Sci: Mater Med, DOI 10.1007/s 10856-012-4577-7, Feb. 2012.
European Search Report and Written Opinion for EP application No. 20175280.5, dated Sep. 11, 2020 in 8 pages.
Fang et al. "Electrospinning: an advanced nanofiber production technology." In: H. Niu, H. Zhou and H. Wang (Eds.), Energy Harvesting Properties of Electrospun Nanofibers (1st ed. [online], pp. 1-1-1-44).IOP Publishing Ltd. (2020). https://iopscience.iop.

(56) **References Cited**

OTHER PUBLICATIONS

org/book/978-0/7503-2005-4/chapter/bk978-0/7503-2005-4ch1 (Accessed Apr. 6, 2021), doi 10.1088/978-0-7503-2005-4ch1.

Huang, et al., "Generation of Synthetic Elastin-Mimetic Small Diameter Fibers and Fiber Networks", Macromolecules 2000, 33, 2989-2997.

Jaeger, et al. "Electrospinning of Ultra-Thin Polymer Fibers", Macromol. Symp. 127, 141-150 (1998).

Khil et al., "Novel Fabricated Matrix Via Electrospinning for Tissue Engineering," Wiley Periodicals, Inc. 2004.

Kumar et al., "Nanofibers: Effective Generation by Electrospinning and Their Applications," Journal of Nanoscience and Nanotechnology, vol. 12, 1-25, 2012.

Liu et al, "Electrospun Fibrous Mats on Lithographically Micropatterned Collectors to Control Cellular Behaviors," Langmuir 28:17134-17142 (2012), doi: 10.1021/la303490x).

Madhugiri, S. et al., "Electrospun MEH-PPV/SBA-15 Composite Nanofibers Using a Dual Syringe Method," J. Am. Chem. Soc., 125: 14531-14538 (2003).

Norris et al. "Electrostatic fabrication of ultrafine conducting fibers: polyaniline/polyethylene oxide blends" Synthetic Metals 114 (2000) pp. 109-114.

Petition for Inter Partes Review of U.S. Pat. No. 10,632,228 dated May 28, 2021 in 91 pages.

Pham et al., "Electrospinning of Polymeric Nanofibers for Tissue Engineering Applications: A Review", Tissue Engineering, 12(5): 1197-1211 (2006).

Rieger et al. "Designing electrospun nanofiber mats to promote wound healing—a review," J. Mater. Chem. B, 2013, 1, 4531.

Subbiah et al. "Electrospinning of Nanofibers," J. of Applied Polymer Science, 96: 557-569 (2005).

Valizadeh et al., "Electrospinning and electrospun nanofibres," IET Nanobiotechnol., 2014, vol. 8, Iss. 2, pp. 83-92.

Yarin, et al., "Taylor Cone and Jetting from Liquid Driplets in Electrospinning of Nanofibers," (2001). College of Polymer Science and Polymer Engineering. 85.

Yogeshwar et al., "Electrospinning of Type I Collagen and PCL Nanofibers Using Acetic Acid," Wiley Online Library, Feb. 1, 2012.

* cited by examiner

FIG. 1

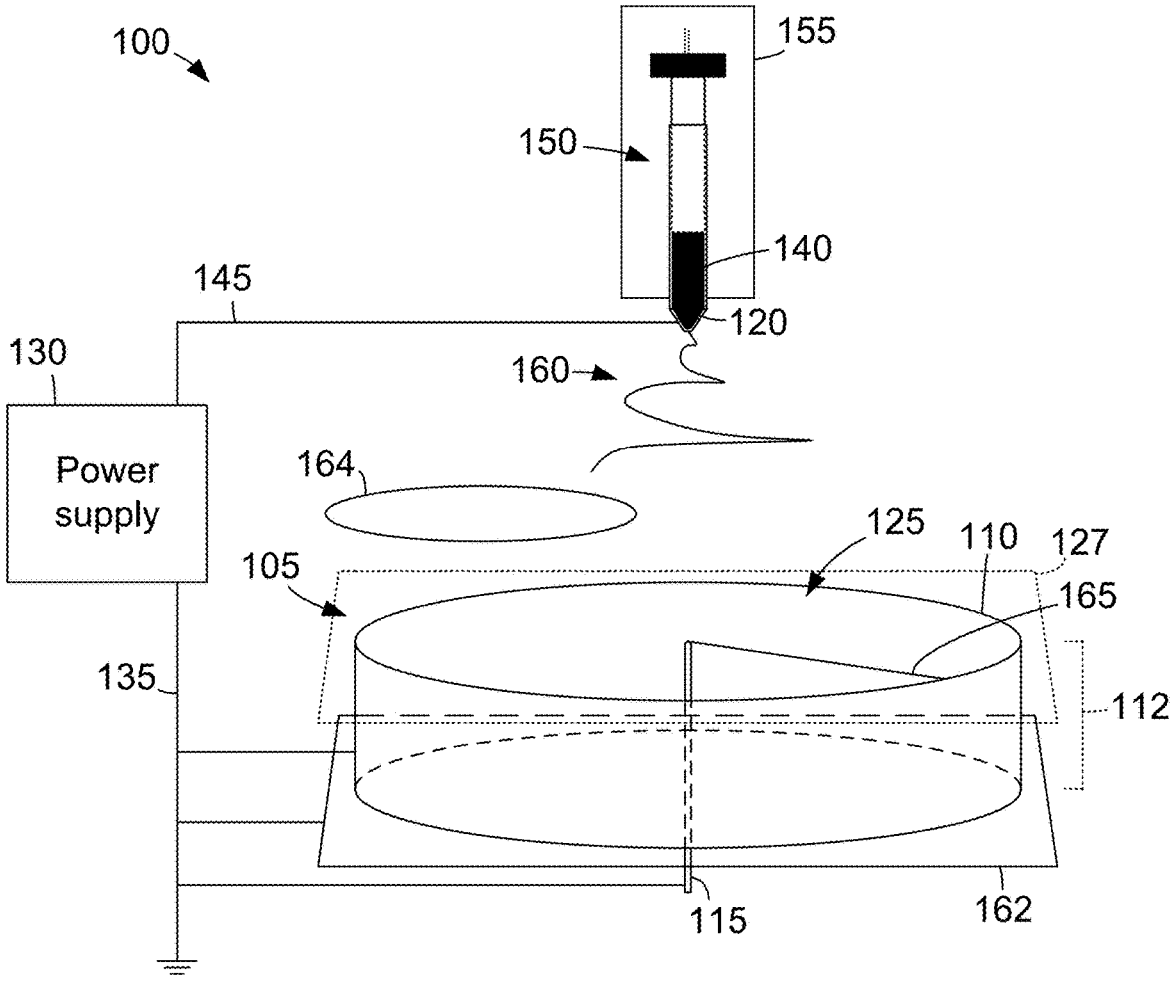
100
155
150
140
145
120
130
160
Power supply
164
125
110
127
105
165
135
112
115
162

FIG. 2

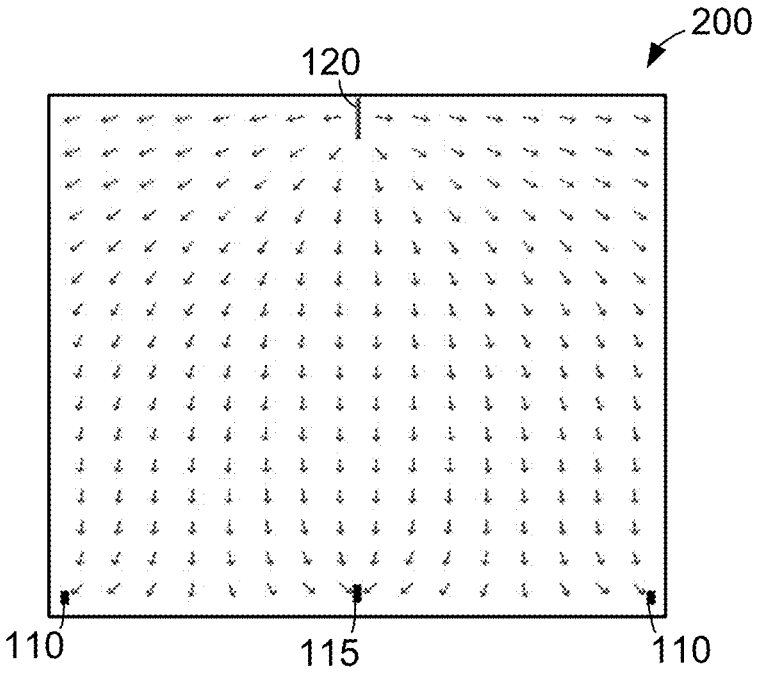

FIG. 3

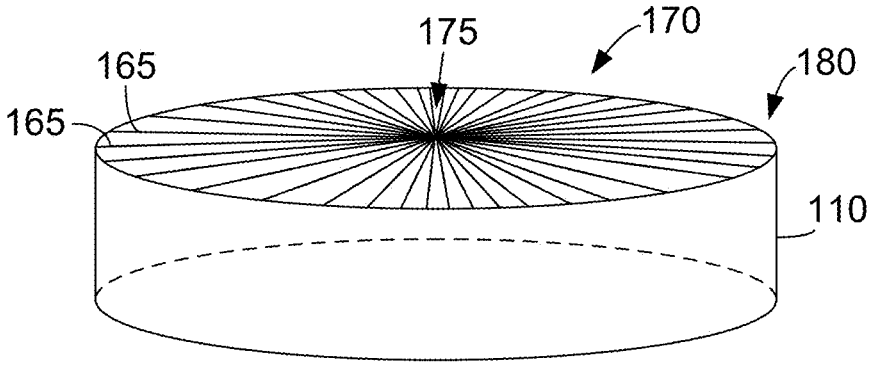

FIG. 4

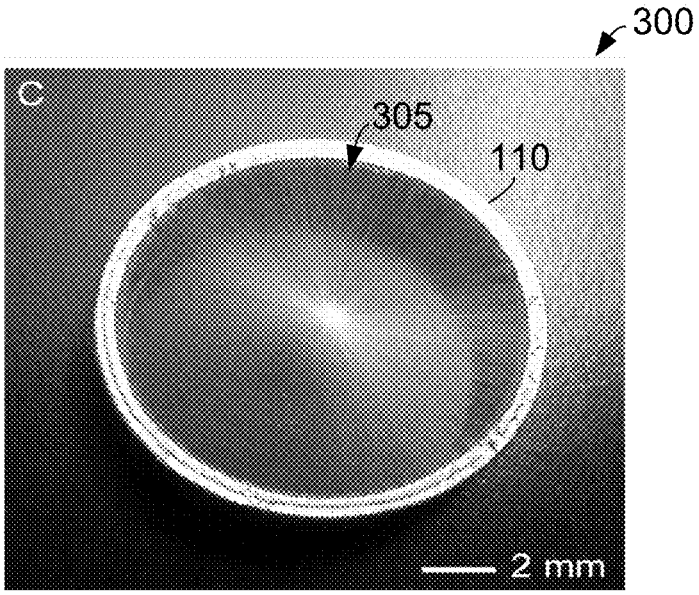

FIG. 5

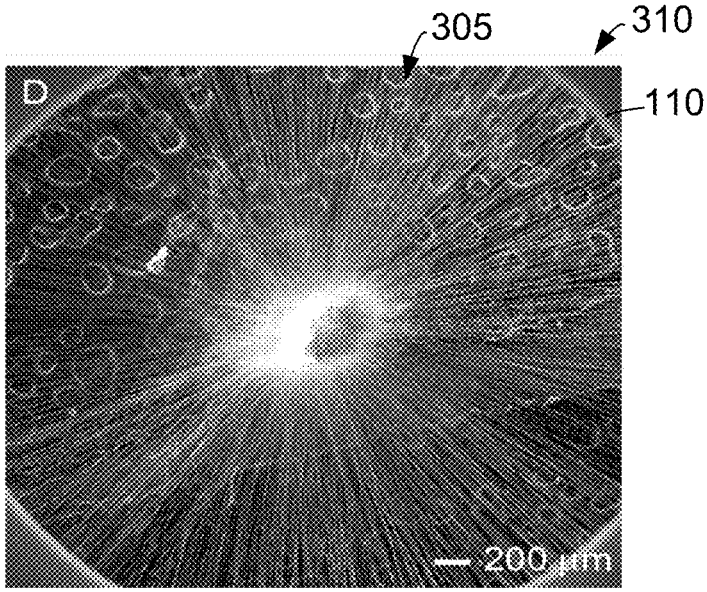

FIG. 6

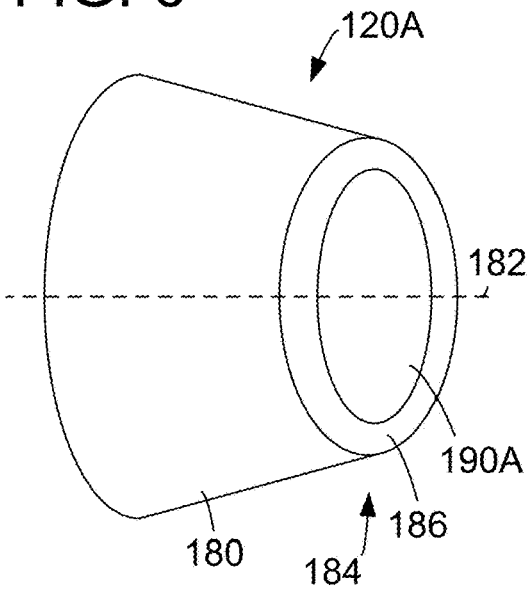

FIG. 7

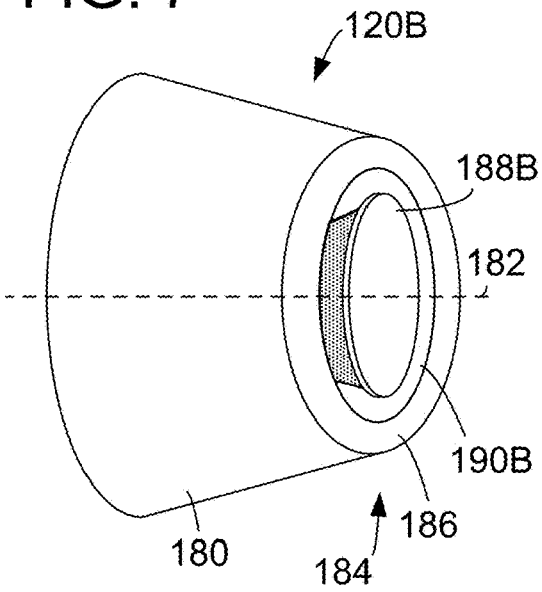

FIG. 8

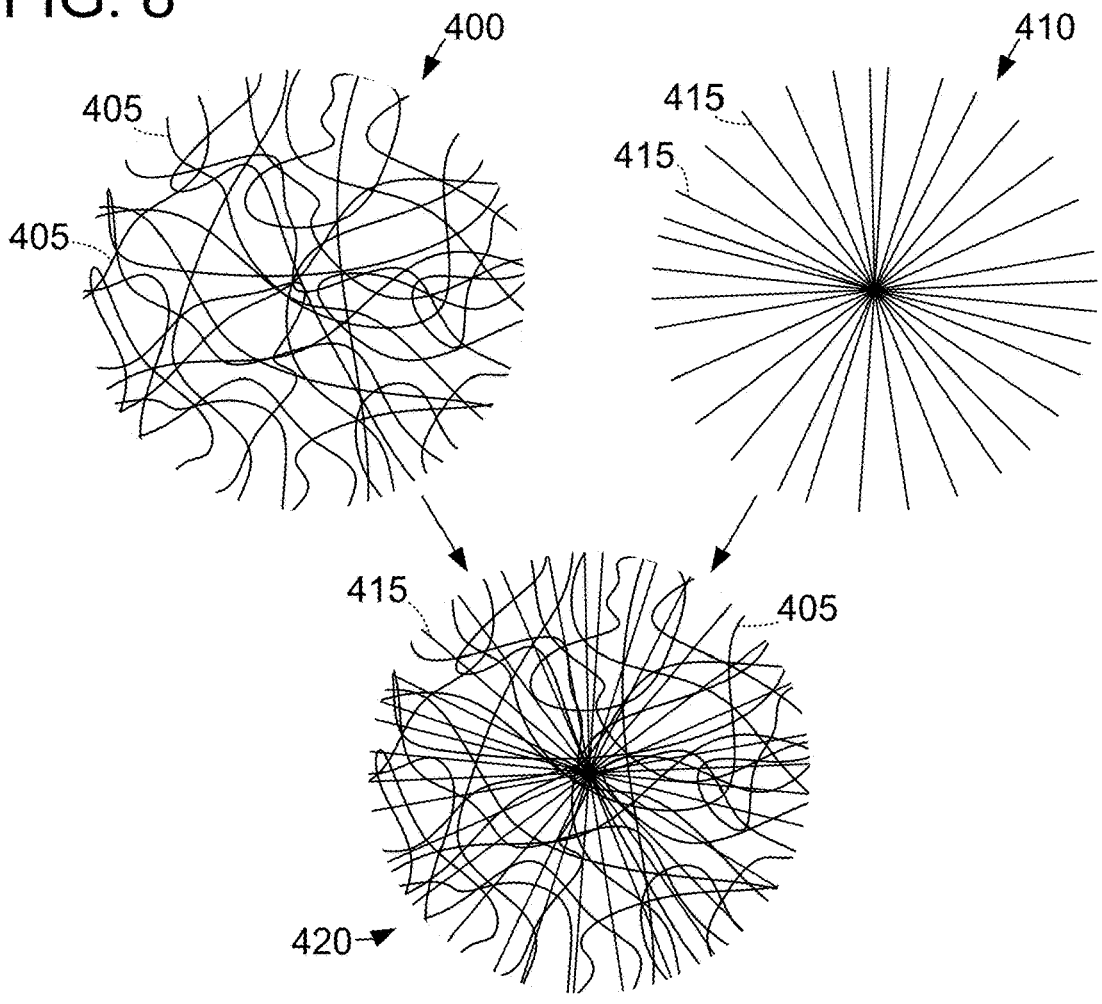

FIG. 9

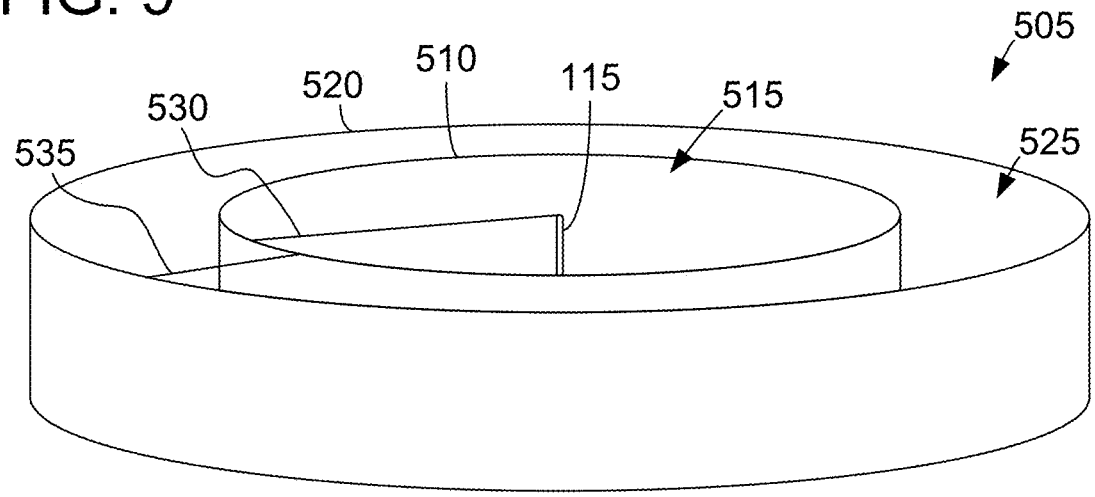
505
510
520
115
530
515
535
525

FIG. 10

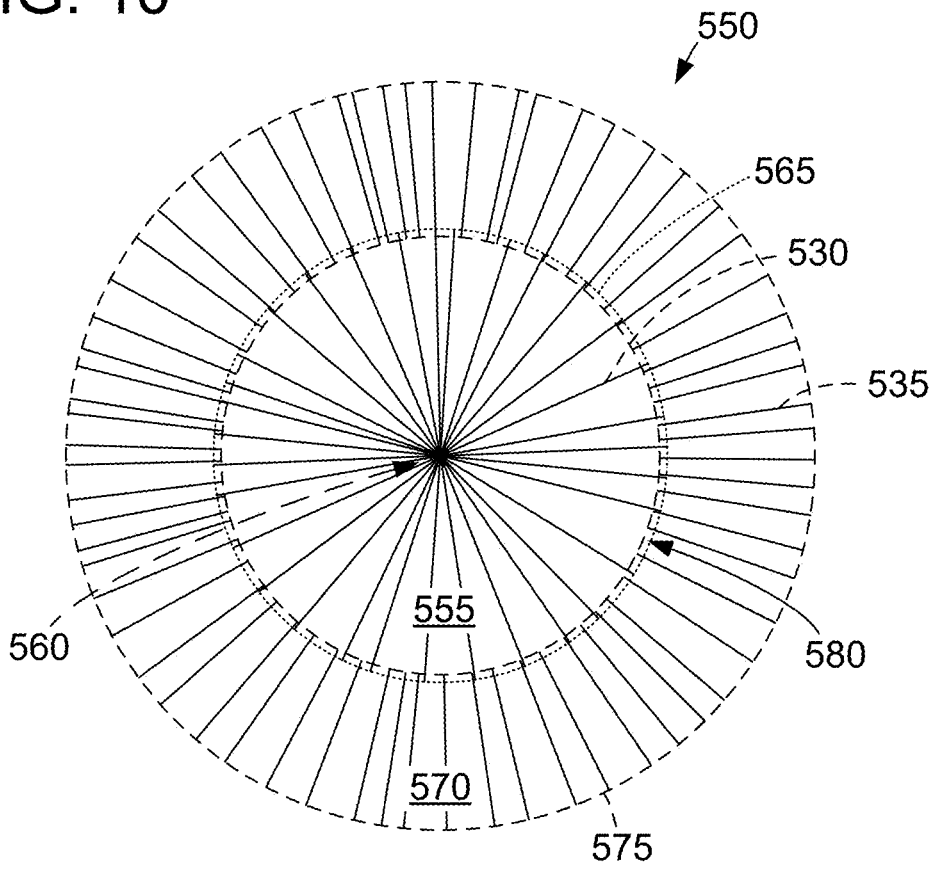
550
565
530
535
555
560
580
570
575

FIG. 11

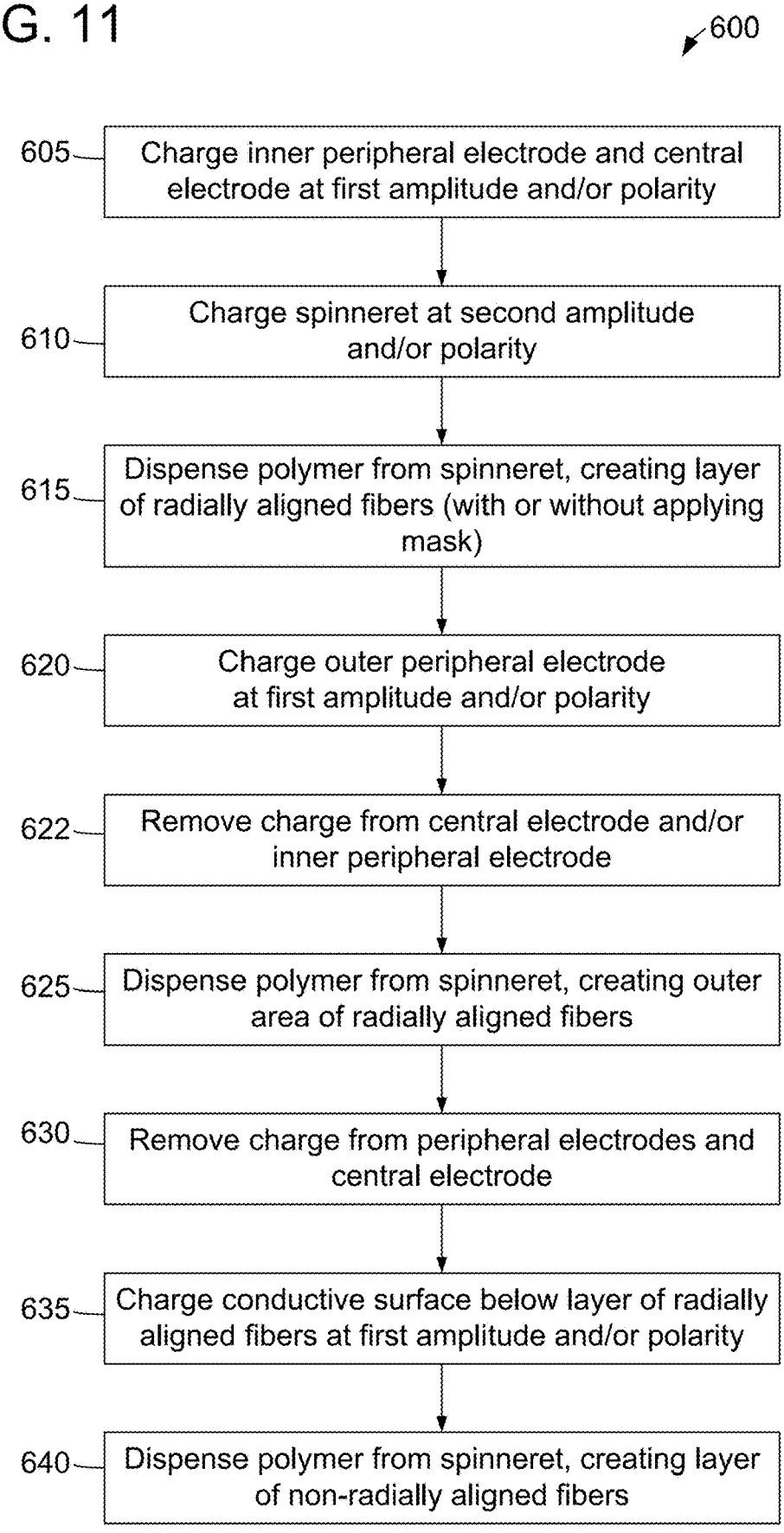
600
605
Charge inner peripheral electrode and central electrode at first amplitude and/or polarity
610
Charge spinneret at second amplitude and/or polarity
615
Dispense polymer from spinneret, creating layer of radially aligned fibers (with or without applying mask)
620
Charge outer peripheral electrode at first amplitude and/or polarity
622
Remove charge from central electrode and/or inner peripheral electrode
625
Dispense polymer from spinneret, creating outer area of radially aligned fibers
630
Remove charge from peripheral electrodes and central electrode
635
Charge conductive surface below layer of radially aligned fibers at first amplitude and/or polarity
640
Dispense polymer from spinneret, creating layer of non-radially aligned fibers

FIG. 12

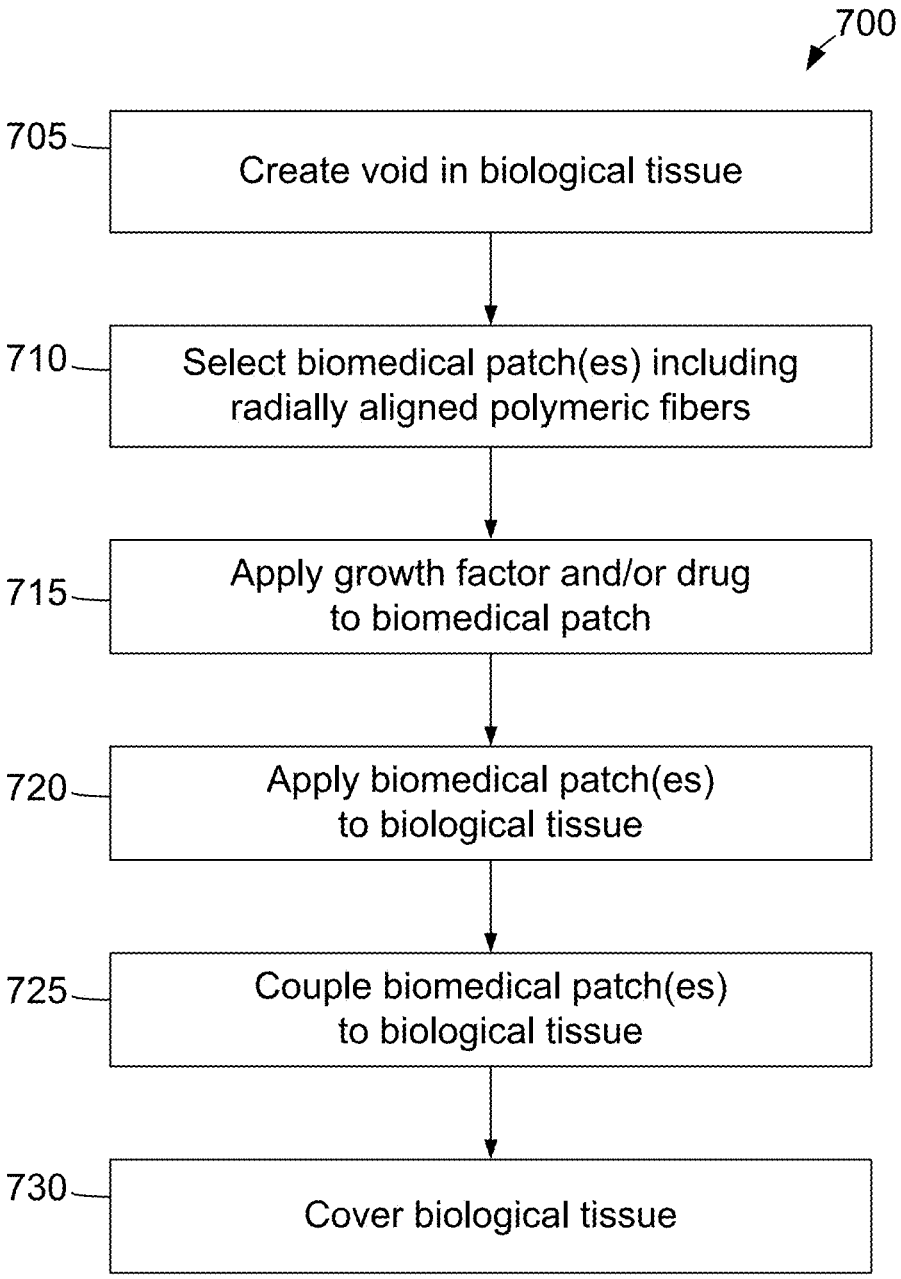
700
705
Create void in biological tissue
710
Select biomedical patch(es) including radially aligned polymeric fibers
715
Apply growth factor and/or drug to biomedical patch
720
Apply biomedical patch(es) to biological tissue
725
Couple biomedical patch(es) to biological tissue
730
Cover biological tissue

FIG. 13

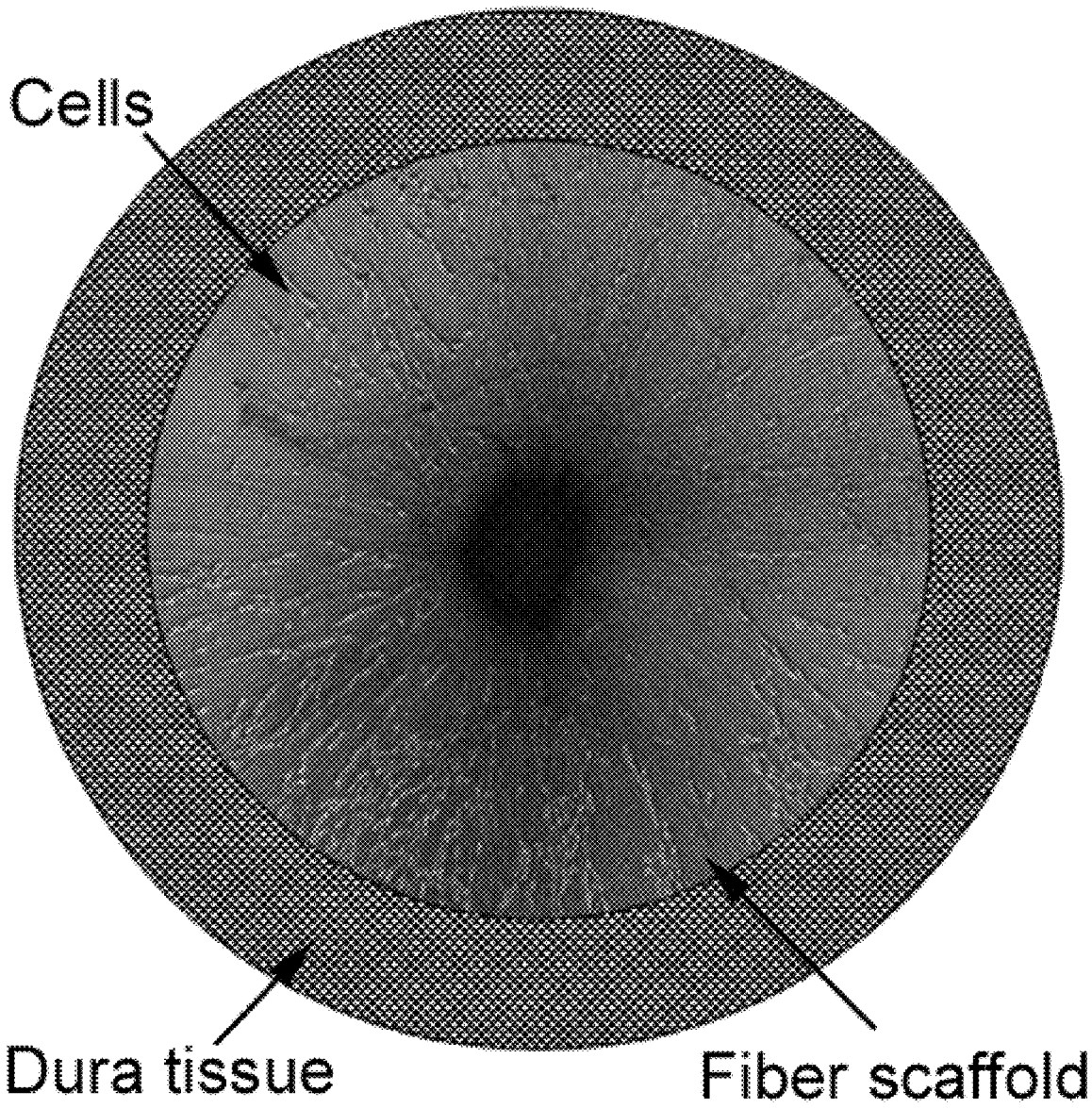

FIG. 14A

FIG. 14B

Radially aligned

Random

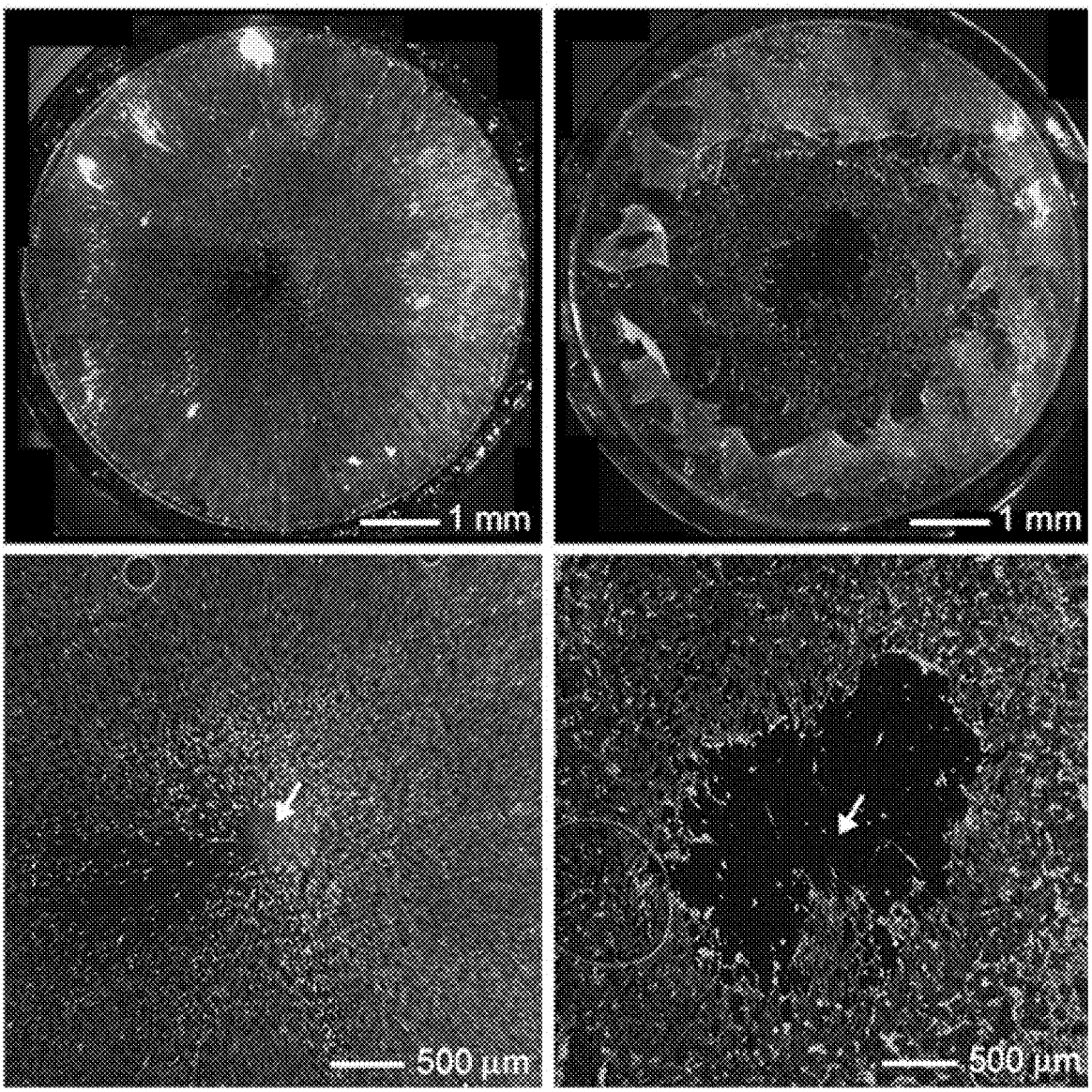

FIG. 14C

FIG. 14D

FIG. 15A

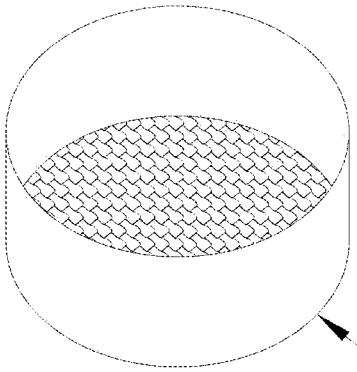

FIG. 15B

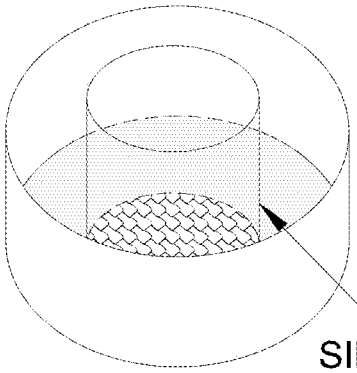

FIG. 15C

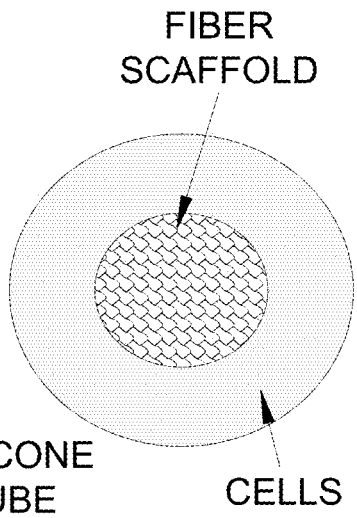

FIG. 16A

FIG. 16B

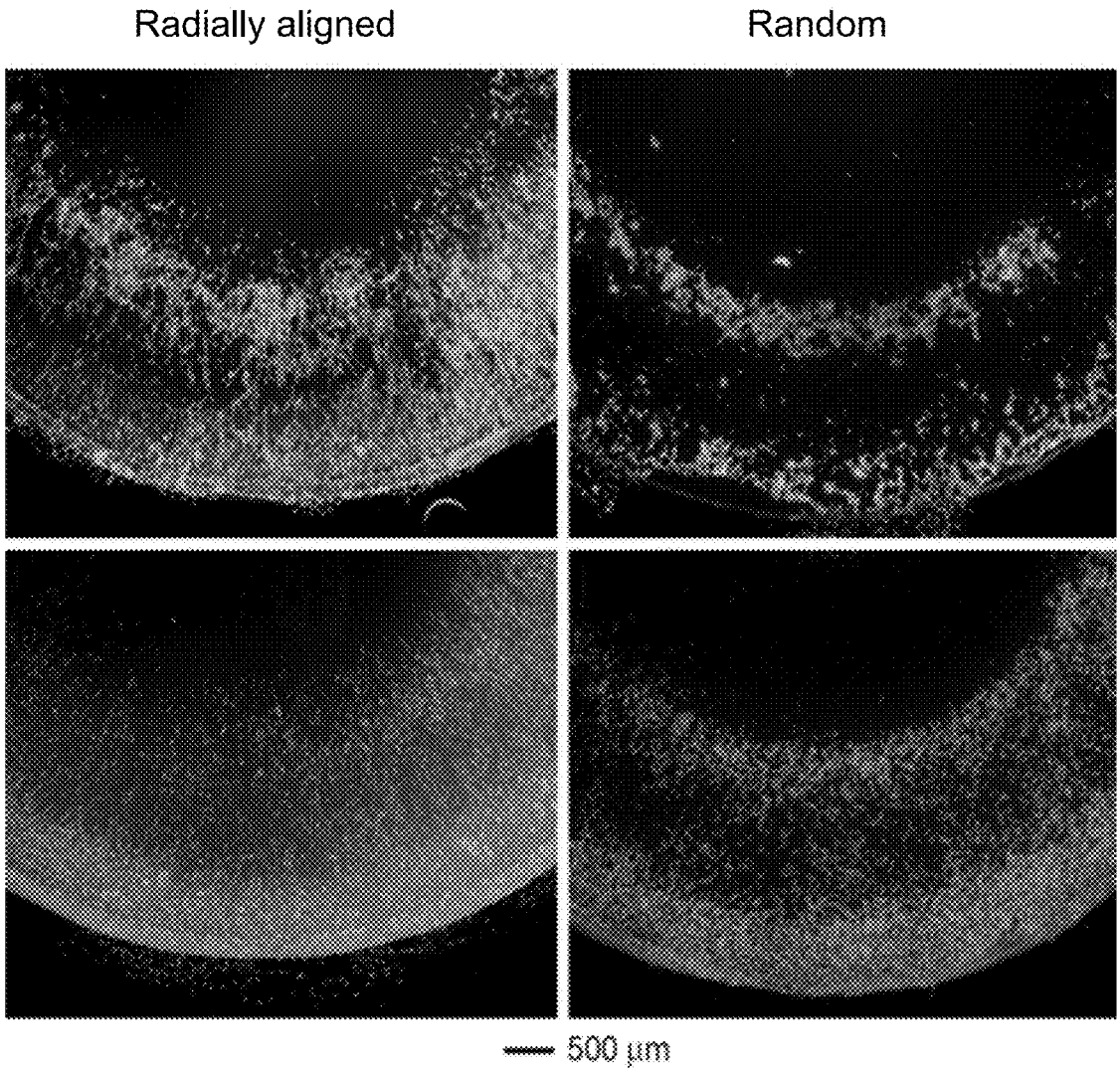

FIG. 16C

FIG. 16D

FIG. 17A

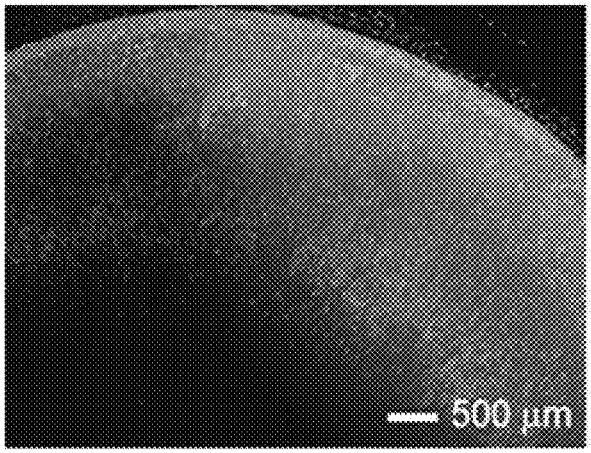

FIG. 17B

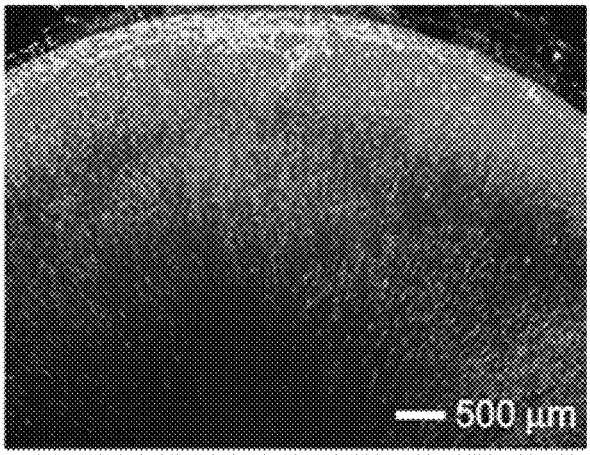

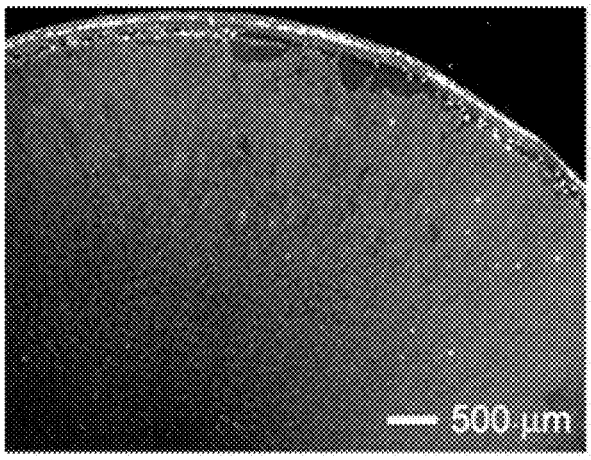

FIG. 17C

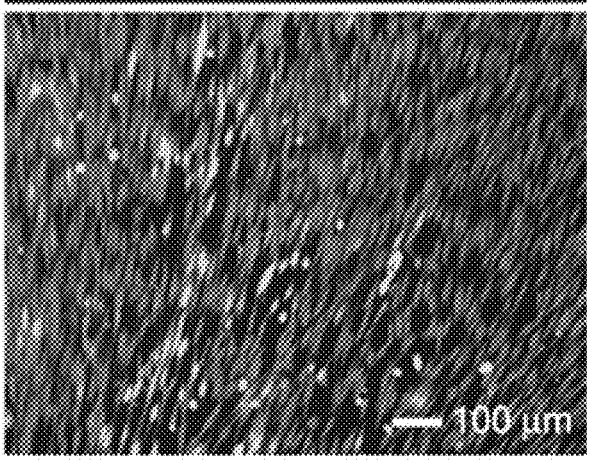

FIG. 17D

FIG. 18

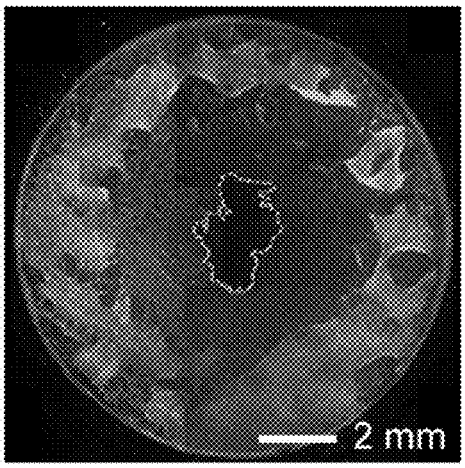

FIG. 19

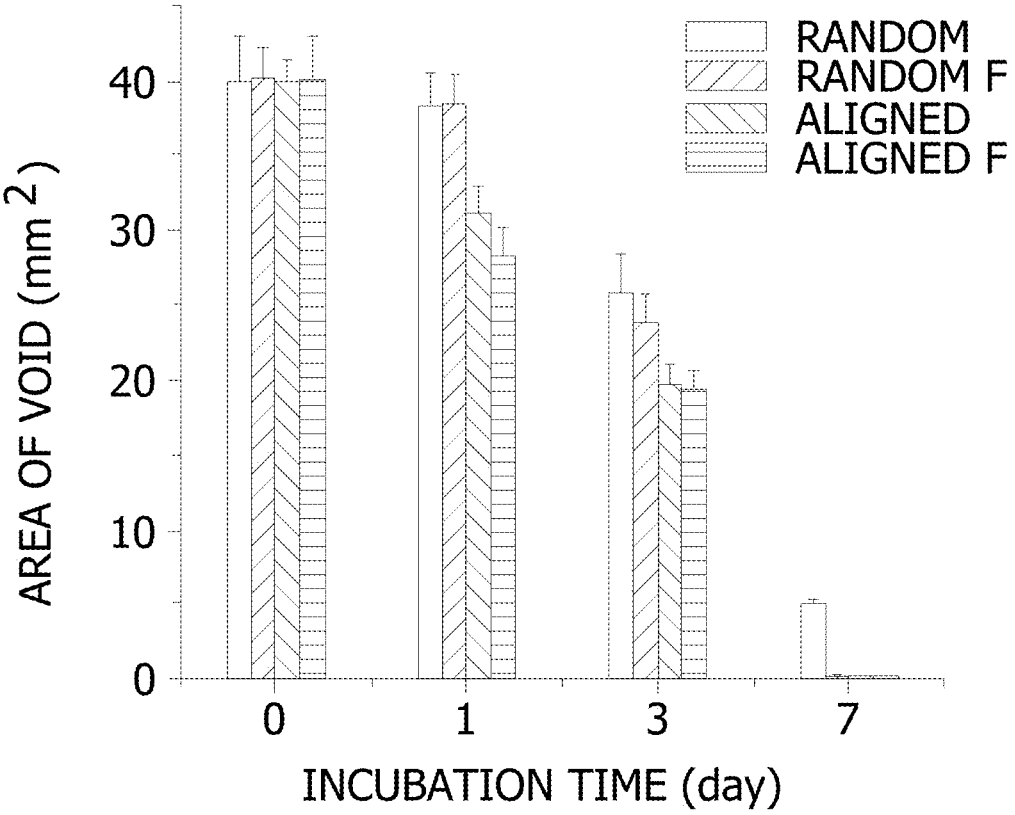
RANDOM
RANDOM F
ALIGNED
ALIGNED F
AREA OF VOID (mm 2)
40
30
20
10
0
0
1
3
7
INCUBATION TIME (day)

FIG. 20A

FIG. 20B

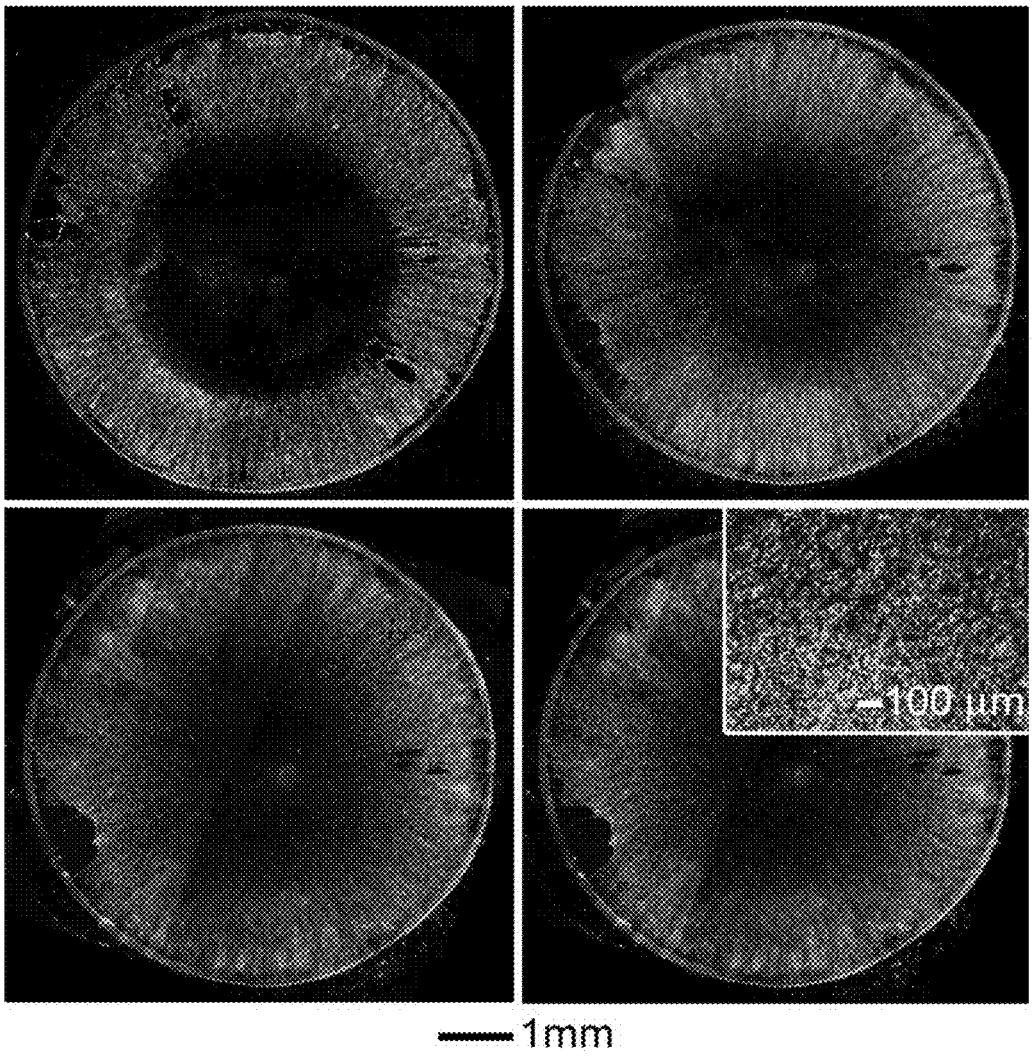

FIG. 20C

FIG. 20D

FIG. 21A

FIG. 21B

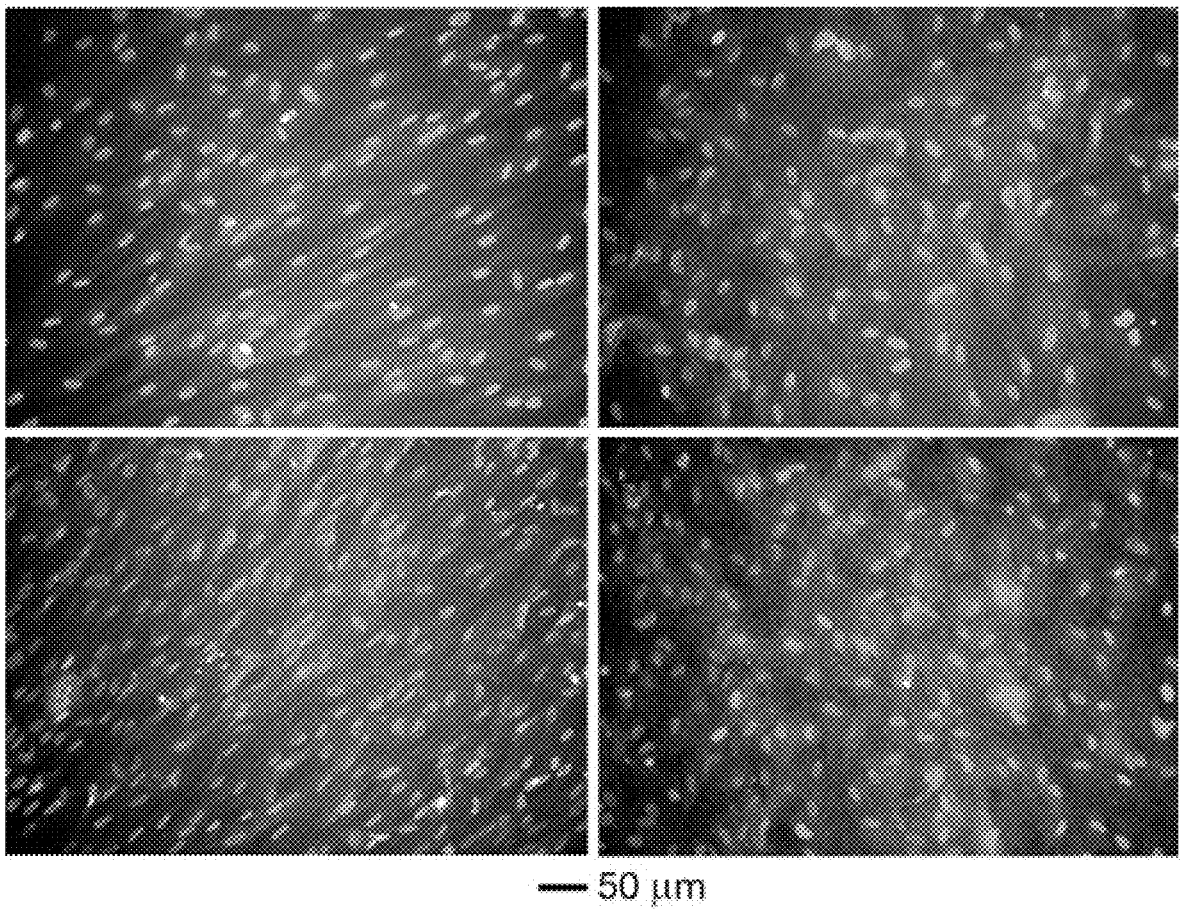

FIG. 21C

FIG. 21D

FIG. 22

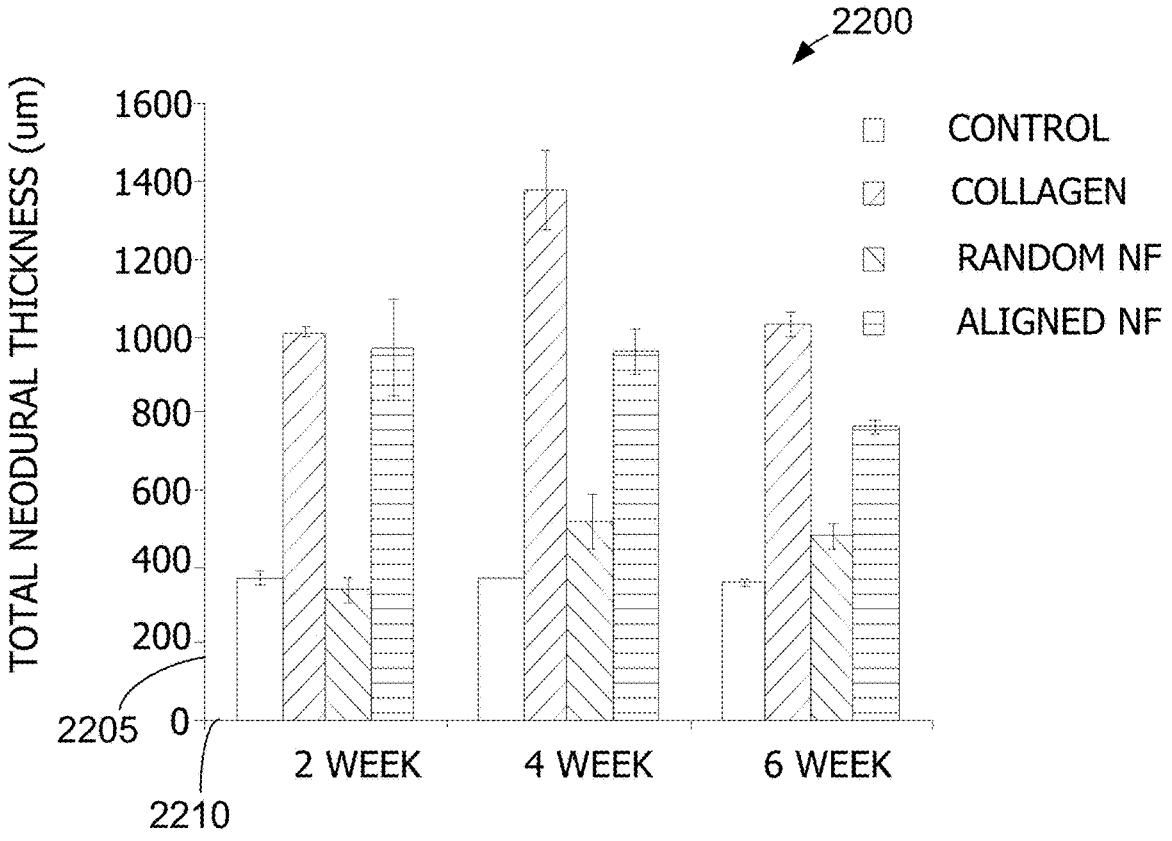
2200
TOTAL NEODURAL THICKNESS (um)
1600
1400
1200
1000
800
600
400
200
0
2205
2210
2 WEEK
4 WEEK
6 WEEK
CONTROL
COLLAGEN
RANDOM NF
ALIGNED NF

FIG. 23

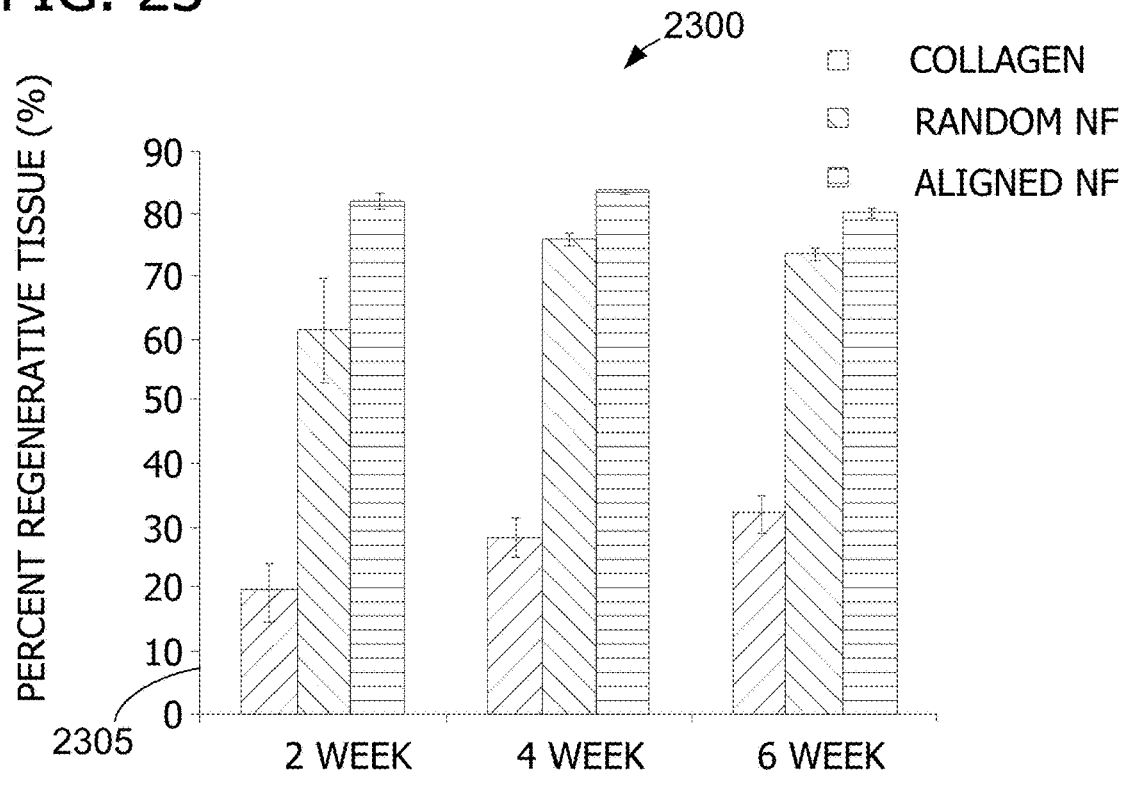
2300
PERCENT REGENERATIVE TISSUE (%)
90
80
70
60
50
40
30
20
10
0
2305
2 WEEK
4 WEEK
6 WEEK
COLLAGEN
RANDOM NF
ALIGNED NF

FIG. 24

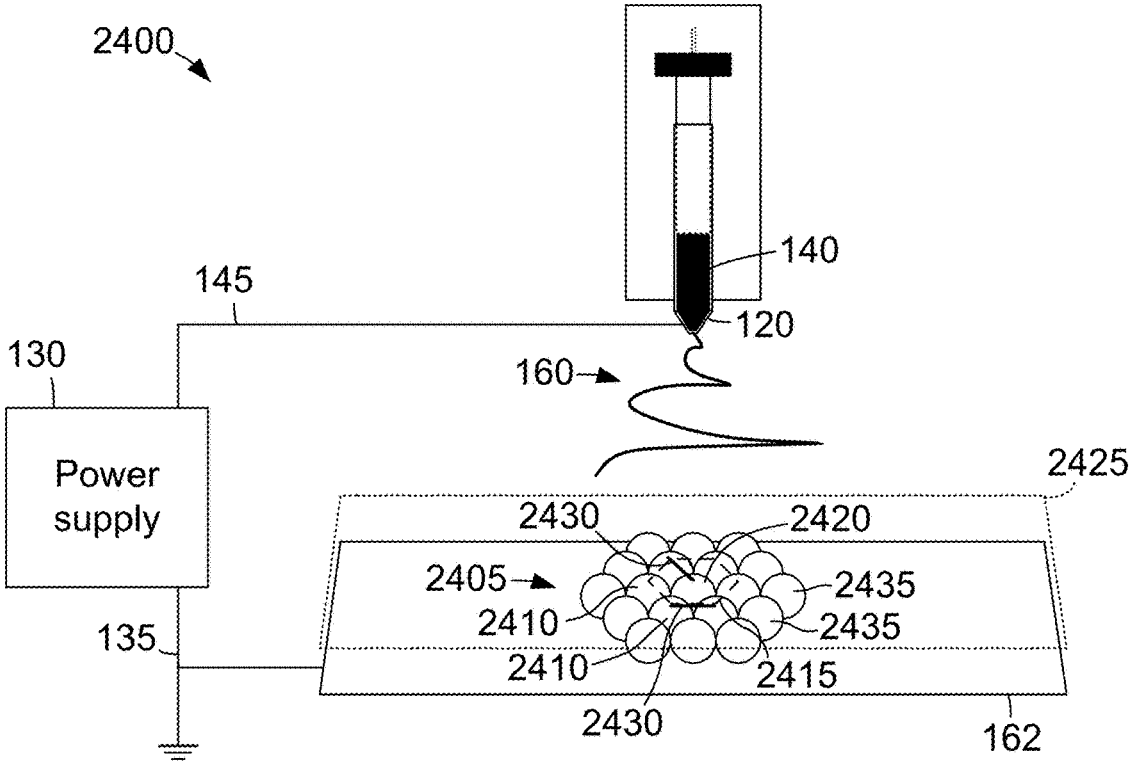
2400
140
145
120
130
160
Power supply
2425
2430
2420
2405
2435
2410
2435
135
2410
2415
2430
162

FIG. 25

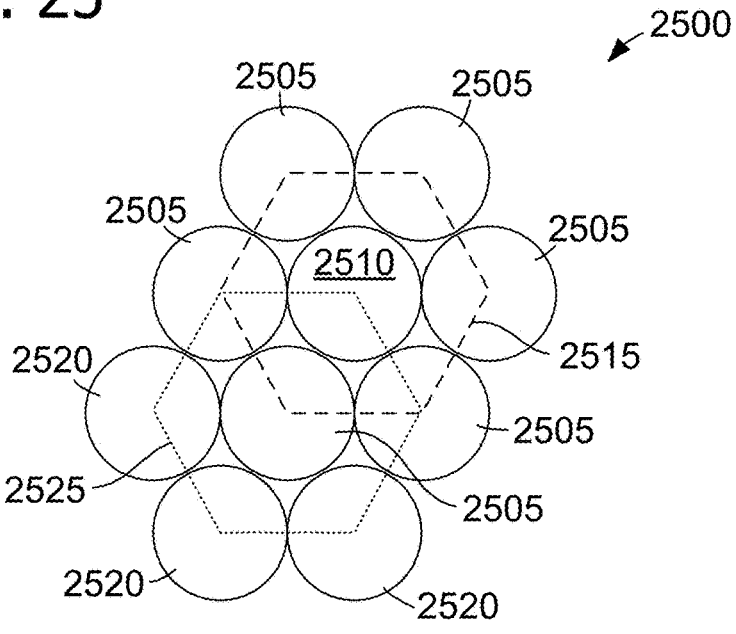
2500
2505
2505
2505
2505
2510
2515
2520
2505
2525
2505
2520
2520

FIG. 26

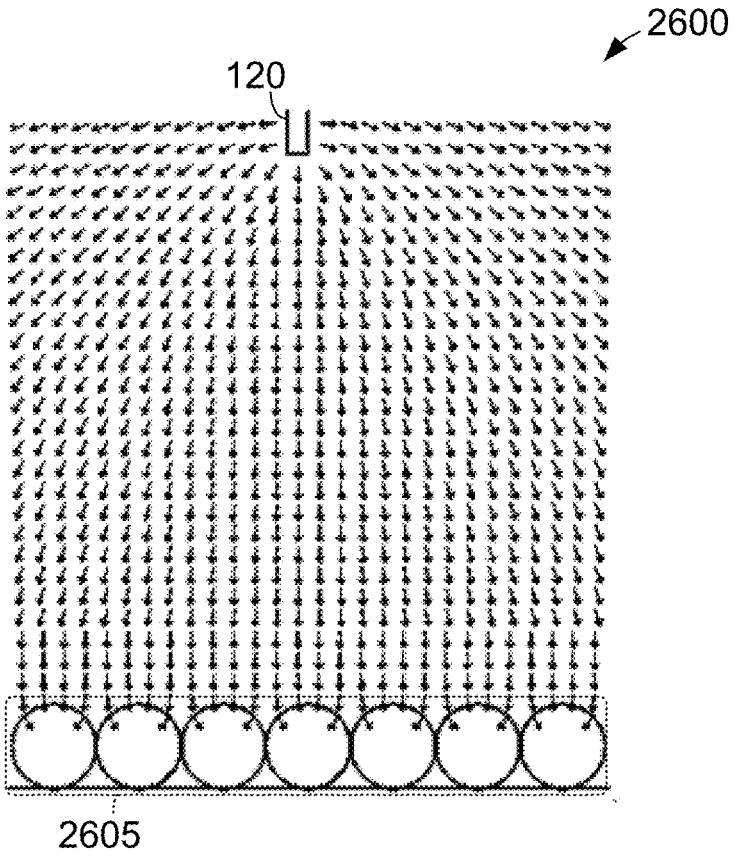

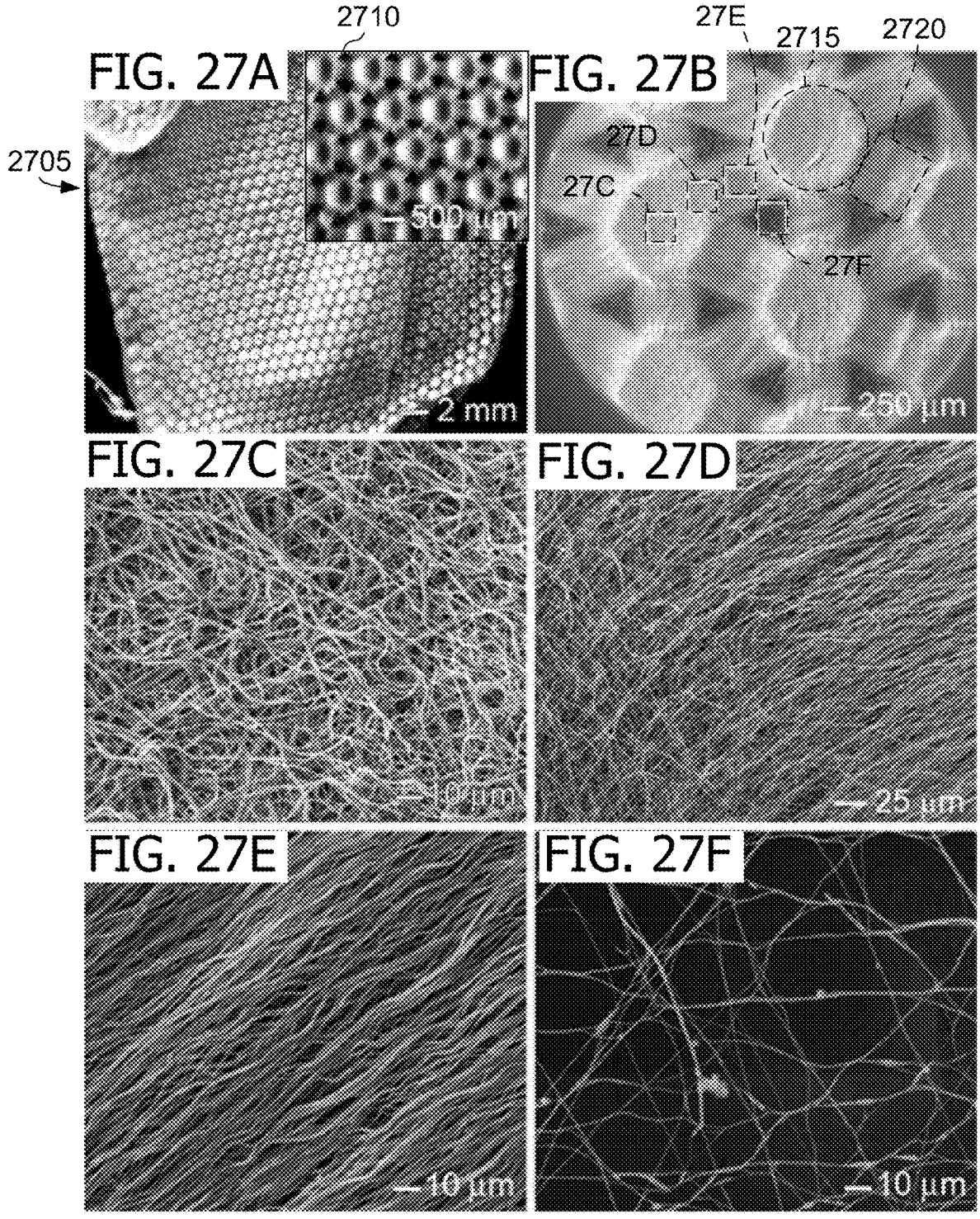

FIG. 27A

FIG. 27B

FIG. 27C

FIG. 27D

FIG. 27E

FIG. 27F

FIG. 28A

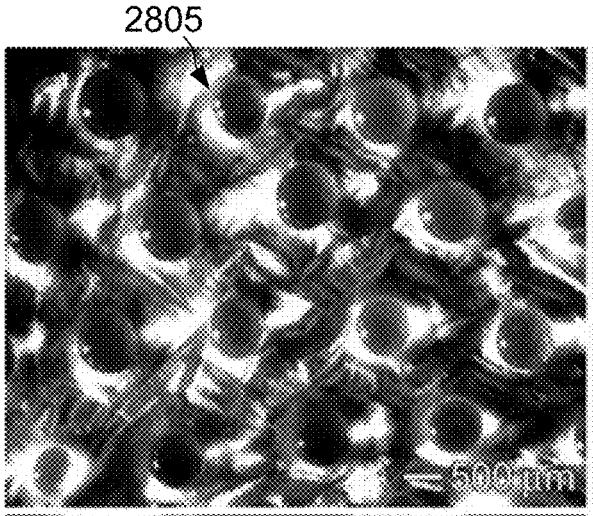

FIG. 28B

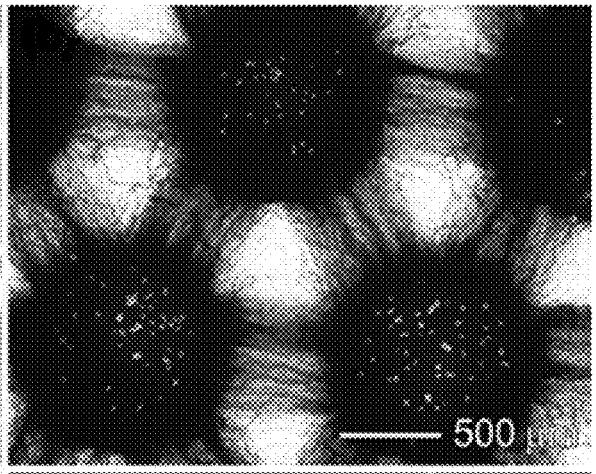

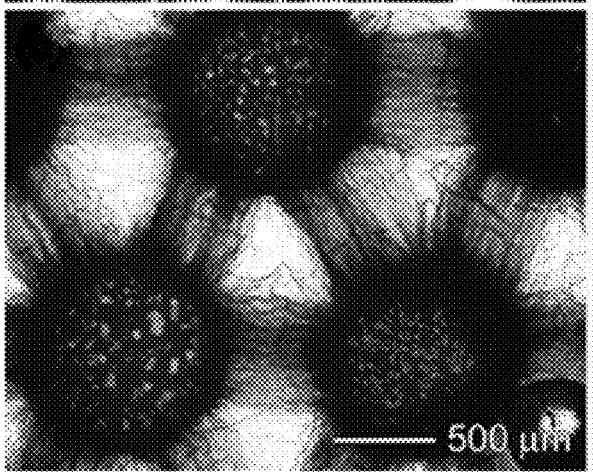

FIG. 28C

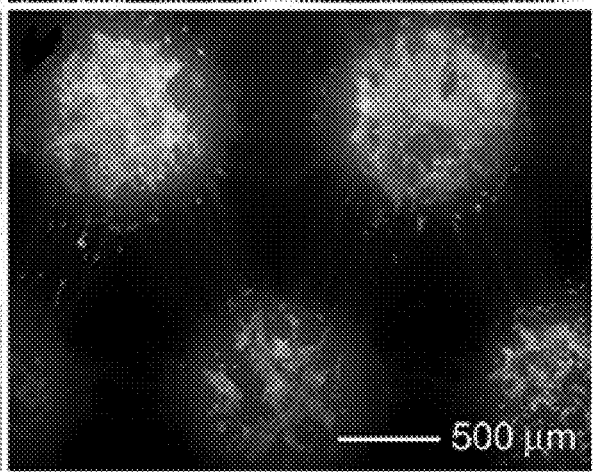

FIG. 28D

FIG. 29A

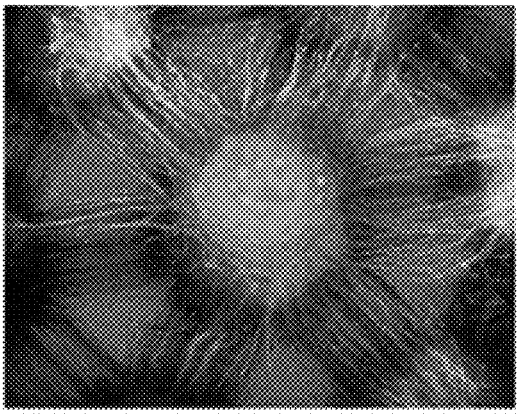

FIG. 29B

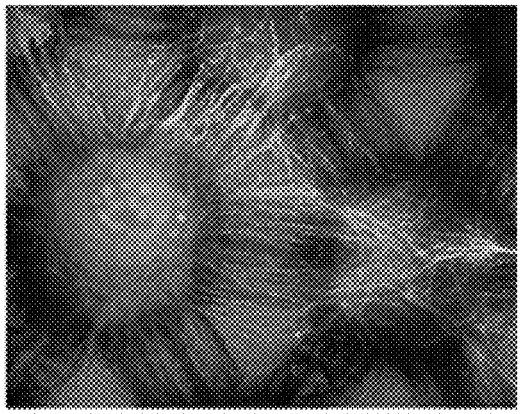

FIG. 30A

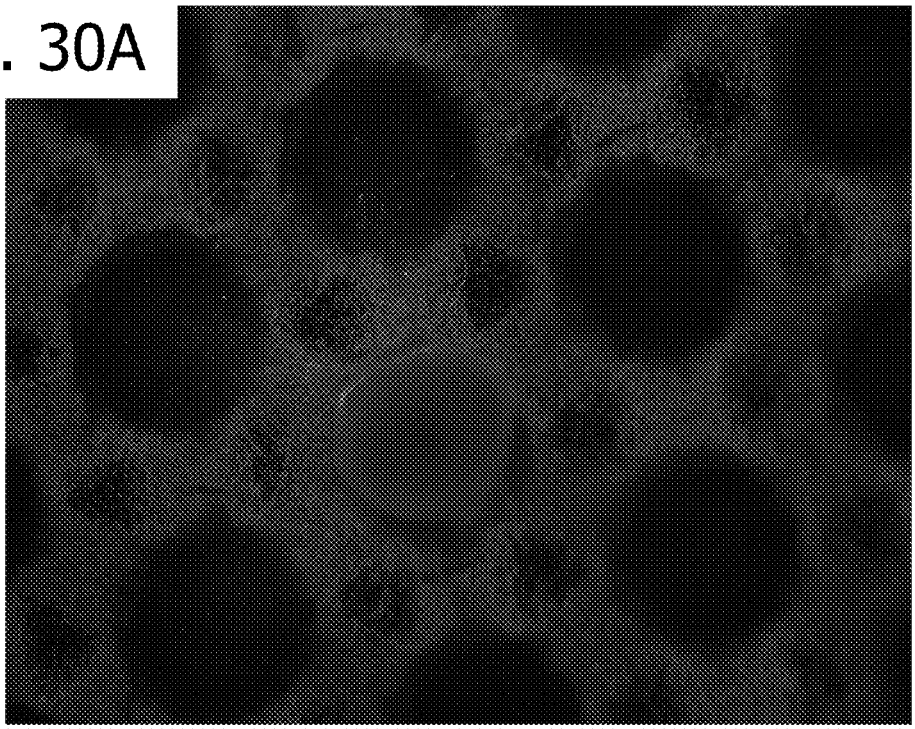

FIG. 30B

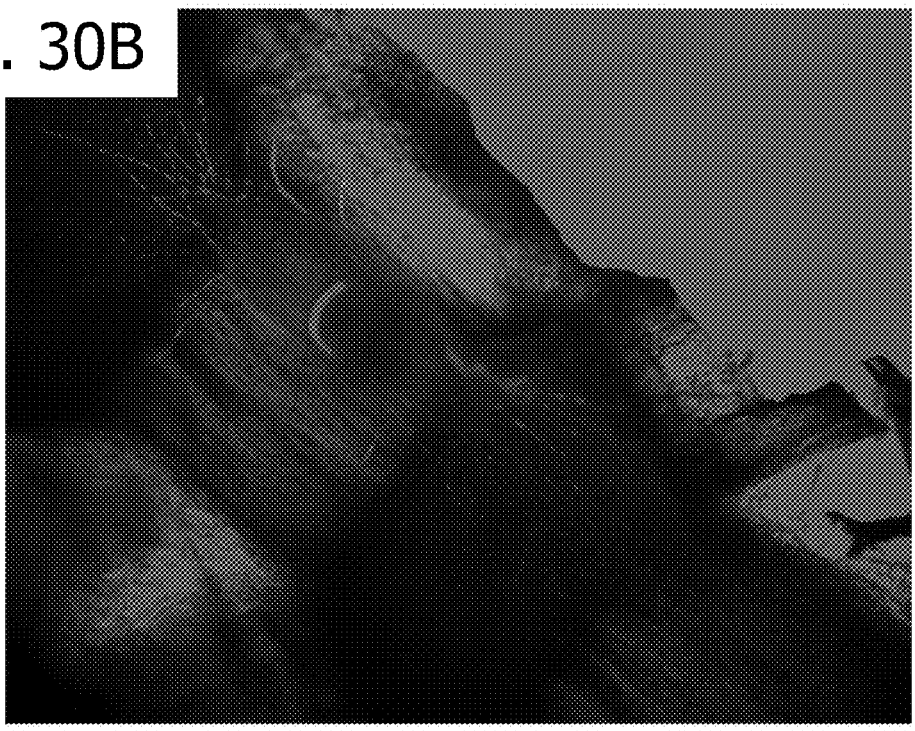

FIG. 31A

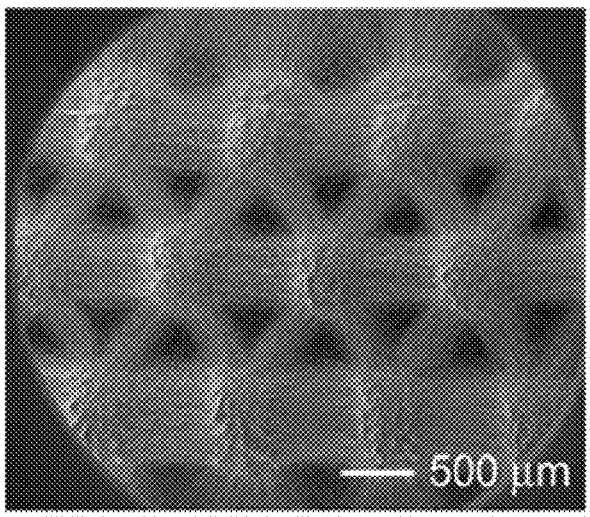

FIG. 31B

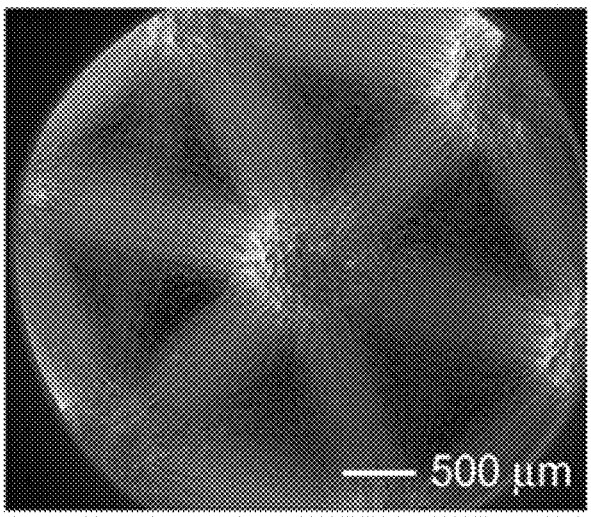

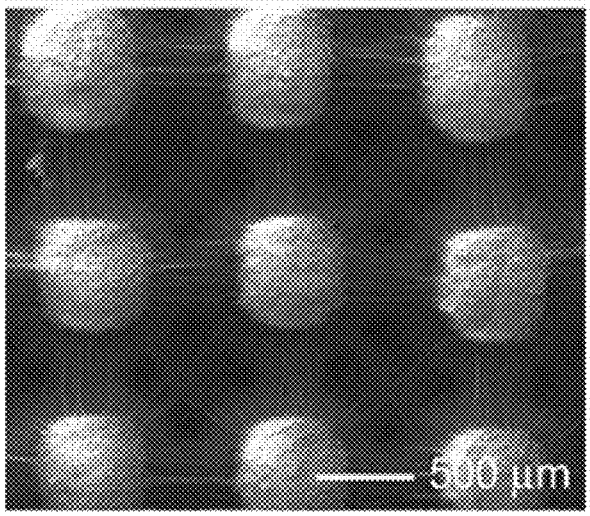

FIG. 31C

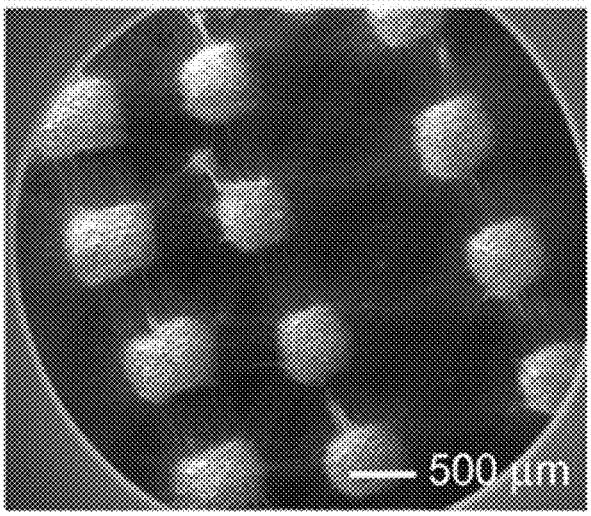

FIG. 31D

FIG. 32

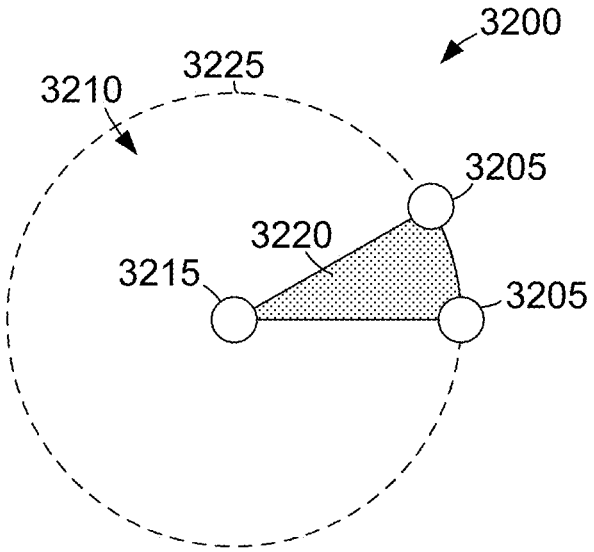

BIOMEDICAL PATCHES WITH ALIGNED FIBERS

CROSS-REFERENCE TO RELATED APPLICATIONS

This application is a continuation of U.S. patent application Ser. No. 16/795,057, filed Feb. 19, 2020, which is a continuation of U.S. patent application Ser. No. 16/540,548, filed Aug. 14, 2019, now U.S. Pat. No. 10,617,512, which is a continuation of U.S. patent application Ser. No. 15/497,691, filed Apr. 26, 2017, which is a continuation of U.S. patent application Ser. No. 13/703,210, filed on Mar. 20, 2013, now U.S. Pat. No. 10,149,749, which is a national stage application under 35 U.S.C. § 371 of International Patent Application No. PCT/US2011/040691 filed on Jun. 16, 2011, which claims the benefit of U.S. Provisional Application No. 61/355,712, filed Jun. 17, 2010, all of which are incorporated herein by reference in their entirety.

STATEMENT REGARDING FEDERALLY SPONSORED RESEARCH & DEVELOPMENT

This invention was made with government support under OD000798 awarded by the National Institutes of Health and under ECS0335765 awarded by the National Science Foundation. The government has certain rights in the invention.

BACKGROUND

Numerous surgical procedures result in the perforation or removal of biological tissue, such as the water-tight fibrous membrane surrounding the brain known as the dura mater. In some instances, such as minimally invasive neurosurgical procedures, relatively few small holes are created in the dura mater, while in others, such as the surgical resection of advanced tumors, large sections of the dura mater may be removed. In all of these cases, the tissue barrier surrounding the brain must be repaired in order to prevent damage to cortical tissues and leakage of cerebrospinal fluid. To facilitate this repair, neurosurgeons utilize sheets of polymeric materials or processed tissue that act like native dura, known as dural substitutes.

At least some known dural substitutes utilized in neurosurgical clinics are composed of an acellular collagen matrix obtained from isolated bovine or porcine tissues. While generally accepted in the field, such xenogenic dural substitutes may increase the incidence of adhesions and contractures, transmit various zoonotic diseases to patients, and generally reduce patient outcome following surgery. Furthermore, processed collagenous grafts are exceedingly expensive, costing patients and insurance companies thousands of dollars per procedure.

In addition while cell microarrays may be useful in biomedical research and tissue engineering, at least some known techniques for producing such cell microarrays may be costly and time consuming, and may require the use of specialized, sophisticated instrumentation.

SUMMARY

One or more embodiments described herein provide structures having a plurality of aligned (e.g., radially aligned and/or polygonally aligned) fibers. When such a structure is used as a biomedical patch, the alignment of fibers as described herein may provide directional cues that influence cell propagation. For example, the structures provided may promote new cell growth along the fibers, such that cell propagation in one or more desired directions may be achieved.

One or more structures provided may be created using an apparatus that includes one or more first electrodes that define an area and/or partially circumscribe an area. For example, a single first electrode may enclose the area, or a plurality of first electrode(s) may be positioned on at least a portion of the perimeter of the area. A second electrode is positioned within the area. In exemplary embodiments, when the electrodes are electrically charged at a first polarity, and a spinneret dispensing a polymer (e.g., toward the second electrode) is electrically charged at a second polarity opposite the first polarity, the dispensed polymer forms a plurality of fibers extending from the second electrode to the first electrodes. Further, electrodes with rounded (e.g., convex) surfaces may be arranged in an array, and a fibrous structure created using such electrodes may include an array of wells at positions corresponding to the positions of the electrodes.

In some embodiments, an artificial dura mater comprising at least a hydrophobic and biodegradable electrospun layer, wherein said layer comprises (a) at least one synthetic biomedical polymer and (b) fibers with a diameter of 1-1000 nm is disclosed. In some embodiments, the artificial dura mater consists essentially of synthetic materials.

In some embodiments, a method of treating a subject having a defective dura mater, the method comprising selecting an artificial dura mater that comprises at least one synthetic polymer and fibers with a diameter of 1-1000 nm, and applying said artificial dura mater proximate to said defective dura mater in said subject, is disclosed. In some embodiments, the artificial dura mater is as described elsewhere herein.

A multi-laminar electrospun nanofiber scaffold for use in repairing a defect in a tissue substrate is provided. The multi-laminar electrospun nanofiber scaffold includes a first layer formed by a first plurality of electrospun polymeric fibers, and a second layer formed by a second plurality of electrospun polymeric fibers. The second layer is combined with the first layer. At least a first portion of the multi-laminar electrospun nanofiber scaffold includes a higher density of fibers than a second portion of the multi-laminar electrospun nanofiber scaffold, and the first portion comprises a higher tensile strength than the second portion. The multi-laminar electrospun nanofiber scaffold is configured to degrade via hydrolysis after at least one of a predetermined time or an environmental condition. The multi-laminar electrospun nanofiber scaffold is configured to be applied to the tissue substrate containing the defect. The multi-laminar electrospun nanofiber scaffold is sufficiently flexible to facilitate application of the multi-laminar electrospun nanofiber scaffold to uneven surfaces of the tissue substrate, and is sufficiently flexible to enable movement of the multi-laminar electrospun nanofiber scaffold by the tissue substrate.

A multi-laminar electrospun nanofiber scaffold for use in repairing a defect in a tissue substrate is provided. The multi-laminar electrospun nanofiber scaffold includes a first layer formed by a first plurality of electrospun polymeric fibers, and a second layer formed by a second plurality of electrospun polymeric fibers. The second layer is combined with the first layer. At least a first portion of the multi-laminar electrospun nanofiber scaffold includes a higher density of fibers than a second portion of the multi-laminar electrospun nanofiber scaffold, and the first portion includes a higher tensile strength than the second portion. The first

layer and the second layer are configured to separate via hydrolysis after at least one of a predetermined time or an environmental condition. The multi-laminar electrospun nanofiber scaffold is configured to be applied to the tissue substrate containing the defect. The multi-laminar electrospun nanofiber scaffold is sufficiently flexible to facilitate application of the multi-laminar electrospun nanofiber scaffold to uneven surfaces of the tissue substrate, and is sufficiently flexible to enable movement of the multi-laminar electrospun nanofiber scaffold by the tissue substrate.

A three-dimensional electrospun nanofiber scaffold for use in repairing a defect in a tissue substrate is provided. The three-dimensional electrospun nanofiber scaffold includes a first layer formed by a first plurality of electrospun polymeric fibers, and a second layer formed by a second plurality of electrospun polymeric fibers. The second layer is combined with the first layer. At least a first portion of the three-dimensional electrospun nanofiber scaffold includes a higher density of fibers than a second portion of the three-dimensional electrospun nanofiber scaffold, and the first portion comprises a higher tensile strength than the second portion. The three-dimensional electrospun nanofiber scaffold is configured to degrade via hydrolysis after at least one of a predetermined time or an environmental condition. The three-dimensional electrospun nanofiber scaffold is configured to be applied to the tissue substrate containing the defect. The three-dimensional electrospun nanofiber scaffold is sufficiently flexible to facilitate application of the three-dimensional electrospun nanofiber scaffold to uneven surfaces of the tissue substrate, and is sufficiently flexible to enable movement of the three-dimensional electrospun nanofiber scaffold by the tissue substrate.

This summary introduces a subset of concepts that are described in more detail below. This summary is not meant to identify essential features, and should not be read as limiting in any way the scope of the claimed subject matter.

BRIEF DESCRIPTION OF THE DRAWINGS

The embodiments described herein may be better understood by referring to the following description in conjunction with the accompanying drawings.

FIG. **1** is a diagram illustrating a perspective view of an example electrospinning system for producing a structure of radially aligned fibers.

FIG. **2** is a diagram illustrating an electric field generated by the electrospinning system shown in FIG. **1**.

FIG. **3** is a diagram of an electrode removed from the electrospinning system shown in FIG. **1** and having a plurality of fibers deposited thereon forming a biomedical patch.

FIG. **4** is a photograph of a biomedical patch including a plurality of radially aligned electrospun fibers deposited on a peripheral electrode.

FIG. **5** is a scanning electron microscope (SEM) image of the biomedical patch shown in FIG. **4**, further illustrating that the fibers of the biomedical patch are radially aligned.

FIG. **6** is an illustration of a solid fiber spinneret.

FIG. **7** is an illustration of a hollow fiber spinneret.

FIG. **8** is an illustration of a biomedical patch layer with a plurality of randomly oriented fibers, a biomedical patch layer with a plurality of radially aligned fibers, and a multi-layer biomedical patch including multiple orders of fibers.

FIG. **9** is a diagram of a collector with a central electrode, an inner peripheral electrode defining an inner enclosed area, and an outer peripheral electrode defining an outer enclosed area.

FIG. **10** is a diagram of a concentric biomedical patch that may be produced utilizing the collector shown in FIG. **9** in conjunction with the electrospinning system shown in FIG. **1**.

FIG. **11** is a flowchart of an exemplary method for producing a structure of radially aligned fibers using a peripheral electrode defining an enclosed area and a central electrode positioned approximately at a center of the enclosed area.

FIG. **12** is a flowchart of an exemplary method for repairing a defect, insult, or void in a biological tissue.

FIG. **13** is a schematic illustration of a cellular infiltration of a biomedical patch from intact dural tissue apposing the edge of a biomedical patch.

FIG. **14**A, FIG. **14**B, FIG. **14**C, and FIG. **14**D are fluorescence micrographs comparing the migration of cells when dura tissues were cultured on scaffolds of radially aligned nanofibers and randomly oriented nanofibers for 4 days. FIG. **14**A is a fluorescence micrograph of dural fibroblasts stained with fluorescein diacetate (FDA) migrating along radially aligned nanofibers. FIG. **14**B is a fluorescence micrograph of dural fibroblasts stained with FDA migrating along random fibers. FIG. **14**C is a fluorescence micrograph of dural fibroblasts stained with FDA migrating along radially aligned nanofibers. FIG. **14**D is a fluorescence micrograph of dural fibroblasts stained with FDA migrating along random fibers.

FIG. **15**A, FIG. **15**B, and FIG. **15**C are schematic diagrams of a custom cell culture system designed to model the wound healing response of defects or voids in a biological tissue. FIG. **15**A is a diagram of a custom cell culture system including a metal ring. FIG. **15**B is a diagram of a custom cell culture system including a central silicone tube. FIG. **15**C is a top view of a diagram of a custom cell culture system showing the location of a central fiber scaffold and a surrounding region seeded with fibroblast cells.

FIG. **16**A, FIG. **16**B, FIG. **16**C, and FIG. **16**D are fluorescence micrographs showing cell morphology and distribution on scaffolds of radially aligned nanofibers and randomly oriented nanofibers with and without fibronectin coating after incubation for 1 day. FIG. **16**A is a micrograph showing cell morphology and distribution on scaffolds of radially aligned nanofibers. FIG. **16**B is a micrograph showing cell morphology and distribution on scaffolds of randomly aligned nanofibers. FIG. **16**C is a micrograph showing cell morphology and distribution on scaffolds of radially aligned nanofibers. FIG. **16**D is a micrograph showing cell morphology and distribution on scaffolds of randomly aligned nanofibers.

FIG. **17**A, FIG. **17**B, FIG. **17**C, and FIG. **17**D are fluorescence micrographs showing the migration of dura fibroblasts seeded on fibronectin-coated scaffolds of radially aligned nanofibers. FIG. **17**A is a fluorescence micrograph showing the migration of dura fibroblasts seeded on fibronectin-coated scaffolds of radially aligned nanofibers for 1 day. FIG. **17**B is a fluorescence micrograph showing the migration of dura fibroblasts seeded on fibronectin-coated scaffolds of radially aligned nanofibers for 3 days. FIG. **17**C is a fluorescence micrograph showing the migration of dura fibroblasts seeded on fibronectin-coated scaffolds of radially aligned nanofibers for 7 days. FIG. **17**D is a magnified view of the fluorescence micrograph of FIG.

17C showing the migration of dura fibroblasts seeded on fibronectin-coated scaffolds of radially aligned nanofibers for 7 days.

FIG. **18** is an illustration of a method utilized to determine the area of remaining acellular region of the nanofiber scaffolds within the simulated tissue defect.

FIG. **19** is a graph illustrating the acellular area remaining on the nanofiber scaffold within the simulated tissue defect as a function of incubation time.

FIG. **20**A, FIG. **20**B, FIG. **20**C, and FIG. **20**D are fluorescence micrographs showing live dural fibroblasts labeled with membrane dye on scaffolds of radially aligned nanofibers with fibronectin coating. FIG. **20**A is a fluorescence micrographs showing live dural fibroblasts labeled with membrane dye on scaffolds of radially aligned nanofibers with fibronectin coating after a 1-day culture. FIG. **20**B is a fluorescence micrographs showing live dural fibroblasts labeled with membrane dye on scaffolds of radially aligned nanofibers with fibronectin coating after a 3-day culture. FIG. **20**C is a fluorescence micrographs showing live dural fibroblasts labeled with membrane dye on scaffolds of radially aligned nanofibers with fibronectin coating after a 7-day culture. FIG. **20**D is a fluorescence micrographs showing live dural fibroblasts labeled with membrane dye on scaffolds of radially aligned nanofibers with fibronectin coating after a 7-day culture and includes an inset of a high magnification image of the same.

FIG. **21**A, FIG. **21**B, FIG. **21**C, and FIG. **21**D are fluorescence micrographs demonstrating the organization of cells and extracellular matrix adherent on scaffolds by immunostaining for type I collagen (green) and cell nuclei (blue). FIG. **21**A is a fluorescence micrograph demonstrating the organization of cells and extracellular matrix adherent on scaffolds of radially aligned fibers by immunostaining for type I collagen (green) and cell nuclei (blue). FIG. **21**B is a fluorescence micrograph demonstrating the organization of cells and extracellular matrix adherent on scaffolds of randomly oriented fibers by immunostaining for type I collagen (green) and cell nuclei (blue). FIG. **21**C is a fluorescence micrograph demonstrating the organization of cells and extracellular matrix adherent on scaffolds of radially aligned fibers by immunostaining for type I collagen (green) and cell nuclei (blue). FIG. **21**D is a fluorescence micrograph demonstrating the organization of cells and extracellular matrix adherent on scaffolds of randomly oriented fibers by immunostaining for type I collagen (green) and cell nuclei (blue).

FIG. **22** is a graph illustrating the thickness of regenerated dura at the center of repaired dural defects over time.

FIG. **23** is a graph illustrating regenerative collagenous tissue content over time.

FIG. **24** is a diagram illustrating a perspective view of an example electrospinning system for producing a structure of fibers aligned in polygons using an array of electrodes.

FIG. **25** is a diagram illustrating an elevation view of an example modular electrospinning collector.

FIG. **26** is a diagram illustrating an electric field generated by an electrospinning system such as the electrospinning system shown in FIG. **24**.

FIG. **27**A, FIG. **27**B, FIG. **27**C, FIG. **27**D, FIG. **27**E, and FIG. **27**F are microscopy images of a membrane produced using a collector with an array of electrodes, such as the collector shown in FIG. **24**. FIG. **27**A is an optical microscopy image of a membrane including an inset illustrating a magnification of the same. FIG. **27**B is an optical microscopy image of a membrane including highlighted areas. FIG. **27**C is a magnified optical microscopy image of the highlighted area labeled **27**C of FIG. **27**B. FIG. **27**D is a magnified optical microscopy image of the highlighted area labeled **27**D of FIG. **27**B. FIG. **27**E is a magnified optical microscopy image of the highlighted area labeled **27**E of FIG. **27**B. FIG. **27**F is a magnified optical microscopy image of the highlighted area labeled **27**F of FIG. **27**B.

FIG. **28**A, FIG. **28**B, FIG. **28**C, and FIG. **28**D are fluorescence microscopy images illustrating cell growth in a membrane such as the membrane shown in FIGS. **27**A-**27**F. FIG. **28**A is an optical fluorescence microscopy image of droplets containing cells placed within the wells of a fiber membrane. FIG. **28**B is a fluorescence microscopy image array of cells selectively adhered to the microwells within a nanofiber membrane. FIG. **28**C is a fluorescence microscopy image of seeded cell microarrays. FIG. **28**D is a fluorescence microscopy image of the same cell microarray shown in FIG. **28**C after incubation for three days. **28**A-**28**D are microscopy images illustrating cell growth in a membrane such as the membrane shown in FIGS. **27**A-**27**F.

FIG. **29**A and FIG. **29**B are microscopy images illustrating neurite propagation in a membrane such as the membrane shown in FIGS. **27**A-**27**F. FIG. **29**A is an overlay of an optical microscopy image and a fluorescence microscopy image. FIG. **29**B is an overlay of an optical microscopy image and a fluorescence microscopy image adjacent to the region shown in FIG. **29**A.

FIG. **30**A and FIG. **30**B are overlays of an optical microscopy image and a fluorescent microscopy image illustrating neuronal network formation from embryoid bodies in a membrane such as the membrane shown in FIGS. **27**A-**27**F. FIG. **30**A is an overlay of an optical microscopy image and a fluorescent microscopy image illustrating an embryoid body confined within a microwell, while neurites extend peripherally along an underlying fiber pattern. FIG. **30**B is an overlay of an optical microscopy image and a fluorescent microscopy image illustrating an embryoid body seeded on regions of uniaxially aligned nanofibers within a nanofiber array.

FIG. **31**A, FIG. **31**B, FIG. **31**C, and FIG. **31**D are scanning electron microscopy images illustrating membranes produced using a variety of electrode arrays. FIG. **31**A is a scanning electron microscopy image of a fiber membrane fabricated using a collector composed of hexagonal arrays of stainless steel beads. FIG. **31**B is a scanning electron microscopy image of a fiber membrane fabricated using a collector composed of hexagonal arrays of stainless steel beads having a larger diameter than the stainless steel beads used to produce the membrane shown in FIG. **31**A. FIG. **31**C is a scanning electron microscopy image of a fiber membrane fabricated using a collector composed of a close-packed square array of stainless steel beads. FIG. **31**D is a scanning electron microscopy image of a fiber membrane produced using a collector composed of square arrays of stainless steel microbeads with a gradual increase of the inter-electrode distance in one direction.

FIG. **32** is a diagram of a collector with peripheral electrodes partially circumscribing an area.

DETAILED DESCRIPTION

Embodiments provided herein facilitate repairing biological tissue with the use of a biomedical patch including a plurality of fibers. Such fibers may have a very small cross-sectional diameter (e.g., from 1-1000 nanometers) and, accordingly, may be referred to as nanofibers. While biomedical patches are described herein with reference to dura mater and use as a dural substitute, embodiments described may be applied to any biological tissue. Moreover,

although described as biomedical patches, structures with aligned fibers may be used for other purposes. Accordingly, embodiments described are not limited to biomedical patches.

In operation, biomedical patches provided herein facilitate cell growth and may be referred to as "membranes," "scaffolds," "matrices," or "substrates." Such biomedical patches further facilitate cell migration from a perimeter of the patch to a center of the biomedical patch. Biomedical patches with aligned fibers, as described herein, may promote significantly faster healing and/or regeneration of tissue such as the dura mater than substitutes lacking nanoscopic organization and directional cues.

Dura mater is a membranous connective tissue located at the outermost of the three layers of the meninges surrounding the brain and spinal cord, which covers and supports the dural sinuses and carries blood from the brain towards the heart. Dural substitutes are often needed after a neurosurgical procedure to repair, expand, or replace the incised, damaged, or resected dura mater.

Although many efforts have been made, the challenge to develop a suitable dural substitute has been met with limited success. Autografts (e.g., fascia lata, temporalis fascia, and pericranium) are preferable because they do not provoke severe inflammatory or immunologic reactions. Potential drawbacks of autografts include the difficulty in achieving a watertight closure, formation of scar tissue, insufficiently accessible graft materials to close large dural defects, increased risk of infection, donor site morbidity, and the need for an additional operative site. Allografts and xenografts are often associated with adverse effects such as graft dissolution, encapsulation, foreign body reaction, scarring, adhesion formation, and toxicity-induced side effects from immunosuppressive regimens. Lyophilized human dura mater as a dural substitute has also been reported as a source of transmittable diseases, specifically involving prions, such as Creutzfeldt-Jakob disease.

In terms of materials, non-absorbable synthetic polymers, such as silicone and expanded polytetrafluoroethylene (ePTFE), often cause serious complications that may include induction of granulation tissue formation due to their chronic stimulation of the foreign body response. Natural absorbable polymers, including collagen, fibrin, and cellulose, may present a risk of infection and disease transmission. As a result, synthetic polymers such as poly(3-hydroxybutyrate-co-3-hydroxyvalerate) (PHBV), poly(lactic acid) (PLA), polyglycolic acid (PGA), PLA-PCL-PGA ternary copolymers, and hydroxyethylmethacrylate hydrogels have recently attracted attention as biodegradable implant materials for dural repair. Methods and systems described herein may be practiced with these materials and/or any biomedical polymer.

In order to facilitate successful regeneration and/or repair of the dura mater following surgery, a synthetic dural substitute or biomedical patch should promote: i) adhesion of dural fibroblasts (the primary cell type present in the dura) to the surface of the biomedical patch; ii) migration of dural fibroblasts from the periphery of the biomedical patch toward the center; and iii) minimal immune response. To date, synthetic dural substitutes have been tested only in the form of foils, films, meshes, glues, and hydrogels. Due to the isotropic surface properties, such substitutes are not well-suited for cell attachment and directed, inward migration.

This problem can be potentially solved by fabricating the polymers as nanoscale fibers with a specific order and organization. For example, the speed of cell migration may be very low on flat, isotropic surfaces, whereas cells may migrate over a very long distance in a highly correlated fashion with constant velocity on a uniaxially aligned, fibrous scaffold.

Electrospinning is an enabling technique which can produce nanoscale fibers from a large number of polymers. The electrospun nanofibers are typically collected as a randomly-oriented, nonwoven mat. Uniaxially aligned arrays of nanofibers can also be obtained under certain conditions, specifically when employing an air-gap collector or a mandrel rotating at a high speed. However, uniaxially aligned nanofiber scaffolds promote cell migration only along one specific direction and are thus not ideally suited as dural substitutes.

In order to promote cell migration from the surrounding tissue to the center of a dural defect and shorten the time for healing and regeneration of dura mater, a surface patterned with aligned (e.g., aligned radially and/or in one or more polygons), nanoscale features would be highly advantageous as an artificial dural substitute. More specifically, scaffolds constructed with aligned nanofibers could meet such a demand by guiding and enhancing cell migration from the edge of a dural defect to the center.

Many polymers are available for use in electrospinning. In some embodiments described herein, nanofibers for dura substitutes are produced as the electrospun polymer from poly(ε-caprolactone) (PCL), an FDA approved, semicrystalline polyester that can degrade via hydrolysis of its ester linkages under physiological conditions with nontoxic degradation products. This polymer has been extensively utilized and studied in the human body as a material for fabrication of drug delivery carriers, sutures, or adhesion barriers. As described herein, electrospun PCL nanofibers may be aligned to generate scaffolds that are useful as dural substitutes.

Embodiments provided herein facilitate producing a novel type of artificial tissue substitute including a polymeric nanofiber material, which is formed through a novel method of electrospinning. This polymeric material includes non-woven nanofibers (e.g., fibers having a diameter of 1-1000 nanometers) which are aligned within a material sheet.

In exemplary embodiments, a material with aligned nanofibers is formed through a novel method of electrospinning that employs a collector including one or more first, or "peripheral," electrodes defining an area and/or at least partially circumscribing the area, and a second, or "inner," electrode positioned within the area. When the electrodes are electrically charged at a first polarity, and a spinneret dispensing a polymer (e.g., toward the inner electrode) is electrically charged at a second polarity opposite the first polarity, the dispensed polymer forms a plurality of fibers extending from the inner electrode to the peripheral electrode(s). Electrodes may include a rounded (e.g., convex) surface, such that a depression, or "well", is formed in the electrode-facing side of a structure of fibers. Alternatively, electrodes may include a concave surface, such that a well is formed in the side of the structure facing away from the electrodes.

In some embodiments, the collector includes a single inner electrode and a single peripheral electrode. In other embodiments, the collector includes a plurality of peripheral electrodes, and the dispensed polymer may form fibers extending between such peripheral electrodes in addition to fibers extending from the inner electrode to one or more of the peripheral electrodes.

Further, in some embodiments, multiple areas are defined and/or partially circumscribed by peripheral electrodes. For

example, an inner peripheral electrode may define an inner enclosed area surrounding the inner electrode, and an outer peripheral electrode may define an outer enclosed area surrounding the inner peripheral electrode. In other embodiments, electrodes are arranged in an array, such as a grid and/or other polygonal pattern (e.g., a hexagonal pattern), and multiple, partially overlapping areas may be defined by such electrodes. For example, an inner electrode of one area may function as a peripheral electrode of another area. In such embodiments, the dispensed polymer may form fibers extending between the electrodes of the collector, such that the fibers define the sides of a plurality of polygons, with the electrodes positioned at the vertices of the polygons.

Unlike known nanofiber structures, aligned nanofiber materials provided herein are capable of presenting nanoscale topographical cues to local cells that enhance and direct cell migration (e.g., throughout the material sheet or into the center of the material sheet). As a result, aligned nanofiber materials may induce faster cellular migration and population than randomly oriented materials, such as processed gold-standard collagen matrices. Materials described herein may be particularly useful as a substrate for various types of biomedical patches or grafts designed to induce wound protection, closure, healing, repair, and/or tissue regeneration.

A scaffold of aligned nanofibers, as described herein, possesses significant potential as an artificial dural substitute, in that it is capable of encouraging robust cell migration from apposed intact dura and promoting rapid cellular population of the nanofiber matrix required to induce dural repair. In addition, such nanofiber materials offer the advantage of being inexpensive to produce, fully customizable, and resorbable. Nanofiber dural substitutes may also reduce the risk of contractures and fully eliminate the risk of transmitted zoonotic disease when applied intraoperatively, generally improving patient outcomes following surgery.

Inner Electrode and Peripheral Electrode(s)

FIG. **1** is a diagram illustrating a perspective view of an exemplary electrospinning system **100** for producing a structure of radially aligned fibers. System **100** includes a collector **105** with a first electrode **110**, which may be referred to as a peripheral electrode, and a second electrode **115**, which may be referred to as an inner electrode or central electrode. System **100** also includes a spinneret **120**. Peripheral electrode **110** defines an enclosed area **125**, and central electrode **115** is positioned approximately at a center of enclosed area **125**.

System **100** is configured to create an electric potential between collector **105** and spinneret **120**. In one embodiment, peripheral electrode **110** and central electrode **115** are configured to be electrically charged at a first amplitude and/or polarity. For example, peripheral electrode **110** and central electrode **115** may be electrically coupled to a power supply **130** via a conductor **135**. Power supply **130** is configured to charge peripheral electrode **110** and central electrode **115** at the first amplitude and/or polarity via conductor **135**.

In the embodiment illustrated in FIG. **1**, peripheral electrode **110** is a ring defining an enclosed area **125** which is circular. For example, circular enclosed area **125** may have a diameter of between 1 centimeter and 20 centimeters. In other embodiments, peripheral electrode **110** may be any shape suitable for use with the methods described herein. For example, peripheral electrode **110** may define an elliptical, ovular, rectangular, square, triangular, and/or other rectilinear or curvilinear enclosed area **125**. In some embodiments, peripheral electrode **110** defines an enclosed area **125** of between 5 square centimeters and 100 square centimeters. Peripheral electrode **110** may have a height **112** of between 0.5 and 2.0 centimeters. Central electrode **115** may include a metallic needle and/or any other structure terminating in a point or set of points.

In one embodiment, enclosed area **125** defines a horizontal plane **127**. Spinneret **120** is aligned with central electrode **115** and vertically offset from horizontal plane **127** at a variable distance. For example, spinneret **120** may be vertically offset from horizontal plane **127** at a distance of 1 centimeter to 100 centimeters.

Spinneret **120** is configured to dispense a polymer **140** while electrically charged at a second amplitude and/or polarity opposite the first polarity. As shown in FIG. **1**, spinneret **120** is electrically coupled to power supply **130** by a conductor **145**. Power supply **130** is configured to charge spinneret **120** at the second amplitude and/or polarity via conductor **145**. In some embodiments, power supply **130** provides a direct current (DC) voltage (e.g., between 10 kilovolts and 17 kilovolts). In one embodiment, conductor **145** is charged positively, and conductor **135** is charged negatively or grounded. In some embodiments, power supply **130** is configured to allow adjustment of a current, a voltage, and/or a power.

In one embodiment, spinneret **120** is coupled to a syringe **150** containing polymer **140** in a liquid solution form. Syringe **150** may be operated manually or by a syringe pump **155**. In an exemplary embodiment, spinneret **120** is a metallic needle having an aperture between 100 micrometers and 2 millimeters in diameter.

As syringe **150** pressurizes polymer **140**, spinneret **120** dispenses polymer **140** as a stream **160**. Stream **160** has a diameter approximately equal to the aperture diameter of spinneret **120**. Stream **160** descends toward collector **105**. For example, stream **160** may fall downward under the influence of gravity and/or may be attracted downward by a charged conductive surface **162** positioned below collector **105**. For example, conductive surface **162** may be electrically coupled to conductor **135** and charged at the same amplitude and/or polarity as peripheral electrode **110** and central electrode **115**. As stream **160** descends, polymer **140** forms one or more solid polymeric fibers **165**.

In some embodiments, a mask **164** composed of a conducting or non-conducting material is applied to collector **105** to manipulate deposition of fibers **165**. For example, mask **164** may be positioned between spinneret **120** and collector **105** such that no fibers **165** are deposited on collector **105** beneath mask **164**. Moreover, mask **164** may be used as a time-variant mask by adjusting its position while spinneret **120** dispenses polymer **140**, facilitating spatial variation of fiber density on collector **105**. While mask **164** is shown as circular, mask **164** may have any shape (e.g., rectangular or semi-circular) and size suitable for use with system **100**. Alternatively, or in addition, deposition of fibers **165** on collector **105** may be manipulated by adjusting the position of collector **105** with respect to spinneret **120** or by spatially varying the electrical potential applied between the spinneret **120** and/or the electrodes making up the collector **105**. For example, positioning one side of collector **105** directly beneath spinneret **120** may cause more fibers **165** to be deposited on that side than are deposited on the opposite side of collector **105**.

FIG. **2** is a diagram **200** illustrating an electric field generated by system **100**. Diagram **200** shows a two dimensional, cross-sectional view of electric field strength vectors between spinneret **120** and peripheral electrode **110** and central electrode **115** of collector **105** (shown in FIG. **1**).

Unlike known electrospinning systems, the electric field vectors (stream lines) in the vicinity of the collector are split into two populations, pointing toward the peripheral electrode **110** and pointing toward the central electrode **115**.

Neglecting the effect of charges on the polymeric fibers, the electrical potential field can be calculated using the Poisson equation,

$$\nabla^2 V = \frac{-\rho}{\varepsilon},$$

where V is the electrical potential, ε is the electrical permittivity of air, and ρ is the spatial charge density. The electrical field, E, can then be calculated by taking the negative gradient of the electrical potential field, E=−∇V. Here, the electrical field was calculated to verify the alignment effect demonstrated by deposited fibers, which was performed using the software COMSOL3.3.

FIG. **3** is a diagram of peripheral electrode **110** removed from electrospinning system **100** (shown in FIG. **1**) and having a plurality of fibers **165** deposited thereon forming a biomedical patch **170**. Fibers **165** extend radially between a center **175** corresponding to the position of central electrode **115** (shown in FIG. **1**) and a perimeter **178** corresponding to the position of peripheral electrode **110**. For example, perimeter **178** may be a circular perimeter about center **175** defining a diameter of between 1 centimeter and 6 centimeters.

Biomedical patch **170** is illustrated with a small quantity of fibers **165** in FIG. **3** for clarity. In some embodiments, biomedical patch **170** includes thousands, tens of thousands, hundreds of thousands, or more fibers **165**, evenly distributed throughout enclosed area **125** (shown in FIG. **1**) of peripheral electrode **110**. Even with millions of fibers **165**, biomedical patch **170** is flexible and/or pliable, facilitating application of biomedical patch **170** to uneven biological tissue surfaces, such as the surface of the dura mater.

The radial alignment of fibers **165** demonstrates the shortest possible path between perimeter **178** and center **175**. Accordingly, biomedical patch **170** also facilitates cell migration directly from perimeter **178** to center **175**, enabling a reduction in time required for cells to infiltrate and populate applied biomedical patch, and for native tissue to regenerate.

Fibers **165** have a diameter of 1-1000 nanometers. In one embodiment, fibers have a diameter of approximately 220 nanometers (e.g., 215 nm to 225 nm). The diameter of the fibers **165**, thickness of the biomedical patch **170**, and/or fiber density within the biomedical patch **170** may affect the durability (e.g., tensile strength) of biomedical patch **170**. Biomedical patch **170** may be produced with various mechanical properties by varying the thickness and/or the fiber density of the biomedical patch **170** by operating electrospinning system **100** for relatively longer or shorter durations.

FIG. **4** is a photograph **300** of a biomedical patch **305** including a plurality of radially aligned electrospun fibers deposited on a peripheral electrode **110**. FIG. **5** is a scanning electron microscope (SEM) image **310** of biomedical patch **305**, further illustrating that the fibers of biomedical patch **305** are radially aligned.

Referring to FIGS. **1** and **3**, fibers **165** may be solid or hollow. In some embodiments, the size and/or structure of fibers **165** is determined by the design of spinneret **120**. FIG. **6** is an illustration of a solid fiber spinneret **120**A. Solid fiber spinneret **120**A includes a conical body **180** defining a center line **182**. At a dispensing end **184**, conical body **180** includes an annulus **186**. Annulus **186** defines a circular aperture **190**A, through which polymer **140** may be dispensed. Fibers **165** produced with solid fiber spinneret **120**A have a solid composition.

FIG. **7** is an illustration of a hollow fiber spinneret **120**B. Like solid fiber spinneret **120**A, hollow fiber spinneret **120**B includes a conical body **180** with an annulus **186** at a dispensing end **184**. Hollow fiber spinneret **120**B also includes a central body **188**B positioned within annulus **186**. Annulus **186** and central body **188**B define an annular aperture **190**B. Accordingly, when polymer **140** is dispensed by hollow fiber spinneret **120**B, fibers **165** have a hollow composition, with an exterior wall surrounding a cavity. The exterior wall of a fiber **165** dispensed by hollow fiber spinneret **120**B defines an outer diameter corresponding to the inner diameter of annulus **186** and an inner diameter corresponding to the diameter of central body **188**B. Accordingly, the outer diameter and inner diameter of hollow fibers **165** may be adjusted by adjusting the diameters of annulus **186** and central body **188**B.

Hollow fiber spinneret **120**B facilitates incorporating a substance, such as a biological agent, growth factor, and/or a drug (e.g., a chemotherapeutic substance), into biomedical patch **170**. For example, the substance may be deposited within a cavity defined by hollow fibers **165** of biomedical patch **170**. In one embodiment, polymer **140** is selected to create porous and/or semi-soluble fibers **165**, and the substance is dispensed from the cavity through fibers **165**. In another embodiment, polymer **140** is degradable, and the substance is dispensed as fibers **165** degrade in vivo. For example, fibers **165** may be configured to degrade within 12 months, 6 months, or 3 months. The degradation rate of polymer **140** may be manipulated by adjusting a ratio of constituent polymers within polymer **140**.

In another embodiment, a substance is delivered by solid fibers **165**. For example, a solid fiber **165** may be created from a polymer **140** including the substance in solution. As solid fiber **165** degrades, the substance is released into the surrounding tissue.

As shown in FIGS. **6** and **7**, annulus **186** is perpendicular to center line **182**. In an alternative embodiment, annulus **186** is oblique (e.g., oriented at an acute or obtuse angle) with respect to center line **182**. The outside diameter of fibers **165** may be determined by the inside diameter of annulus **186**.

Some embodiments facilitate producing a biomedical patch having radially aligned fibers and non-radially aligned fibers. For example, radially aligned fibers may be deposited into a first layer, and non-radially aligned fibers may be deposited into a second layer. Alternatively, radially aligned non-radially aligned fibers may be deposited into a single layer (e.g., simultaneously, sequentially, and/or alternately). Referring to FIG. **1**, system **100** may be used to create randomly oriented fibers by charging or grounding conductive surface **162**. Optionally, peripheral electrode **110** and central electrode **115** may be uncharged or ungrounded (e.g., decoupled from conductor **135**).

FIG. **8** is an illustration of a biomedical patch layer **400** with a plurality of randomly oriented fibers **405** and a biomedical patch layer **410** with a plurality of radially aligned fibers **415**. As shown in FIG. **8**, biomedical patch layers **400** and **410** may be combined (e.g., overlaid) to produce a multi-layer biomedical patch **420** with both randomly oriented fibers **405** and radially aligned fibers **415**, or any other combination of any number or type of fiber layers.

Combining non-radially aligned fibers **405** and radially aligned fibers **415** facilitates providing a biomedical patch that promotes cell migration to a center of the biomedical patch while exhibiting potentially greater durability (e.g., tensile strength) than a biomedical patch having only radially aligned fibers **415**. Combining non-radially aligned fibers **405** and radially aligned fibers **415** may also enable spatial control of cell migration and infiltration along an axis perpendicular to the plane of the biomedical patch, facilitating the formation and organization of specific layers of cells and/or extracellular matrix proteins resembling natural tissue strata.

In some embodiments, multiple biomedical patch layers **410** with radially aligned fibers **415** may be combined to create a multi-layer biomedical patch. For example, referring to FIGS. **1** and **3**, after depositing a first set of fibers on collector **105**, one may wait for the first set of fibers **165** to solidify completely or cure and then deposit a second set of fibers **165** on collector **105**. The second set of fibers **165** may be deposited directly over the first set of fibers **165** on collector **105**. Alternatively, the first set of fibers **165** may be removed from collector **105**, and the second set of fibers **165** may be deposited on conductive surface **162** and/or collector **105** and then removed and overlaid on the first set of fibers **165**. Such embodiments facilitate increased durability of the biomedical patch, and added spatial control of cell migration/activity, even where only radially aligned fibers are used. In some embodiments, a hydrogel or polymeric scaffold may be disposed between biomedical patch layers **400** and/or biomedical patch layers **410**.

A multi-layered biomedical patch may be useful for dural grafts as well as other tissue engineering applications. Sequential layers of fibers can be created with varying orders (e.g., radially aligned or randomly oriented) and densities (e.g., low or high fiber density), which may allow specific types of cells to infiltrate and populate select layers of the artificial biomedical patch. For example, biomedical patches containing a high fiber density generally prohibit cellular migration and infiltration, while biomedical patches containing a low fiber density generally enhance cellular migration and infiltration.

Overall, the ability to form multi-layered fiber materials, as described herein, may be extremely beneficial in the construction of biomedical patches designed to recapitulate the natural multi-laminar structure of not only dura mater, but also other biological tissues such as skin, heart valve leaflets, pericardium, and/or any other biological tissue. Furthermore, one or more layers of a biomedical patch may be fabricated from biodegradable polymers such that the resulting nanofiber materials fully resorb following implantation. Manipulation of the chemical composition of the polymers utilized to fabricate these scaffolds may further allow for specific control of the rate of degradation and/or resorption of a biomedical patch following implantation.

Some embodiments provide a biomedical patch including a plurality of nested (e.g., concentric) areas. FIG. **9** is a diagram of a collector **505** with a central electrode **115**, a first or inner peripheral electrode **510** defining a first or inner enclosed area **515**, and a second or outer peripheral electrode **520** defining a second or outer enclosed area **525** that is larger than the inner enclosed area **515**. In some embodiments, outer peripheral electrode **520** is concentrically oriented with inner peripheral electrode **510**. While inner peripheral electrode **510** and outer peripheral electrode **520** are shown as defining circular enclosed areas **515**, **525** in FIG. **9**, inner peripheral electrode **510** and outer peripheral electrode **520** may define enclosed areas **515**, **525** of any shape suitable for use with the methods described herein. Moreover, inner enclosed area **515** and outer enclosed area **525** may have different shapes and/or different centers.

In operation with electrospinning system **100** (shown in FIG. **1**), central electrode **115** and inner peripheral collector **505** are charged at the first amplitude and/or polarity (opposite the polarity at which spinneret **120** is charged) while spinneret **120** dispenses polymer **140** as stream **160**. Stream **160** descends toward collector **505** and forms one or more fibers **530** extending from central electrode **115** to inner peripheral electrode **510**.

The charge of the first polarity is removed from central electrode **115** (e.g., by decoupling central electrode **115** from conductor **135**), and outer peripheral electrode **520** is charged at the first amplitude and/or polarity. Spinneret **120** dispenses polymer **140** as stream **160**, which descends toward collector **505** and forms one or more fibers **535** extending from inner peripheral electrode **510** to outer peripheral electrode **520**. Together, fibers **530** and **535** form a concentric biomedical patch **550**, as shown in FIG. **10**. In some embodiments, the charge is not removed from central electrode **115** prior to depositing fibers **535** between inner peripheral electrode **510** and outer peripheral electrode **520**.

FIG. **10** is a diagram of a concentric biomedical patch **550** that may be produced with collector **505** (shown in FIG. **9**). Fibers **530** define an inner area **555**, shown as a circle extending from a center **560** to an inner perimeter **565**. An outer area **570** includes fibers **535** extending approximately from inner perimeter **565** (e.g., about 100 μm to 2000 μm inside inner perimeter **565**) to an outer perimeter **575**. Fibers **535** are oriented radially or approximately (e.g., within 1, 3, or 5 degrees) radially with respect to center **560**.

As shown in FIG. **10**, inner area **555** and outer area **570** may overlap in an overlapping area **580**. In one embodiment, overlapping area **580** corresponds to a thickness of inner peripheral ring **510** (shown in FIG. **8**). Similar to FIG. **3**, concentric biomedical patch **550** is shown in FIG. **10** with a small quantity of fibers **530** and **535** for clarity. In some embodiments, inner area **555** and outer area **570** each include thousands, tens of thousands, hundreds of thousands, or more fibers **530** and **535**, respectively. Fibers **530** and fibers **535** may be coupled to each other in overlapping area **580**. For example, fibers **535** may be deposited before fibers **530** have completely solidified (or vice versa). In some embodiments, fibers **530** and fibers **535** are deposited on collector **505** (shown in FIG. **9**) simultaneously or in an alternating manner.

Embodiments such as those shown in FIGS. **9** and **10** facilitate providing a biomedical patch having a relatively consistent fiber density throughout. For contrast, if fibers **530** extended from center **560** to outer perimeter **575**, the fiber density at center **560** would be considerably higher than the fiber density at outer perimeter **575**. Low peripheral fiber density may compromise durability of a biomedical patch near an outer perimeter, especially at large diameters (e.g., above 5 or 6 centimeters). Accordingly, such embodiments further facilitate providing a biomedical patch of large diameter (e.g., up to 10 or 12 centimeters) while maintaining durability of the biomedical patch. In some embodiments, a layer of non-radially aligned fibers is combined with biomedical patch **550**, as described above with regard to FIG. **8**, which may further enhance durability of biomedical patch **550**.

In some embodiments, the spatial fiber density within inner area **555** is different from the spatial fiber density within outer area **570**. In one example, fibers **530** are deposited between central electrode **115** and inner peripheral

electrode **510** for a first duration, and fibers **535** are deposited between inner peripheral electrode **510** and outer peripheral electrode **520** for a second duration.

While collector **505** and concentric biomedical patch **550** are illustrated with circular inner and outer areas, any quantity and shape of peripheral electrodes may be used to create any number of distinct fiber areas within a biomedical patch.

FIG. **11** is a flowchart of an exemplary method **600** for producing a structure of radially aligned fibers using a peripheral electrode defining an enclosed area and a central electrode positioned approximately at a center of the enclosed area. While one embodiment of method **600** is shown in FIG. **11**, it is contemplated that any of the operations illustrated may be omitted and that the operations may be performed in a different order than is shown.

Method **600** includes electrically charging **605** the peripheral electrode and the central electrode at a first amplitude and/or polarity (e.g., negatively charging or grounding). A spinneret approximately aligned with the central electrode is electrically charged **610** at a second amplitude and/or polarity opposite the first amplitude and/or polarity (e.g., positively charged).

A polymer (e.g., a liquid polymer) is dispensed **615** from the spinneret. In an exemplary embodiment, dispensing **615** the polymer forms a plurality of polymeric fibers extending from the central electrode to the peripheral electrode to create a layer of radially aligned fibers.

Some embodiments facilitate creating a concentric structure of radially aligned fibers using multiple peripheral electrodes. In one embodiment, the peripheral electrode is an inner peripheral electrode. An outer peripheral electrode defining an outer enclosed area larger than the inner enclosed area is electrically charged **620** at the first amplitude and/or polarity. The electrical charge may or may not be removed **622** from the central electrode and/or the inner peripheral electrode. The polymer is dispensed **625** from the spinneret to create an outer area of radially aligned fibers extending from the inner peripheral electrode to the outer peripheral electrode.

Furthermore, some embodiments facilitate creating a multi-layered structure including both radially aligned fibers and non-radially aligned fibers. The electrical charge is removed **630** from the peripheral electrode(s) and the central electrode. A conductive surface below the layer of radially aligned fibers is electrically charged **635** at the first amplitude and/or polarity. The polymer is dispensed **640** from the spinneret to create a layer of non-radially aligned (e.g., randomly oriented and/or uniaxially aligned) fibers over the layer of radially aligned fibers.

FIG. **12** is a flowchart of an exemplary method **700** for repairing a defect in a biological tissue. The defect may include a void, an insult, and/or any other condition resulting in diminished function of the biological tissue. In one embodiment, method **700** includes creating **705** a void in the biological tissue, and the defect is the created void. For example, the void may be created **705** by surgical incision to provide access to an underlying tissue (e.g., a tumor). In another example, the void is created **705** by excising necrotic tissue (e.g., skin cells). One or more biomedical patches capable of covering the defect are selected **710**. For example, a plurality of biomedical patches may be selected **710** for a large and/or complex (e.g., irregularly shaped) defect. The biomedical patch includes a plurality of radially aligned polymeric fibers extending from a center of the biomedical patch to a perimeter of the biomedical patch. For example, a biomedical patch having a diameter greater than the diameter of an approximately circular defect may be selected **710**.

The biomedical patch selected **710** may also include non-radially aligned (e.g., randomly oriented and/or uniaxially aligned) polymeric fibers. For example, radially aligned fibers and non-radially aligned fibers may be arranged in separate layers.

In some embodiments, the biomedical patch includes multiple areas of radially aligned fibers. In one embodiment, a first set of radially aligned fibers extends from a center of the biomedical patch to a first perimeter and define an inner area. A second set of radially aligned fibers extends from the first perimeter to a second perimeter and defines an outer area.

A substance such as a growth factor and/or a drug (e.g., a chemotherapeutic drug) may be applied **715** to the biomedical patch. For example, the biomedical patch may be immersed in the substance to allow the substance to occupy a cavity within hollow fibers of the biomedical patch, dope the polymer comprising the fibers in the biomedical patch, or coat the surface of the fibers within the biomedical patch.

The biomedical patch is applied **720** to (e.g., overlaid on) the biological tissue to cover at least a portion of the defect. For example, the biomedical patch may be applied **720** to dura mater tissue, cardiac tissue, and/or any biological tissue including a defect. In one embodiment, the perimeter of the biomedical patch extends past the perimeter of the defect, such that the entire defect is covered by the biomedical patch. In some embodiments, the biomedical patch is coupled **725** to the biological tissue with a plurality of sutures, adhesive, and/or any other means of attaching the biomedical patch to the biological tissue. In an alternative embodiment, the biomedical patch is simply allowed to fuse to the biological tissue, such as by adhesion of biological cells to the biomedical patch.

After the biomedical patch is applied **720** and, optionally, coupled **725**, to the biological tissue, the biological tissue is covered **730**. In one embodiment, other tissue overlaying the defect (e.g., dermis and/or epidermis) is repaired (e.g., sutured closed). In another embodiment, one or more protective layers are applied over the biological tissue. For example, a bandage may be applied to a skin graft, with or without a protective substance, such as a gel, an ointment, and/or an antibacterial agent. In one embodiment, the protective layer includes a nanofiber structure, such as an additional biomedical patch, as described herein.

Embodiments described herein are operable with any neurosurgical procedure involving the repair, replacement, or expansion of the dura mater, including, but not limited to, a transphenoidal procedure (e.g., surgical removal of pituitary adenomas), various types of skull base surgeries, and/or surgical removal of cranial or spinal tumors (e.g., meningiomas and/or astrocytomas). In one embodiment, a biomedical patch may be applied to a bone fracture (e.g., a complex fracture). In another embodiment, a biomedical patch may be applied to a defect in the skin (e.g. a burn).

Moreover, such embodiments are operable to provide a dura mater substitute, a biomedical patch for a skin graft (e.g., dermal or epidermal), a biomedical patch for tracheal repair, a scaffold for an artificial heart valve leaflet, an artificial mesh for surgical repair of a gastrointestinal tract (e.g., an abdominal hernia or an ulcer), an artificial mesh for surgical repair of cardiac defects. For example, a cardiac biomedical patch including radially aligned fibers may be used to promote cardiomyocyte regeneration. Embodiments described herein facilitate providing a cardiac patch of

sufficient flexibility to enable movement of the biomedical patch by a biological tissue (e.g., cardiomyocytes).

In some embodiments, a biomedical patch has a thickness less than a thickness of the biological tissue being repaired. As cells migrate along the radial fibers of the biomedical patch, the biological tissue is regenerated.

Biomedical patches with radially aligned polymeric fibers facilitate reducing the expense of tissue repair, improving tissue healing time, and reducing or eliminating the risk of zoonotic infection. Moreover, such biomedical patches are relatively simple to manufacture, enabling customization of shape, size, and chemical composition and improved availability and non-immunogenicity. In addition, biomedical patches with radially aligned polymeric fibers exhibit excellent handling properties due to their cloth-like composition, eliminate the need for a second surgery to harvest autologous graft tissue, and reduce the risk of contracture and adhesion when compared with known products.

Experimental Results

Dura mater is a complex, fibrous membrane that consists of numerous cells and cell types, extracellular matrix proteins, and trophic factors, all of which play an important role in the colonization and duralization of artificial dural substitutes, and the successful implementation of such biomedical patches in vivo. In order to evaluate the capability of radially aligned nanofibers to interface with natural dura, promote host cell adhesion to the graft, and enhance host cell migration along the graft, an ex vivo model of the surgical repair of a small dural defect was developed.

In a typical procedure, an "artificial dural defect" was introduced into a piece of dura (1 cm×1 cm) by microsurgically cutting a small circular hole, 7 mm in diameter, in the center of the specimen. A nanofiber-based scaffold was then utilized to repair the artificial defect by overlaying the graft onto the dural specimen.

FIG. **13** is a schematic illustration of biological cells extending from intact dural tissue, apposed to the edge of a scaffold, into the central portion of the scaffold along radially-aligned nanofibers. The graft covered the entire simulated dural defect while simultaneously contacting the dural tissue at the periphery of the specimen, and demonstrates the ability of native cells in intact tissue to easily adhere to and migrate across the nanofiber scaffolds.

FIGS. **14**A-**14**D are a collection of fluorescence micrographs comparing the migration of cells when dural tissues were cultured on scaffolds of radially aligned nanofibers (FIGS. **14**A, **14**C) and randomly oriented nanofibers (FIGS. **14**B, **14**D) for 4 days using a custom cell culture system (FIG. **15**). FIGS. **14**C and **14**D are magnified views of the center portion shown in FIGS. **14**A and **14**B, respectively. The arrow marks the center of the scaffold.

As shown in FIG. **14**A, dural fibroblasts stained with fluorescein diacetate (FDA) migrated from the surrounding tissue along the radially aligned nanofibers and further to the center of the circular scaffold after incubation for 4 days. It was found that the cells could completely cover the entire surface of the scaffold in 4 days. In contrast, a void was observed after the same period of incubation time for a scaffold made of random fibers (FIG. **14**B), indicating faster migration of native cells on radially-aligned nanofiber scaffolds than the random counterparts. It is clear that the scaffold made of radially aligned nanofibers (shown in FIGS. **14**A and **14**C) was completely populated with dural cells which had migrated from the borders of the apposed dural tissue. On the contrary, an acellular region is clearly visible at the center of the scaffold made of randomly oriented nanofibers after the same incubation time, indicating cellular infiltration was incomplete and occurred at a slower rate.

In order to further investigate the effect of fiber alignment and nanofiber scaffold post-modification on cell migration, primary dural fibroblasts isolated from dura tissue were cultured on scaffolds of radially aligned and randomly oriented nanofibers with and without fibronectin coating. FIGS. **15**A-C are schematic diagrams of a custom-made cell culture system designed to model wound healing of tissue defects. Specifically, dural fibroblasts were selectively seeded around the periphery of a circular scaffold of nanofibers, effectively forming a 7-mm "simulated dural defect" in the center of the sample.

FIGS. **16**A-**16**D are fluorescence micrographs showing cell morphology and distribution on scaffolds of radially aligned nanofibers (FIGS. **16**A, **16**C) and randomly oriented nanofibers (FIGS. **16**B, **16**D) without and with fibronectin coating after incubation for 1 day. As shown in FIG. **16**A, many cells could attach to the uncoated scaffolds including radially aligned nanofibers. In comparison, fewer cells poorly attached to the uncoated scaffold of randomly oriented nanofibers and cell aggregations were noticed (FIG. **16**B). Seeded cells were distributed evenly over the entire surface of the fibronectin-coated scaffold of radially aligned nanofibers, and they exhibited an elongated shape parallel to the axis of nanofiber alignment (FIG. **16**C). This result indicates that fibronectin coating could enhance the influence of topographic cues on cell morphology provided by aligned fibers. The cells could also adhere well to the fibronectin-coated scaffold of randomly oriented nanofibers and cell distribution was more uniform than the uncoated samples, though no cell elongation or alignment was observed (FIG. **16**D). The random organization of cells on the randomly-oriented nanofiber scaffolds also mimics the organization of cells in scar tissue. This suggests that the aligned scaffolds may assist in reducing scar tissue formation by promoting more regular cell organization/function.

To characterize cell motility on the scaffold, cells were stained with FDA and fluorescence images were taken at different time points. FIGS. **17**A-**17**D are fluorescence micrographs showing the migration of dura fibroblasts seeded on fibronectin-coated scaffolds of radially aligned nanofibers for 1 day (FIG. **17**A), 3 days (FIG. **17**B), and 7 days (FIG. **17**C). FIG. **17**D is a magnified view of FIG. **17**C. The cells were radially aligned, replicating the alignment of fibers underneath, as shown in FIG. **17**D.

The ability of dural fibroblasts to migrate into and repopulate a simulated dural defect was measured at various time points throughout the experiment as an estimate of the regenerative capacity of the substitute. FIG. **18** is an illustration of the determination (e.g., calculation) of the area of simulated dural defect remaining on the scaffold at a given time point. FIG. **19** is an illustration of the area of void space as a function of incubation time. In FIG. **19**, "Random" indicates samples with a scaffold of random fibers; "Random F" indicates samples with a fibronectin-coated scaffold of random fibers; "Aligned" indicates samples with a scaffold of radially aligned fiber; and "Aligned F" indicates samples with a fibronectin-coated scaffold of radially aligned fibers. An asterisk (*) and a hash (#) indicate $p<0.05$ for samples compared with Random samples and Random F samples in the same period of incubation time.

The area of void decreased with increasing incubation time for all the scaffolds tested due to the inward migration of cells. As illustrated by FIGS. **17**A-**17**D, aligned fibers may significantly enhance cell migration compared to ran-

dom fibers, and cells migrated fastest on the fibronectin-coated scaffold of radially aligned nanofibers for the first 3 days of incubation. Around 5 mm^2 of surface area remained uncovered by cells on the uncoated random scaffolds even after incubation for 7 days. In contrast, cells covered almost the entire area of the simulated defect within the same period of incubation for other three types of scaffolds.

FIGS. **20**A-**20**D are fluorescence micrographs showing live dural fibroblasts labeled with membrane dye on scaffolds of radially aligned nanofibers with fibronectin coating after a 1-day culture (FIG. **20**A), a 3-day culture (FIG. **20**B), a 7-day culture (FIG. **20**C), and a 10-day culture (FIG. **20**D). FIG. **20**D includes an inset of a high magnification image of FIG. **20**D indicating that the cells were radially aligned on the aligned scaffolds. Cell migration towards the center of a fibronectin-coated scaffold of radially aligned nanofibers was further confirmed by time lapse imaging shown in FIGS. **20**A-**20**D.

Dural tissue is primarily composed of type I collagen. The production of type I collagen from dural fibroblasts was also examined. FIGS. **21**A-**21**D are fluorescence micrographs obtained by immunostaining of type I collagen with cell nuclei with 4',6-diamidino-2-phenylindole (DAPI) in blue for scaffolds of radially aligned fibers (FIGS. **21**A, **21**C) and randomly oriented fibers (FIGS. **21**B, **21**D). It was observed that comparable levels of type I collagen were produced by cells on the scaffolds of radially aligned fibers as compared to the scaffolds of random fibers although one previous study showed more elongated cells expressed higher collagen type I than did less elongated cells. Additionally, fibronectin coating had no significant influence on the production of type I collagen. The type I collagen was oriented haphazardly for the random scaffolds, resembling the extracellular composition of amorphous scar tissue, and had a high degree of organization for the radially aligned scaffolds, resembling healthy connective tissue

Recent advances in cell-biomaterial interaction have shown that both chemical and topographical properties of the materials surface can regulate and control cell shape and function. Cell orientation, motility, adhesion and shape can be modulated by specific surface micro- and nano-topographies. Cells can align along microgrooves or similar topographical features on a surface. It was demonstrated that fibroblasts were the most sensitive cell-type compared to endothelial cells and smooth muscle cells, and responded with a strong alignment, elongation, and migration along such topographical features.

Simultaneously, electrospinning has been widely used for producing nanofibers for a rich variety of applications in tissue engineering including skin grafts, artificial blood vessels, nerve repair, and others. Yet previous studies were limited to the use of scaffolds made of random and uniaxially-aligned nanofibers. Scaffolds composed of uniaxially-aligned nanofibers are not practical for wound healing applications due to the commonality of irregularly shaped wounds. The work described herein demonstrated for the first time the fabrication of a new type of scaffolds made of radially aligned nanofibers. This novel type of scaffold can guide dural fibroblasts spreading along the direction of fiber alignment and direct cell motility towards the center of the scaffold, resulting in faster cell migration and infiltration compared to scaffolds composed of randomly oriented nanofibers.

In addition, uniaxially aligned nanofiber scaffolds cannot match such a capability in that they can guide cell migration only in one direction. It was reported that controlling cellular orientation or morphology by topography, the so-called "contact guidance", could allow for the organization of extracellular matrix. For most injuries, repair results in previously functional tissue becoming a disorganized amalgam of cell (e.g., fibroblasts) and extracellular matrix (e.g., collagen fibers) known as a scar. Highly organized cells and extracellular matrix is required for proper tissue regeneration and function, which is normally vastly different from tissue repair with scarring. It has been demonstrated in the present work that extracellular matrix type I collagen on scaffolds of radially aligned nanofibers showed a high degree of organization, suggesting that radially-aligned nanofiber scaffolds may reduce the possibility of scar tissue formation following wound healing.

A dura substitute should be safe, efficacious, easy to handle, watertight, and easily integrated into the surrounding tissue to form new tissue similar to the native tissue. Also, it should avoid harmful foreign body reactions, be free of any potential risk of infections, have mechanical properties similar to those of natural dura mater, in particular with respect to flexibility and strength, be stable and/or storable, and be available for immediate use. In the present work, biodegradable polymer PCL was chosen as a material for dural substitute in that PCL has some advantages compared with other bioabsorbable polyesters. Heterogeneous degradation of PGA and poly(L-lactic acid) (PLLA) could lead to a sudden increase of degradation products, resulting in acidic conditions and toxic reactions in the surrounding tissue. The degradation of PCL is slower and produces less-acidic degradation products and has been studied as a wound dressing materials since the 1970s.

In order to obtain water-tight property, the radially-aligned nanofiber scaffold can be combined with nonwoven mat to form two-layered or even multi-layered substitutes. Simultaneously, antibiotics can be readily encapsulated inside nanofibers to further reduce inflammatory response, improve wound healing, and prevent postsurgery adhesion. Alternatively, PCL can be blended with other polymers to further improve its biocompatibility, as well as mechanical, physical, and chemical properties. Moreover, extracellular proteins and/or growth factors can be immobilized on the surface of the nanofibers using various surface modification approaches to enhance cell adhesion. The current work demonstrates the effect of fibronectin coating on the PCL nanofibers through electrostatic interaction on dural fibroblast adhesion and motility. The results presented herein demonstrate that fibronectin coating enhanced adhesion of dural fibroblasts and improved cell migration on randomly oriented nanofiber scaffolds. In contrast, the coating had marginal contribution to cell motility on radially aligned nanofiber scaffolds, compared to the bare scaffolds, indicating the predominant role played by nanofiber alignment and resulting surface topography.

In summary, the fabrication of a new type of electrospun nanofiber scaffold including radially aligned fibers and the potential application of such structures as dural substitutes are described herein. Dural fibroblasts cultured on scaffolds of radially aligned nanofibers were elongated parallel to the fiber axis, and cell migration towards the center of the scaffold was accelerated along with the development of a regular arrangement of extracellular matrix like type I collagen, potentially promoting fast regeneration and formation of neodura. Taken together, these results suggest that radially aligned nanofibers possess great potential as an artificial dural substitute, may offer an alternative in the repair of dural defects, and furthermore occupy a unique, desirable niche within the neurosurgical community.

Additional Experimental Results

In a typical procedure for electrospinning PCL (Mw=65 kDa, Sigma-Aldrich) nanofibers, a solution of 20% (w/v) PCL in a mixture of dichloromethane (DCM) and N, N-dimethylformamide (DMF) (Fisher Chemical) with a volume ratio of 8:2 was used. The fibers were spun at 10-17 kV with a feeding rate ranging from 0.5 mL/h, together with a 23 gauge needle as the spinneret. A piece of aluminum foil was used as a collector to obtain random nanofiber scaffolds. Radially aligned nanofiber scaffolds were fabricated utilizing a collector consisting of a ring electrode (e.g., metal ring) and a point electrode (e.g., a sharp needle). Electrospun PCL nanofibers were coated with fibronectin (Millipore, Temecular, Calif.) as the following. The electrospun fiber scaffolds were sterilized by soaking in 70% ethanol overnight and washed three times with phosphate buffered saline (PBS). Then, the scaffolds were immersed in a 0.1% poly-$_L$-lysine (PLL) (Sigma-Aldrich) solution for one hour at room temperature, followed by washing with PBS buffer (Invitrogen) three times. Subsequently, the samples were immersed in a fibronectin solution (26 μL 50 μg/mL fibronectin solution diluted with 5 mL PBS buffer) at 4° C. overnight. Prior to cell seeding, the fibronectin solution was removed and the nanofiber scaffolds were rinsed with PBS buffer.

The PCL nanofiber scaffolds were sputter-coated with gold before imaging with scanning electron microscope (Nova 200 NanoLab, FEI, Oregon, USA) at an accelerating voltage of 15 kV. Samples prepared for use in cell culture were inserted into a 24-well TCPS culture plate and sterilized by soaking scaffolds in 70% ethanol.

Fibroblasts were isolated from sections of explanted dura. Specifically, a 2.0 cm×1.5 cm section of dura was removed through sharp dissection and washed three times with cold PBS. Dural fibroblasts were then isolated by digesting minced dura three times in 4 mL of warm Hank's Balanced Salt Solution (HBSS) containing 0.05% Trpsin and 0.04% EDTA (Sigma-Aldrich, St. Louis, Mo.). Following digestion collected supernatant was centrifuged and the pellet of dural cells was isolated and resuspended in Dulbecco's modified Eagle's medium (DMEM) supplemented with 10% calf serum and 1% penicillin and streptomycin. Dural cells obtained in this manner were then plated in 75 cm^2 flaks and expanded (subpassaged no more than 5 times).

Large continuous pieces of dura mater were placed in cold PBS and microsurgically trimmed into 1 cm×1 cm sections. An artificial defect was then introduced into each section of dura by microsurgically cutting a small circular hole, 7 mm in diameter, in the middle of the section. Sections of dura were then introduced into individual wells of 6-well culture plates containing 4 mL of DEMEM supplemented with 10% calf serum and 1% penicillin and streptomycin. Random and radially aligned nanofiber scaffolds 1 cm in diameter were then utilized to repair the artificial defects by overlaying the graft onto the dural specimen. Nanofiber scaffolds were placed on the dura such that the graft covered with entire defect while simultaneously contacting the dural tissue at the periphery of the specimen. Nanofiber scaffolds were held in this position throughout the experiment by placing a sterilized metal ring over both the scaffold and the dura. After 4 days of culture, the cells were stained with FDA in green color and imaged with fluorescence microscope. Fluorescent images were taken using a QICAM Fast Cooled Mono 12-bit camera (Q Imaging, Burnaby, BC, Canada) attached to an Olympus microscope with OCapture 2.90.1 (Olympus, Tokyo, Japan). Similarly, around 1×10^5 dural fibroblast cells were seeded onto the periphery of nanofiber scaffolds using the custom-made culture system shown in FIGS. **15**A-C. After different periods of time, the cells were stained with FDA in green color and imaged with fluorescence microscope. The total surface area of nanofiber scaffold devoid of migrating cells was then quantified using Image J software (National Institute of Health).

Living cells were labeled with membrane dye using VYBRANT DiO cell-labeling solution (Invitrogen) according to the manufacturer's instructions and then imaged at day 1, 3, 7, and 10.

Production of collagen type I by the dural fibroblasts on the fiber scaffolds was assessed using immunohistochemistry. At day 7, the cells were rinsed with PBS and fixed with 3.7% formalin for 1 h (N=4). Cells were permeabilized using 0.1% Triton X-100 (Invitrogen) in PBS for 20 min, followed by blocking in PBS containing 5% normal goat serum (NGS) for 30 min. Monoclonal antibodies for type I collagen (1:20 dilution) was obtained from EMD Chemicals (Calbiochem, San Diego, Calif.). Cells were washed three times with PBS containing 2% FBS. The secondary antibody Gt×Rb IgG Fluor (Chemicon, Temecula, Calif.) (1:200 dilution) was applied for 1 h at room temperature. Fluorescent images were taken using a QICAM Fast Cooled Mono 12-bit camera (Q Imaging, Burnaby, BC, Canada) attached to an Olympus microscope with OCapture 2.90.1 (Olympus, Tokyo, Japan).

Mean values and standard deviation were reported. Comparative analyses were performed using the Turkey post hoc test by analysis of variance at a 95% confidence level.

As a secondary study, an ex vivo model of the surgical repair of a small dural defect was developed. Large pieces of healthy dura mater (3 cm×3 cm) were placed into cold, supplemented Dulbecco's Modified Eagle Media (DMEM) and microsurgically trimmed into smaller (1 cm×1 cm) pieces. Artificial defects were introduced into the pieces of dura by microsurgically cutting small circular holes, 6-8 mm in diameter, into the middle of the specimens. Radially aligned nanofiber scaffolds, randomly oriented nanofiber scaffolds, and DURA MATRIX collagen scaffolds (1 cm×1 cm) were then utilized to repair the artificial defects by overlaying the graft onto the dural specimen, such that the graft covered the entire defect while simultaneously contacting the dural tissue at the periphery of the specimen.

Assemblies of dural/dural substitute were then cultured in vitro in supplemented DMEM for a period of four days. At the terminal time point, optical and fluorescent microscopy was utilized to assess the regenerative capacity of the substitute, defined as the ability of dural cells to migrate onto the artificial substitute and repopulate the acellular region of the dural substitute within the artificial defect.

Results demonstrated that native cells present in intact dura (primarily dural fibroblasts) readily migrated onto apposed polymeric nanofiber dural substitutes in high concentrations within 24 to 48 hours after coming into contact with pieces of explanted dura. Dural cell migration onto gold-standard collagen matrices followed a similar time course, though slightly lower concentrations of dural cells were observed migrating onto collagen matrices compared to nanofiber dural substitutes. This observation suggests that nanofiber dural substitutes easily adhere to native dural tissue, an important quality regarding the intraoperative handling and/or placement of the material, and that nanofiber dural substitutes provide an ideal substrate for dural fibroblast adhesion.

Further examination of the various dural substitutes after four days of culture revealed that dural fibroblast migration into the central, acellular region of the material proceeded

significantly faster on radially aligned nanofiber substitutes than on randomly oriented nanofiber substitutes or collagen matrices. This finding was evidenced by the fact that after four days of culture, a prominent acellular region ("void space") remained on samples of both the random nanofiber substitute and the collagen matrix.

In contrast, samples of radially aligned nanofiber materials examined at the same time point were completely populated with dural cells which had migrated from the borders of the apposed dural tissue. In effect, radially aligned nanofiber substitutes were able to induce significantly faster "healing" of this simulated dural defect than both randomly oriented materials. High magnification views of dural substitutes within this ex vivo culture further demonstrated the ability of radially aligned nanofiber materials to align and direct native, migratory dural cells, a result similar to that of the previous study conducted using pre-seeded dural fibroblasts. Specifically, dural cells were noted to align and extend parallel to individual nanofibers within the artificial substrate, as well as deposit organized extracellular matrix proteins (namely type I collagen) on the aligned nanofiber materials. This observation suggests that the topographical cues presented by aligned nanofiber substitutes are capable of organizing and directing native dural cells migrating from intact dura, and may enhance the ability of these migratory cells to deposit extracellular matrix proteins necessary to heal and repair dural defects.

Results of this secondary study demonstrate that nanofiber dural substitutes not only provide a favorable scaffold for dural cell adhesion and migration, but readily support the ingrowth of dural cells from whole, intact dura mater. The ability of nanofiber materials to intimately interface intact dura mater and facilitate rapid cellular population of the polymeric scaffold strongly suggest that this material may function exceptionally well as an artificial graft in the surgical repair of complex dural defects. In addition, dural substitutes constructed of radially aligned nanofibers were demonstrated to promote faster "healing" of simulated dural defects than randomly oriented materials, suggesting that aligned nanofiber scaffolds imparting nanoscale topographical features may represent a significant technological advance over clinical gold-standard collagen matrices.

Although experiments described herein were limited in duration, the results of these experiments suggest that biomedical patches including radially aligned fibers are viable for use in tissue repair at longer durations. For example, it is expected that the observed accelerated cellular ingrowth would continue until the biological tissue at the site of a defect is completely regenerated and/or until degradation of the biomedical patch is complete.

In Vivo Experimental Results

In vivo experimentation was performed by imposing a 12 millimeter diameter dural defect in native porcine dura. The defect was repaired with a collagen dural substitute, a mono-layer dural substitute with randomly oriented nanofibers, and a bi-layer dural substitute with one layer of radially aligned nanofibers fused to a second layer of randomly oriented nanofibers through layer-by-layer stacking (e.g., as described above with reference to FIG. **8**). In a control group, the defect was unrepaired.

FIG. **22** is a graph **2200** illustrating the thickness of regenerated dura at the center of repaired dural defects over time. In graph **2200**, a y-axis **2205** represents the total thickness of regenerated dura, including both regenerative tissue and the integrated dural substitute material, at the center of a dural defect. Samples with no dural substitute (control samples), a collagen dural substitute, a mono-layer randomly oriented nanofiber dural substitute, and a bi-layer radially aligned nanofiber dural substitute are grouped by elapsed time on an x-axis **2210**.

FIG. **23** is a graph **2300** illustrating regenerative collagenous tissue content over time. In graph **2300**, a y-axis **2305** represents the percentage of regenerated dura that is composed of regenerative collagenous tissue. Samples with a collagen dural substitute, a mono-layer randomly oriented nanofiber dural substitute, and a bi-layer radially aligned nanofiber dural substitute are grouped by elapsed time on an x-axis **2310**.

Electrode Arrays

In some embodiments, a collector includes a plurality of electrodes at least partially circumscribing an area and a second electrode positioned within the area. The electrodes may be arranged in an array, such as a grid and/or other polygonal pattern, and a polymer deposited on the electrodes may form fibers extending between the electrodes of the collector, such that the fibers define the sides of a plurality of polygons, with the electrodes positioned at the vertices of the polygons. In some embodiments, the structure created by such fibers may be used to create a cell microarray, such as by seeding the structure with cells and incubating the cells to promote propagation of the cells throughout the structure.

Cell microarrays may provide powerful experimental tools for high-throughput screening useful in a number of applications ranging from drug discovery and toxicology to stem cell research and tissue engineering. For example, cell microarrays may represent an effective means of fabricating ordered neuronal networks useful in studying synapse formation and neuronal plasticity in vitro. At least some known techniques for fabrication of neuronal microarrays have concentrated on the use of spatial patterning of cell adhesive and/or cell repulsive materials and agents. Unfortunately, such fabrication techniques may be time consuming and costly, and involve the use of sophisticated instrumentation (e.g., photolithography, soft lithography, contact printing, microfluidics, nanoprinting, and inkjet printing).

Electrospinning is capable of producing one-dimensional fibers with diameters ranging from several nanometers to several microns. The large surface area to volume ratio and nanoscale morphology of electrospun nanofibers may suggest that these materials effectively mimic the architecture of extracellular matrix (ECM). As a result, electrospun nanofiber materials have been utilized in a wide variety of biomedical applications. Electrospun nanofibers may be deposited on a conductive collector in a random fashion and/or aligned into uniaxial arrays through manipulation of an electric field and/or application of mechanical force.

Embodiments described herein facilitate producing a complex cell microarray using electrospun nanofibers. In exemplary embodiments, a collector with an array of electrodes is used to fabricate electrospun nanofiber scaffolds that include a complex, ordered architecture and numerous multiwells. Such a scaffold may be valuable at least for i) cell microarray formation; and ii) neuronal network formation. The use of presented complex nanofiber arrays may facilitate the creation of advanced substrates useful in neural engineering applications and cell arrays useful in bio-sensing and drug screening applications.

FIG. **24** is a diagram illustrating a perspective view of an example electrospinning system **2400** for producing a structure of polygonally aligned fibers using an array of electrodes. System **2400** is similar to system **100** (shown in FIG. **1**) in structure and operation. A collector **2405** includes a plurality of first electrodes **2410**, which may be referred to as peripheral electrodes. First electrodes **2410** define and/or

at least partially circumscribe an area **2415**, such as a polygon. As illustrated in FIG. **24**, the area **2415** defined by first electrodes **2410** is a hexagon. A second electrode **2420**, which may be referred to as an inner electrode, is positioned within (e.g., approximately at the center of) area **2415**, such that first electrodes **2410** surround second electrode **2420**. In exemplary embodiments, first electrodes **2410** and second electrodes are metallic (e.g., stainless steel) beads having a diameter between 0.5 millimeters (mm) and 5.0 mm (e.g., 1.0 mm or 2.0 mm).

System **2400** also includes a spinneret **120** and is configured to create an electric potential between collector **2405** and spinneret **120**, as described above with reference to FIG. **1**. In exemplary embodiments, peripheral electrodes **2410** and inner electrode **2420** are electrically coupled to a power supply **130** via a conductor **135**, and spinneret **120** is coupled to power supply **130** via a conductor **145**. Power supply **130** is configured to charge peripheral electrodes **2410** at a first amplitude and/or polarity via conductor **135**, and to charge spinneret **120** at a second amplitude and/or polarity, opposite the first polarity, via conductor **145**.

In the embodiment illustrated in FIG. **24**, peripheral electrodes **2410** and inner electrode **2420** are metallic (e.g., stainless steel) beads or balls, which may be referred to as "microbeads," arranged in a hexagonal pattern. In some embodiments, circular enclosed area **125** may have a diameter of between 1 centimeter and 20 centimeters. In other embodiments, peripheral electrodes **2410** and inner electrode **2420** may be any shape and/or may be arranged in any pattern suitable for use with the methods described herein. For example, peripheral electrodes **2410** and inner electrode **2420** may be pins, rods, domes, and/or ridges. Further, peripheral electrodes **2410** and inner electrode **2420** may be arranged in an octagonal, pentagonal, and/or square pattern, for example, though other polygonal and non-polygonal arrangements, regular and/or irregular, are also contemplated.

In one embodiment, area **2415** defines a horizontal plane **2425**. Spinneret **120** is aligned with inner electrode **2420** and vertically offset from horizontal plane **2425** at a variable distance. For example, spinneret **120** may be vertically offset from horizontal plane **2425** at a distance of 1 centimeter to 100 centimeters. In exemplary embodiments, inner electrode **2420** and/or peripheral electrodes **2410** include a rounded (e.g., convex) surface, such as the surface of the metallic beads shown in FIG. **24**, oriented toward horizontal plane **2425**.

As described above with reference to FIG. **1**, spinneret **120** is configured to dispense a polymer **140** while spinneret **120** is electrically charged at the second amplitude and/or polarity, and peripheral electrodes **2410** and inner electrode **2420** are electrically charged at the first amplitude and/or polarity. Spinneret **120** dispenses polymer **140** as a stream **160**. Stream **160** has a diameter approximately equal to the aperture diameter of spinneret **120**. Stream **160** descends toward collector **2405**. For example, stream **160** may fall downward under the influence of gravity and/or may be attracted downward by a charged conductive surface **162** positioned below collector **2405**. For example, conductive surface **162** may be electrically coupled to conductor **135** and charged at the same amplitude and/or polarity as peripheral electrodes **2410** and central electrode **2420**. As stream **160** descends and is deposited on collector **2405**, polymer **140** forms one or more solid polymeric fibers **2430** extending from inner electrode **2420** to a peripheral electrode **2410** and/or between peripheral electrodes **2410**.

In some embodiments, collector **2405** includes peripheral electrodes **2410** that define a plurality of areas **2415**. For example, peripheral electrodes **2410** immediately surrounding inner electrode **2420** may be considered inner peripheral electrodes, and a plurality of outer peripheral electrodes **2435** may surround inner peripheral electrodes **2410**, such that inner peripheral electrodes **2410** are nested within outer peripheral electrodes **2435**. Collector **2405** may include any quantity of nested sets of peripheral electrodes. While collector **2405** includes electrodes in a closely-packed arrangement (e.g., with electrodes contacting each other), it is contemplated that electrodes may be displaced from each other by an inter-electrode distance, which may be constant throughout the collector or may vary between different pairs of electrodes.

Further, in some embodiments, a collector may include electrodes that define a plurality of partially overlapping areas in a modular fashion. FIG. **25** is a diagram illustrating a perspective view of an example modular electrospinning collector **2500**. Collector **2500** includes first electrodes **2505** surrounding a second electrode **2510**. First electrodes **2505** define a first hexagonal area **2515**. With respect to first hexagonal area **2515**, second electrode **2510** may be considered an inner electrode, and first electrodes **2505** may be considered peripheral electrodes.

Collector **2500** also includes a plurality of third electrodes **2520** that are positioned outside first hexagonal area **2515**. Third electrodes **2520**, second electrode **2510**, and a subset of first electrodes **2505** define a second hexagonal area **2525** that partially overlaps first hexagonal area **2515**. One of the first electrodes **2505** (e.g., a peripheral electrode with respect to first hexagonal area **2515**) is positioned within second hexagonal area **2525**. With respect to second hexagonal area **2525**, this first electrode **2505** may be considered an inner electrode. Third electrodes **2520**, the subset of the first electrodes **2505**, and the second electrode **2510** may be considered peripheral electrodes. Although electrodes defining two partially overlapping areas are illustrated in FIG. **25**, it is contemplated that the modular nature of collector **2500** facilitates including any quantity of electrodes that define any quantity of areas, such that collector **2500** may be extended in one or more directions by adding electrodes to the perimeter of collector **2500**.

As described above with reference to system **2400** (shown in FIG. **24**), collector **2500** (e.g., first electrodes **2505**, second electrode **2510**, and third electrodes **2520**) is configured to be electrically charged at an amplitude and/or a polarity opposed the amplitude and/or polarity at which spinneret **120** is electrically charged. When these components are so charged, a polymer dispensed by spinneret **120** may form fibers extending between the electrodes (e.g., first electrodes **2505**, second electrode **2510**, and/or third electrodes **2520**) of collector **2500**.

FIG. **26** is a diagram **2600** illustrating an electric field generated by an electrospinning system such as electrospinning system **2400** (shown in FIG. **24**). Diagram **2600** shows a two dimensional, cross-sectional view of electric field strength vectors between a spinneret **120** and a plurality of electrodes **2605**.

Electric field vectors near the surface of electrodes **2605** are oriented perpendicular to the surface of electrodes **2605**. Electric field vectors between two neighboring electrodes split into two main streams, pointing towards the centers of the two adjacent electrodes **2605**. Accordingly, fibers deposited on the surface of electrodes **2605** may be randomly distributed, while the fibers deposited in the region between

two neighboring electrodes **2605** may be uniaxially aligned between these two adjacent electrodes **2605**.

FIGS. **27**A-**27**F are microscopy images of a nanofiber membrane **2705** produced using a collector with an array of electrodes, such as collector **2405** (shown in FIG. **24**). For example, membrane **2705** may be produced using an array of stainless steel beads. FIG. **27**A is an optical microscopy image of a membrane **2705**. FIG. **27**A includes an inset **2710** illustrating a magnification of membrane **2705** with a light source on the right-hand side of the image. Shadows in inset **2710** indicate wells within membrane **2705**, the positions of which correspond to the positions of electrodes in the collector.

FIG. **27**B is a scanning electron microscopy (SEM) image of membrane **2705** illustrating the complex, ordered architecture composed of hexagonally arranged wells **2715** connected with uniaxially aligned fiber arrays **2720**. The depth of the wells formed by depositing electrospun nanofibers on packed stainless steel microbeads 1.0 mm and 2.0 mm in diameter was approximately 200 micrometers (μm) and 400 μm, respectively. Such wells may be referred to as "microwells."

FIGS. **27**C-**27**F are magnifications of corresponding areas within FIG. **27**B. FIG. **27**C suggests that the fibers deposited on the surface of microbead electrodes were randomly distributed. FIG. **27**D shows that the fibers at the interface between the surface of an electrode and a gap between electrodes transitioned from a random orientation to an aligned orientation. FIG. **27**E indicates that fibers deposited along the axis connecting the centers of two adjacent electrodes were uniaxially aligned parallel to that axis. FIG. **27**F shows that the fiber density was significantly lower between neighboring beads and away from the axes connecting the centers of adjacent beads than in other regions (e.g., shown in FIGS. **27**C-**27**E), and that fiber deposited in this region were randomly oriented.

In some embodiments, a fiber membrane, such as membrane **2705**, may be combined with other membranes. For example, a membrane with a plurality of wells interconnected by uniaxially aligned fibers may be used as one layer within a multi-layer structure, as described above with reference to FIG. **8**. In addition, or alternatively, different collector types may be combined, such as by using an electrode array collector as an inner collector (e.g., corresponding to a center of a biomedical patch, and using a ring-type collector (e.g., as shown in FIG. **1**) as an outer collector that surrounds the inner collector.

Experimental Results

Fiber membranes, or "scaffolds," produced by an electrode array collector as described above were evaluated for use as substrates for generating cell microarrays. Cells were selectively seeded onto the surface of the scaffold by placing a small amount of media, containing specified number of cells, onto the microwells present within the nanofiber arrays.

FIGS. **28**A-**28**D are microscopy images illustrating cell growth in a membrane such as membrane **2705** (shown in FIGS. **27**A-**27**F). FIG. **28**A is an optical microscopy image illustrating that droplets **2805** containing cells may be placed within the wells of a fiber membrane. Further, hydrophobic fibers may facilitate maintaining such droplets for over two hours. Cells adherent to the nanofiber matrices after two hours were found to be loosely attached and were easily removed using PBS buffer, suggesting fast, reversible binding of cells within the microarrays. Cells adherent to the nanofiber matrices after twenty-four hours were stained with fluorescein diacetate (FDA) in green to identify living cells.

FIGS. **28**B-**28**D are fluorescence microscopy images illustrating cell microarrays. Live MG-63 cells were stained with fluorescein diacetate and are shown as light areas against a dark background in FIGS. **28**B-**28**D.

FIG. **28**B shows an array of cells selectively adhered to the microwells within the nanofiber membrane. Each well within the scaffold was observed to contain approximately 45 cells, while very few cells were observed outside of the microwells within the fiber membrane. The average number of cells adherent on each microwell was easily manipulated by controlling the density of cells present within the seeding droplets.

FIG. **28**C demonstrates cell microarrays seeded with greater numbers of cells (approximately 150 cells per well) than were used in the arrays shown in FIG. **28**B. Despite increasing cell concentrations, cells remained greatly confined to the wells in the nanofiber scaffold. FIG. **28**D shows the same cell microarray shown in FIG. **28**C after incubation for three days. Comparison of FIG. **28**D to FIG. **28**C demonstrates that seeded cells were capable of proliferating and migrating on the surface of the nanofiber scaffolds, yet generally remained physically confined within the wells of the cell microarray.

In order to examine the potential of these unique nanofiber scaffolds as effective substrates for neural engineering applications, dorsal root ganglia (DRG) were seeded onto fiber membranes functionalized with polylysine and laminin and incubated for 6 days. Resulting neurite fields protruding from DRG were stained with anti-neurofilament **200** to visualize neurite extension along the underlying nanofiber scaffold.

FIGS. **29**A and **29**B are microscopy images illustrating neurite propagation in a membrane such as membrane **2705** (shown in FIGS. **27**A-**27**F). FIG. **29**A is an overlay of an optical microscopy image and a fluorescence microscopy image illustrating that neurites emanated from a DRG main body located at the center of FIG. **29**A and formed an appreciable neuronal network after 6 days of culture. Neurites were observed to grow along the long axes of uniaxially aligned nanofibers and reach neighboring microwells, effectively replicating the geometry of the underlying nanofiber architecture.

FIG. **29**B is an overlay of an optical microscopy image and a fluorescence microscopy image adjacent to the region shown in FIG. **29**A. FIG. **29**B demonstrates that neurites may continue growing along the direction of uniaxial alignment of nanofibers after reaching the neighboring wells and navigate to other neighboring wells along the fiber alignment in several directions. Neurites extending to adjacent microwells were subsequently observed to split into five groups following the aligned fiber arrays which connected to a secondary set of adjacent wells, further indicating capability of the scaffold to form a complex neuronal network in vitro.

FIGS. **30**A and **30**B are overlays of an optical microscopy image and a fluorescent microscopy image illustrating neuronal network formation from embryoid bodies in a membrane such as the membrane shown in FIGS. **27**A-**27**F. Embryonic stem (ES) cells, cultured to aggregate into embryoid bodies (EBs) using the 4−/4+ protocol, were seeded onto electrospun nanofiber scaffolds such as that shown in FIGS. **27**A-**27**F, and incubated with B27 supplement to induce neuronal differentiation. Immunostaining with Tuj1, a neuronal marker, was performed after incubation for 14 days to examine the ability of underlying nanofiber scaffolds to promote neuronal differentiation in vitro.

FIGS. **30**A and **30**B demonstrate the ability of EBs to form neuronal networks on nanofiber membrane substrates. In one case, one EB was confined within one of the microwells, while neurites extended peripherally along the underlying fiber pattern, as shown in FIG. **30**A. Neurites extending from cultured EBs were similarly aligned on the uniaxial portion of the scaffold where fibers were highly organized. Upon reaching the region of the adjacent wells, neurites were haphazardly organized as a result of the random orientation of the underlying fibers.

In another case, EBs were seeded on regions of uniaxially aligned nanofibers within the nanofiber array, as shown in FIG. **30**B. Neurites again extended along the direction of fiber alignment, and, upon reaching the nearest well, exhibited a disordered organization. Notably, when the neurites extended through the microwell region, their uniaxial alignment, parallel to the underlying fiber alignment, was restored. Together, these results suggest that nanofiber architectures described herein represent a simple and effective means of developing complex neuronal networks from either primary neurons or embryonic stem cells.

Experimental Procedure

The electrospinning system used for fabricating and collecting aligned nanofibers was similar to system **2400** (shown in FIG. **24**). The polymer solution used for electrospinning contained 20% PCL (w/v) in a mixed solvent of dichloromethane (DCM) and dimethylformaldehyde (DMF) with a volume ratio of 80:20. The collector included assemblies of stainless steel microbeads with diameters of 1 mm and 2 mm, respectively. The fiber membranes were transferred to culture plates and then fixed by medical grade silicon adhesive. The PCL fibers were sputter-coated with gold before imaging with scanning electron microscope at an accelerating voltage of 15 kV.

For dorsal root ganglia (DRG) culture and immunostaining, DRG were dissected from the thoracic region of embryonic day 8 chicks (E8, stage HH35-36) and collected in Hank's buffered salt solution (HBSS) prior to plating. DRG were seeded on the fiber architectures and incubated for 6 days in modified neurobasal (NB) media containing 1% ABAM, 1% N-2 supplement (Invitrogen), and 30 ng/mL Beta nerve growth factors (B-NGF) (R&D Systems, Minneapolis, Minn.). After incubation for 6 days, the DRG were immunostained with the marker anti-neurofilament **200** (Sigma-Aldrich). Briefly, the DRG were fixed in 3.7% formaldehyde for 45 minutes and permeabilized by 0.1% Triton X-100 for 30 minutes. The samples were blocked in PBS containing 2.5% bovine serum albumin (BSA) (Sigma-Aldrich) for 1 hour. Anti-NF **200** diluted with PBS containing 1.5% BSA was applied to the cells overnight at 4° C. A secondary antibody, AlexaFluor 488 goat anti-mouse IgG (1:200, Invitrogen), was then applied for 1 hour at room temperature. After staining, fluorescence images were captured.

For embryoid body formation and immunostaining, EBs were seeded onto fiber architectures and incubated with neural basal media containing B27 supplement. After 14 days, immunohistochemistry was performed to visualize the spatial distribution of neurites according to our previous study.

The MG-63 cell line was used to demonstrate the formation of cell microarrays. Cells were cultured in alpha minimum essential medium (α-MEM, Invitrogen, Grand Island, N.Y.), supplemented with 10% fetal bovine serum (FBS, Invitrogen) and 1% antibiotics (containing penicillin and streptomycin, Invitrogen). The medium was changed every other day, and the cultures were incubated at 37° C. in a humidified atmosphere containing 5% CO_2. A certain number of cells were seeded into each well of the scaffolds by placing small droplets onto wells. After incubation for 2 hours, the scaffolds were washed with culture media to remove the loosely attached cells. Then, the living cells were stained with fluorescein diacetate (FDA) after incubation for 24 hours and imaged with fluorescence microscope.

Additional Electrode Array Arrangements

In addition to particular examples of electrode arrays described above with reference to experimental results, it is contemplated that nanofiber structures such as those described herein may be produced with various other electrode arrays. FIGS. **31**A-**31**D are scanning electron microscopy images illustrating membranes produced using a variety of electrode arrays.

FIG. **31**A illustrates a fiber membrane fabricated using a collector composed of hexagonal arrays of stainless steel beads. FIG. **31**B illustrates a fiber membrane fabricated using a collector composed of hexagonal arrays of stainless steel beads having a larger diameter than the stainless steel beads used to produce the membrane shown in FIG. **31**A.

Other, non-hexagonal, packing orders may also be employed with the electrodes to achieve different geometries. FIG. **31**C shows a fiber membrane fabricated using a collector composed of a close-packed square array of stainless steel beads. FIG. **31**D shows a fiber membrane produced using a collector composed of square arrays of stainless steel microbeads with a gradual increase of the inter-electrode distance in one direction. The fiber membranes were not removed from the collectors during SEM imaging and can be readily removed (e.g., peeled off) from collectors as needed.

FIG. **32** is a diagram of a collector **3200** with peripheral electrodes **3205** partially circumscribing an area **3210**. Collector **3200** also includes an inner electrode **3215**. Peripheral electrodes **3205** and inner electrode **3215** define a portion **3220** of area **3210**. In exemplary embodiments, peripheral electrodes **3205** are positioned on a perimeter **3225** of area **3210**.

In the embodiment shown in FIG. **32**, area **3210** is shown as an ellipse (e.g., a circle), and portion **3220** is shown as a sector of the ellipse. It is contemplated that area **3210** may be any geometric or non-geometric shape, such as an ellipse, polygon, oval, rectangle, square, triangle, and/or any rectilinear or curvilinear shape, and that portion **3220** may be any portion of such a shape.

Electrode array fiber structures described herein enable the formation of "dimple" structures within a fiber membrane. Accordingly, the production of such membranes represents a significant advance in that the fiber membranes described possess multiple microwells arranged into variable, ordered geometries. Furthermore, such structures possess unique, three-dimensional microwells capable of physically confining cells seeded on the surface of the scaffold and facilitating the fabrication of cell microarrays. Compared to known approaches to microarray fabrication, the use of fiber membranes may be a simpler and less expensive technique for forming complex cell microarrays for in vitro and in vivo use. Further, experimental results described above demonstrate that the neurites on the site of wells presented random distribution, and that neurites could bridge from one well to another along the aligned fibers in between. A neuronal network developed using such a structure could be used for high-throughput applications in neurotoxicology and neurodevelopmental biology.

While the making and use of various embodiments of the invention are discussed in detail above, the embodiments of

the invention provide many applicable inventive concepts that may be embodied in a wide variety of specific contexts. The specific embodiments discussed herein are merely illustrative of specific ways to make and use the invention and do not delimit the scope of the invention.

To facilitate the understanding of this invention, a number of terms are defined below. Terms defined herein have meanings as commonly understood by a person of ordinary skill in the areas relevant to the embodiments of the invention. Terms such as "a," "an" and "the" are not intended to refer to only a singular entity, but include the general class of which a specific example may be used for illustration. The terminology herein is used to describe specific embodiments of the invention, but their usage does not delimit the invention, except as outlined in the claims.

The order of execution or performance of the operations in embodiments of the invention illustrated and described herein is not essential, unless otherwise specified. For example, it is contemplated that executing or performing a particular operation before, contemporaneously with, or after another operation is within the scope of aspects of the invention. Embodiments of the invention may include additional or fewer operations than those disclosed herein.

What is claimed is:

1. A biomedical patch device for tissue repair, the biomedical patch device comprising:

a first polymeric scaffold comprising a first structure of fibers having electrospun nanofibers, the first structure of fibers comprising randomly oriented fiber sections, the first structure of fibers configured to promote cell growth for a first period of time upon application of the biomedical patch to a tissue, wherein the first period of time is less than three months; and

a second polymeric scaffold comprising a second structure of fibers having electrospun nanofibers, the second structure of fibers comprising a plurality of radially aligned fiber sections and a plurality of randomly oriented fiber sections,

wherein one or more of the plurality of radially aliened fiber sections transition into one or more of the plurality of randomly oriented fiber sections of the second structure of fibers, wherein one or more of the plurality of radially aliened fiber sections is overlaid on one or more of the plurality of randomly oriented fiber sections of the second structure of fibers,

the second structure of fibers configured to provide structural reinforcement to the first polymeric scaffold for a second period of time upon application of the biomedical patch to the tissue, wherein the second period of time is less than three months;

the first structure of fibers and the second structure of fibers generated by depositing via electrospinning a first polymer composition and a second polymer composition, the first polymer composition being different from the second polymer composition;

the biomedical patch device further comprising a surface configured to contact tissue upon application of the biomedical patch,

the surface, the first polymeric scaffold, and the second polymeric scaffold of the biomedical patch device sufficiently pliable to facilitate application of the biomedical patch device to uneven surfaces of the tissue,

the surface, the first polymeric scaffold, and the second polymeric scaffold of the biomedical patch device sufficiently pliable to enable movement of the biomedical patch device with the tissue, and

the surface, the first polymeric scaffold, and the second polymeric scaffold of the biomedical patch device comprising sufficient durability to maintain stability of the biomedical patch for a storage period prior to application of the biomedical patch device to the tissue.

2. The biomedical patch of claim **1**, wherein a first portion of the biomedical patch of a particular size comprises a higher number of fibers than a second portion of the biomedical patch of the particular size.

3. The biomedical patch of claim **2**, wherein the surface comprises a surface pattern formed by positioning a mask between a collector and a spinneret, wherein the mask is configured to prevent depositing at least some of the first structure of fibers or the second structure of fibers on the collector.

4. The biomedical patch of claim **2**, wherein the surface comprises a surface pattern formed by depositing the first structure of fibers and the second structure of fibers directly on a collector without a mask.

5. The biomedical patch of claim **4**, wherein the surface pattern comprises a plurality of organized features.

6. The biomedical patch of claim **1**, wherein at least a portion of the first structure of fibers and at least a portion of the second structure of fibers are deposited simultaneously.

7. The biomedical patch of claim **1**, wherein the surface comprises a plurality of structural features configured to align cells.

8. The biomedical patch of claim **1**, wherein the first structure of fibers and the second structure of fibers comprise one or more randomly oriented fibers.

9. The biomedical patch of claim **1**, wherein the first structure of fibers and the second structure of fibers comprise one or more radially aligned fibers.

10. The biomedical patch of claim **1**, wherein the first structure of fibers and the second structure of fibers comprise one or more uniaxially aligned fibers.

11. A biomedical wound matrix for facilitating wound healing, the biomedical wound matrix comprising:

a first polymeric scaffold comprising a first structure of fibers having electrospun nanofibers, the first structure of fibers comprising a plurality of randomly oriented portions of fibers, the first structure of fibers configured to promote cell growth upon application of the biomedical wound matrix to a tissue; and

a second polymeric scaffold comprising a second structure of fibers having electrospun nanofibers, the second structure of fibers comprising a plurality of radially aligned portions of fibers and a plurality of non-radially aligned portions of fibers,

wherein one or more of the plurality of radially aliened portions of fibers transition into one or more of the plurality of non-radially aliened portions of fibers of the second structure of fibers, wherein one or more of the plurality of radially aligned portions of fibers is overlaid on one or more of the plurality of non-radially aliened portions of fibers of the second structure of fibers,

the second structure of fibers configured to provide structural reinforcement to the first polymeric scaffold;

the first structure of fibers and the second structure of fibers generated by depositing via electrospinning a first polymer composition and a second polymer composition, the first polymer composition being different from the second polymer composition;

the biomedical wound matrix further comprising a surface configured to contact tissue upon application of the biomedical wound matrix,

the surface, the first polymeric scaffold, and the second polymeric scaffold of the biomedical wound matrix sufficiently pliable to facilitate application of the biomedical wound matrix to uneven surfaces of the tissue,

the surface, the first polymeric scaffold, and the second polymeric scaffold of the biomedical wound matrix sufficiently pliable to enable movement of the biomedical wound matrix with the tissue, and

wherein the first structure of fibers and the second structure of fibers are configured to degrade after application to the tissue.

12. The biomedical wound matrix of claim **11**, wherein a first portion of the biomedical wound matrix of a particular size comprises a higher number of fibers than a second portion of the biomedical wound matrix of the particular size.

13. The biomedical wound matrix of claim **11**, wherein the first polymeric scaffold comprises a first topographical cue and the second polymeric scaffold comprises a second topographical cue.

14. The biomedical wound matrix of claim **13**, wherein one or more of the first topographical cue or the second topographical cue are randomly oriented to resemble an extracellular matrix.

15. The biomedical wound matrix of claim **11**, wherein the surface comprises a surface pattern comprising a plurality of organized features.

16. The biomedical wound matrix of claim **11**, wherein at least a portion of the first structure of fibers and at least a portion of the second structure of fibers are deposited simultaneously.

17. The biomedical wound matrix of claim **11**, wherein the surface comprises a plurality of structural features configured to facilitate cell growth.

18. The biomedical wound matrix of claim **11**, wherein the first structure of fibers and the second structure of fibers comprise one or more randomly oriented fibers.

19. The biomedical wound matrix of claim **11**, wherein the first structure of fibers and the second structure of fibers comprise one or more radially aligned fibers.

20. The biomedical wound matrix of claim **11**, wherein the first structure of fibers and the second structure of fibers comprise one or more uniaxially aligned fibers.

21. A biomedical wound matrix for facilitating wound healing, the biomedical wound matrix comprising:

a first polymeric scaffold comprising a first structure of fibers having electrospun nanofibers, the first structure of fibers comprising a plurality of randomly oriented fiber portion, the first structure of fibers configured to promote cell growth upon application of the biomedical wound matrix to a tissue; and

a second polymeric scaffold comprising a second structure of fibers having electrospun nanofibers, the second structure of fibers comprising a plurality of radially aligned fiber portions and a plurality of non-radially aligned fiber portions,

wherein one or more of the plurality of radially aliened fiber portions transition into one or more of the plurality of non-radially aliened fiber portions of the second structure of fibers, wherein one or more of the plurality of radially aliened fiber portions is overlaid on one or more of the plurality of non-radially aliened fiber portions of the second structure of fibers,

the second structure of fibers configured to provide structural reinforcement to the first polymeric scaffold;

the first structure of fibers and the second structure of fibers generated by depositing via electrospinning a first polymer composition and a second polymer composition, the first polymer composition being different from the second polymer composition;

the biomedical wound matrix further comprising a surface configured to contact tissue,

the biomedical wound matrix sufficiently flexible to facilitate application of the biomedical wound matrix to uneven surfaces of the tissue,

the biomedical wound matrix sufficiently flexible to enable movement of the biomedical wound matrix with the tissue, and

wherein the first structure of fibers and the second structure of fibers are configured to degrade after application to the tissue.

22. The biomedical wound matrix of claim **21**, wherein a first portion of the biomedical wound matrix of a particular size comprises a higher number of fibers than a second portion of the biomedical wound matrix of the particular size.

23. The biomedical wound matrix of claim **21**, wherein the surface of the biomedical wound matrix lacks a surface pattern.

24. The biomedical wound matrix of claim **21**, further comprising a directional cue configured to promote growth of neurites in one or more directions.

25. The biomedical wound matrix of claim **21**, wherein one or more of the first polymeric scaffold or the second polymeric scaffold is randomly oriented to resemble an extracellular matrix.

26. The biomedical wound matrix of claim **21**, wherein the first structure of fibers and the second structure of fibers are sterilized.

27. The biomedical wound matrix of claim **21**, wherein at least a portion of the first structure of fibers and at least a portion of the second structure of fibers are deposited simultaneously.

28. The biomedical wound matrix of claim **21**, wherein the surface comprises a plurality of structural features configured to facilitate cell growth.

29. The biomedical wound matrix of claim **21**, wherein the first structure of fibers and the second structure of fibers comprise one or more radially aligned fibers.

30. The biomedical wound matrix of claim **21**, wherein the first structure of fibers and the second structure of fibers comprise one or more uniaxially aligned fibers.

* * * * *